Dissertation zur Erlangung des Doktorgrades
der Fakultät für Chemie und Pharmazie
der Ludwig-Maximilians-Universität München

Molecular determinants of Min protein pattern formation

Simon Alexander Thomas Kretschmer
aus
Erlangen, Deutschland

2018

Erklärung

Diese Dissertation wurde im Sinne von § 7 der Promotionsordnung vom 28. November 2011 von Frau Prof. Dr. Petra Schwille betreut und von Herrn Prof. Dr. F. Ulrich Hartl von der Fakultät für Chemie und Pharmazie vertreten.

Eidesstattliche Versicherung

Diese Dissertation wurde eigenständig und ohne unerlaubte Hilfe erarbeitet.

München, den 27.04.2018

_____

Simon Alexander Thomas Kretschmer

Dissertation eingereicht am: 11.05.2018

1. Gutachter: Prof. Dr. F. Ulrich Hartl

2. Gutachterin: Prof. Dr. Petra Schwille

Mündliche Prüfung am: 21.06.2018

"Life is … a chemical incident …" [1]

(Paul Ehrlich)

Publications

Parts of this work have been published.

2018 **MinE conformational switching confers robustness on self-organized Min protein patterns**

Jonas Denk*, Simon Kretschmer*, Jacob Halatek*, Caroline Hartl, Petra Schwille and Erwin Frey

(* J.D., S.K. and J.H. contributed equally to this work)

Proceedings of the National Academy of Sciences of the United States of America

PNAS 201719801; published ahead of print April 16, 2018.

https://doi.org/10.1073/pnas.1719801115

Author contributions:

J.H. and E.F. initiated the project; J.H., C.H., and E.F. performed preliminary research; J.D., **S.K.**, J.H., P.S., and E.F. designed research; J.D., **S.K.**, J.H., P.S., and E.F. performed research; J.D., **S.K.**, J.H., P.S., and E.F. contributed new reagents/analytic tools; J.D., **S.K.**, J.H., P.S., and E.F. analyzed data; J.D., J.H., C.H., and E.F. designed the theoretical models and performed the mathematical analyses; **S.K.** and P.S. designed and carried out the experiments; and J.D., **S.K.**, J.H., P.S., and E.F. wrote the paper.

2018 **Reverse and forward engineering of protein pattern formation**

Simon Kretschmer, Leon Harrington and Petra Schwille

Philosophical Transactions of the Royal Society B *373*: 20170104.

http://dx.doi.org/10.1098/rstb.2017.0104

Author contributions:

S.K. and P.S. designed the research. **S.K.** performed experiments and analysed the data. **S.K**, L.H. and P.S. wrote the manuscript.

2017 **Large-scale modulation of reconstituted Min protein patterns and gradients by defined mutations in MinE's membrane targeting sequence**

Simon Kretschmer, Katja Zieske and Petra Schwille

PLoS ONE *12(6)*: e0179582.

https://doi.org/10.1371/journal.pone.0179582

Author contributions:

S.K.: Conceptualization, data curation, formal analysis, investigation, methodology, resources, validation, visualization, writing – original draft, writing – review and editing

K.Z.: methodology, resources, writing – review and editing

P.S.: conceptualization, funding acquisition, methodology, project administration, resources, validation, supervision, writing – review and editing

Additional Publications

2018 **Optical Control of a Biological Reaction-Diffusion System**
Philipp Glock, Johannes Broichhagen, Simon Kretschmer, Philipp Blumhardt, Jonas Mucksch, Dirk Trauner and Petra Schwille
Angewandte Chemie *57*, 2362-2366

2018 **Protein Pattern Formation**
Erwin Frey, Jacob Halatek, Simon Kretschmer and Petra Schwille
Book chapter in Physics of Biological Membranes, Edited by P. Bassereau and P. C. A. Sens (Springer-Verlag GmbH, Heidelberg)
In press
Preprint: arXiv:1801.01365.

2016 **Pattern formation on membranes and its role in bacterial cell division**
Simon Kretschmer and Petra Schwille
Current Opinion in Cell Biology *38*, 52-59

2015 **Rekonstitution biologischer Selbstorganisation *in vitro***
Simon Kretschmer and Petra Schwille
Biospektrum *21*: 148-150

2014 **Toward Spatially Regulated Division of Protocells: Insights into the *E. coli* Min System from *in Vitro* Studies**
Simon Kretschmer and Petra Schwille
Life *4*, 915-928

Table of Contents

1 Summary

In self-organizing systems, spatiotemporal order can emerge solely out of the interactions of the underlying components far from thermodynamic equilibrium. Inside the cell, protein self-organization enables pattern formation on intracellular surfaces, which regulates essential biological processes in space and time. This thesis aimed at revealing molecular determinants of protein pattern formation. For this, we turned to the *Escherichia coli* Min system, an archetypal example of protein self-organization on lipid membranes. Based on this system, we addressed the following general questions. First, which protein functionalities, or "modules", are strictly required for spatiotemporal pattern formation? Second, which functionalities are non-essential but modulate the characteristics of the large-scale protein patterns? Third, how sensitive are the emergent patterns to molecular changes in the underlying proteins as well as their concentrations and, in turn, how may robustness be conferred?

In the Min system, the ATPase MinD and its activating protein MinE cycle between the membrane and cytoplasm to oscillate between the cell poles in *E. coli*. In this way, a time-averaged concentration gradient with maxima at the poles and minimum at mid-cell is generated, which thereby localizes the cytokinetic machinery through the inhibitory action of the passenger protein MinC. *In vitro* reconstitution has previously shown that MinD, MinE, a lipid membrane and ATP are necessary and sufficient for Min protein self-organization. Moreover, a range of dynamic patterns, including traveling waves on flat membranes and pole-to-pole oscillations in cell-shaped microcompartments has been reconstituted dependent on the experimental conditions. However, it has remained poorly understood how the biochemical properties of MinD and MinE regulate the formation and characteristics of these patterns. Therefore, we applied a reverse engineering approach to the reconstituted Min system. Specifically, we analyzed the effects of altered Min protein functionalities on spatiotemporal pattern formation through the *in vitro* reconstitution of mutant Min proteins. With this approach, we gained novel insights into the minimal requirements and multi-scale regulation of Min protein patterns.

We confirmed that MinD ATPase stimulation by MinE is an essential requirement for self-organization. Moreover, by reconstitution of patterns formed by a mutant with reduced capacity of ATPase stimulation, we found that MinE activity and concentration regulate the spatiotemporal properties of Min patterns in a complementary fashion.

Disrupting MinE's membrane targeting sequence (MTS) by truncation or mutation still allowed for regular wave formation. However, we demonstrate that the MTS restrains MinE's

capacity to stimulate MinD's ATPase activity and regulates the length scale of Min protein patterns. Moreover, we observed that loss of MinE membrane interaction is accompanied by unusual dynamic modes deficient in gradient formation in cell-like geometry. Thus, MinE membrane affinity is a non-essential but regulatory critical modulatory parameter of Min protein patterns.

Recently, it has been discovered that MinE can switch between a "latent" and "reactive" conformation dependent on its interaction with MinD. As the functional role of this switch was unclear, we analyzed pattern formation by MinE mutants locked in the reactive conformation and compared our results with theoretical model predictions. With this approach, it became clear that, while not being strictly required for pattern formation, MinE's conformational switch confers robustness against variations in protein concentrations, thus enabling pattern formation in a broad parameter regime.

Lastly, we investigated the role of MinD membrane interaction in pattern formation. Disrupting the amphipathicity of MinD's MTS resulted in loss of self-organization. On the other hand, increasing the length of the MTS modulated Min protein patterns in multiple ways depending on the MinD/MinE ratio. While traveling waves with slower velocity emerged at high MinD concentrations, lower concentrations supported the formation of a qualitatively distinct pattern, namely standing waves. Thus, MinD membrane affinity is both strictly required for pattern formation and a multifaceted modulatory parameter.

Taken together, our reverse engineering approach enabled the determination of molecular properties of MinD and MinE that play essential roles in pattern formation or serve as important regulatory parameters. From a modular perspective, the cyclic attachment of MinD to the membrane and its subsequent release dependent on ATPase stimulation by MinE forms the core of Min protein dynamics. On top of this cycle, MinE membrane interaction and conformational switching are built for regulation and robustness of Min patterns.

Finally, while pattern formation *per se* is relatively robust to changes in the molecular properties and concentrations of Min proteins, the detailed characteristics of Min protein patterns are highly sensitive to changes in these parameters. Whereas this makes the Min system vulnerable, it also enables transitions between versatile behaviors, which could be advantageous for the Min system's adaptation in the course of evolution.

In a broader context, the results obtained here constitute a promising step toward a molecular blueprint of protein pattern formation, which could also guide future efforts in designing artificial self-organizing networks.

2 Introduction

2.1 Minimalist approaches to biochemical interaction networks

Over the last century, cell biological and biochemical studies have uncovered a wealth of insight about the structure and function of biomolecules (Berman, 2008). Yet, many defining characteristics of living systems, including their ability to organize and replicate themselves, cannot be explained by the properties of these components alone. Instead, such life properties typically emerge from the interactions between biomolecules. Therefore, a major aim is to elucidate how biochemical interaction networks give rise to emergent properties that exceed the features of the underlying molecular players.

Systems and synthetic biology approaches have provided intriguing insights on intracellular interactions (Bader et al., 2008) as well as proteome organization (Kuhner et al., 2009) and have even produced a whole-cell model for a genome-reduced bacterium (Karr et al., 2012). However, despite the inference of protein interaction networks and maps, whole-cell studies typically do not provide information about physicochemical mechanisms underlying basic life processes. In part, this is due to the complexity of even "simple" cells, which contain still unknown as well as partially redundant components. For example, even for a "synthetic" *Mycoplasma mycoides* (JCV-syn3.0) bacterium whose genome was systematically reduced to only 473 genes, the function of around one third of retained genes remains mysterious (Hutchison et al., 2016). This strongly impedes the identification of the minimal set of generalizable modules required for a certain biological process.

Alternatively, minimal systems approaches can be applied to the study of biochemical interaction networks in order to reduce cross-talk from endogenous cellular networks and enable control over the composition of the network and its components. Toward this end, various complementary strategies exist. If a suitable network has been identified *in vivo*, the components can be isolated and reconstituted under defined conditions *in vitro* (Schwille and Diez, 2009). Alternatively, the network can be "transplanted" into a different chassis *in vivo*, where it may function orthogonally to other host machineries (Chen et al., 2015). Lastly, synthetic networks that emulate a phenomenon of interest, but with different components, can be engineered *in vivo* and *in vitro* (Elowitz and Leibler, 2000; Gardner et al., 2000; Isalan et al., 2005). Although all of these approaches have distinct advantages, cell-free systems

provide particularly desirable control over important parameters, such as component types or concentrations as well as geometric boundary conditions. This facilitates the testing of proposed mechanisms and models as well as the elucidation of the minimal requirements for a process of interest.

From a minimal systems perspective, networks that generate emergent temporal and/or spatial behaviors are of particular interest due to their important regulatory roles in cellular organization and morphogenesis (Kondo and Miura, 2010; Kretschmer and Schwille, 2016; Oates et al., 2012). Moreover, it has been shown that complex phenomena such as circadian oscillations or spatiotemporal pattern formation can arise from interactions between even a small number of different components with certain key features. Thus, interaction networks capable of oscillations and pattern formation have both been reconstituted (Loose et al., 2008; Nakajima et al., 2005) and engineered *de novo* (Isalan et al., 2005; Karzbrun et al., 2014; Niederholtmeyer et al., 2015). Although the *de novo* designed networks are typically advantageous with regard to programmability and manipulation, they often comprise a relatively high number of components and reactions, including those involved in transcription and translation. In contrast, reconstituted protein networks only require a handful of different components for function. For example, three proteins in the KaiABC system suffice to generate temporal oscillations in protein phosphorylation (Nakajima et al., 2005). Similarly, in the Min system, spatiotemporal patterns arise solely from the ATP-driven self-organization of two proteins on a lipid membrane (Loose et al., 2008). Due to their known composition and archetypal character, such reconstituted protein networks provide ideal starting points for elucidating design features that give rise to, or regulate, their emergent dynamic behaviors.

2.2 Self-organized pattern formation in cell biology

2.2.1 Self-organized pattern formation

Regulation of intracellular processes in space and time is of pivotal importance for robust cell function. However, such desired spatiotemporal order is counteracted by the thermodynamic drive to equilibrium, or a state of maximum entropy. With regard to this dilemma, Erwin Schrödinger argued in his seminal treatise "What is Life?" that living systems can generate order by maintaining out-of-equilibrium conditions (Schrödinger, 1944). This can be realized by the consumption of chemical fuels like ATP that are, in turn, synthesized by metabolizing energy sources from the environment. Far from equilibrium, large-scale order can then spontaneously emerge solely from the interactions of a few components, given that the latter fulfill certain conditions (Camazine et al., 2001). This process is termed "self-organization" and is inherently different from "self-assembly", a process whereby components assemble into regular structures on a system's path to equilibrium (Misteli, 2001).

Self-organization has long been recognized in inanimate systems with famous examples including wind-generated ripples in sand dunes (Figure 2.1 A) or convection patterns in heated fluids (Camazine et al., 2001). A particularly striking and well-studied example of self-organization in chemistry is presented by the Belousov-Zhabotsinky reaction (Belousov, 1958; Zaikin and Zhabotinsky, 1970). This paradigmatic reaction generates temporal oscillations of the components or spatiotemporal wave patterns dependent on the experimental conditions, as long as reactants are continuously supplied (Belousov, 1958; Sagués and Epstein, 2003; Zaikin and Zhabotinsky, 1970) (Figure 2.1 C). Likewise, self-organization occurs on all scales of biological organization, from molecules to cells, organisms and populations. Famous examples include the social behavior of animals and microbes, developmental programs in multicellular organisms and the formation of dynamic biomolecular assemblies (Figure 2.1 B, D, E) (Camazine et al., 2001; Karsenti, 2008).

All of these self-organizing systems share common features. For example, for order to spontaneously emerge from a random distribution of components, positive feedback loops are required to amplify small, stochastic fluctuations. In turn, delayed negative feedback can balance such amplified changes to prevent their uncontrolled growth. Through the concerted interactions of a large number of components, often of a few distinct types only, the interplay

of positive and negative feedback can shape a large-scale pattern. Thus, the outcomes of self-organization often exceed the spatial and temporal dimensions of the low-level components by several orders of magnitude. In this way, the self-organization of individually small components can give rise to complex large-scale phenomena (Camazine et al., 2001).

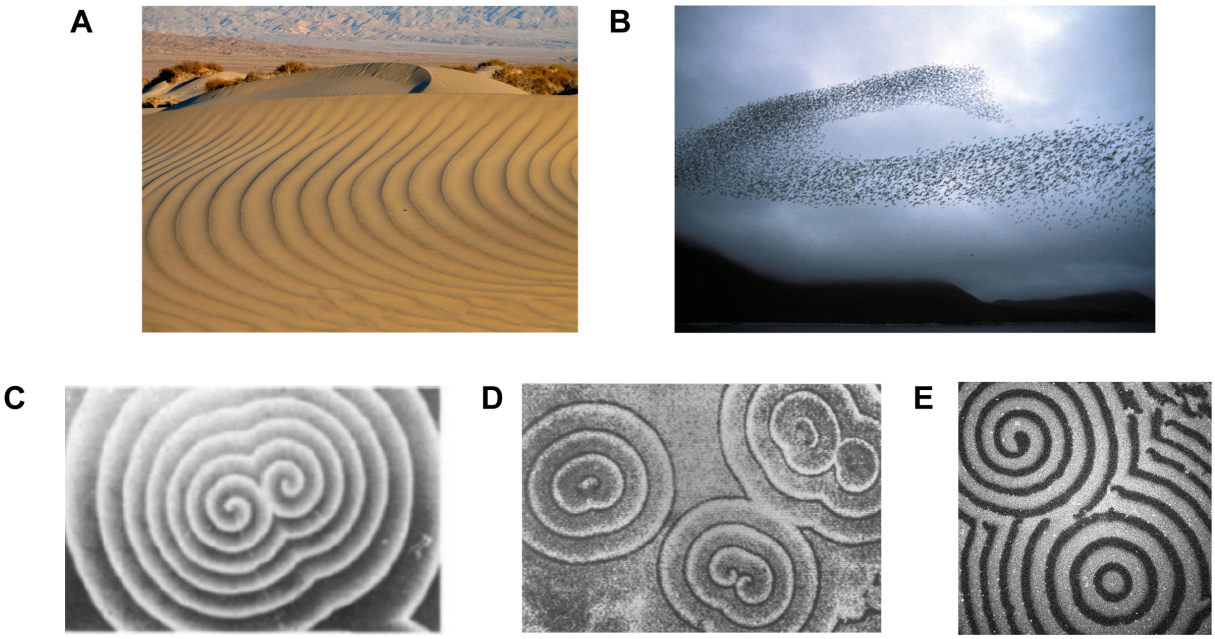

Figure 2.1: Examples of self-organization in inanimate and living systems. A) Wind-generated ripples in a sand dune (Photo by the National Park Service[2]). **B)** Flock of birds (Photo by D. Dibensiki[3]). **C)** Wave patterns emerging in the Belousov-Zhabotinsky reaction. Adapted from (Agladze et al., 1984) by permission from Springer Nature: Nature[4], (Agladze et al., 1984), Copyright 1984. **D)** Wave patterns emerging during aggregation of the slime mold *Dictyostelium discoideum*. Adapted from (Siegert and Steinbock, 1994) by permission from Springer Nature: Springer eBook, Die Natur schlägt Wellen[5], (Siegert and Steinbock, 1994), Copyright 1994. **E)** Wave patterns formed by purified and fluorescently labeled *E. coli* Min proteins on flat lipid membranes (see also section 2.3.4).

Self-organized biological pattern formation has first been proposed in pioneering theoretical studies. In 1952, Alan Turing mathematically described how, for certain parameter configurations, complex spatiotemporal patterns can emerge solely from the reaction and diffusion of two different components (Turing, 1952). Later, Alfred Gierer and Hans Meinhardt developed a framework for reaction-diffusion systems, based on a short-range activator and long-range inhibitor (Gierer and Meinhardt, 1972). Here, an activator catalyzes its own production in a self-enhanced fashion (positive feedback; “autocatalysis”). Furthermore, it produces, or recruits, its own inhibitor, which suppresses accumulation of the activator (negative feedback) (Figure 2.2 A). Importantly, the inhibitor has to diffuse much

faster than the activator (Gierer and Meinhardt, 1972). In such reaction-diffusion models, qualitatively different patterns, such as spots or stripes, emerge depending on the parameter values (Figure 2.2 B) (Gierer and Meinhardt, 1972; Kondo and Miura, 2010; Turing, 1952).

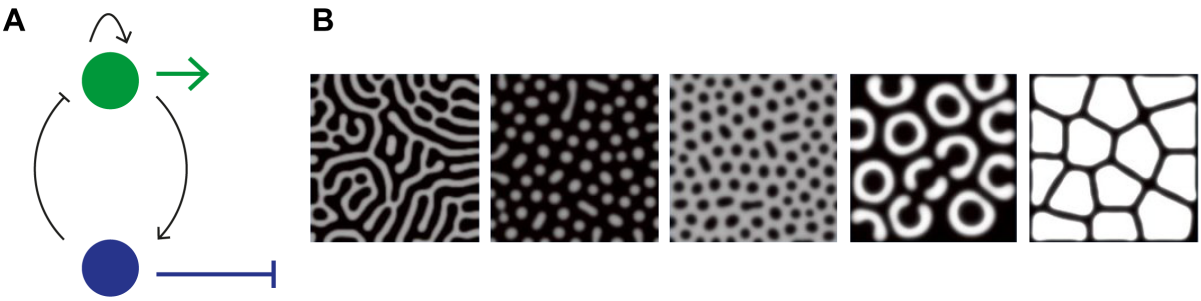

Figure 2.2: Theoretical reaction-diffusion systems composed of a short-range activator and long-range inhibitor can produce a rich variety of patterns depending on the system parameters. A) Activator–inhibitor network topology. The lengths of the colored arrows indicate the diffusive ranges of the activator (green) and inhibitor (blue). **B)** Examples of different types of self-organized patterns emerging in a reaction-diffusion model depending on the parameter values. From (Kondo and Miura, 2010). Reprinted with permission from AAAS.

It is important to note that pattern formation can also occur by mechanisms other than self-organization, e.g. by phase separation or through leveraging of pre-available positional information (Scholes and Isalan, 2017). For example, embryonic development of the fruit fly *Drosophila melanogaster* involves the local deposition of maternal mRNAs, which then give rise to "morphogen" gradients (Driever and Nusslein-Volhard, 1988a, b). Such gradients are then read out to regulate downstream gene expression in a concentration-dependent manner. In this way, a stripe pattern can emerge, which has also been described theoretically (Wolpert, 1969). Importantly, such a patterning mechanism relies on an initial asymmetry given by the spatial distribution of maternal mRNAs, whereas self-organized pattern formation can occur from initially homogeneous conditions by the amplification of stochastic fluctuations (Camazine et al., 2001; Isalan et al., 2005).

2.2.2 Self-organized protein pattern formation inside the cell

Several examples of self-organized pattern formation have been observed in both eukaryotic and bacterial cells. Despite their diverse origins and biological roles, these systems share a set of common features (Kretschmer and Schwille, 2016; Lutkenhaus, 2012). In all of these biochemical networks, self-organizing capabilities are "encoded" in the molecular properties of the involved proteins. First, consumption of chemical energy in the form of ATP or GTP hydrolysis keeps the systems far from thermodynamic equilibrium. Second, positive feedback is typically achieved by "cooperative" or otherwise "autocatalytic" binding of a protein to an intracellular surface, such as a lipid membrane or nucleoid DNA. While exceptions have been described, surface interaction is usually coupled to NTP binding. Moreover, the protein's accumulation on the surface is reversible and typically counteracted by antagonistic partner proteins that effectively exert a negative feedback by stimulating NTP hydrolysis. This combination of positive feedback and coupled antagonism can give rise to an NTP-dependent cycling of the proteins between the cytoplasm and surface (see also Figure 2.9 in 2.3.3.2). Notably, surface binding transiently modulates the diffusion coefficients of the proteins, which is important both for pattern formation (Gierer and Meinhardt, 1972) and for localized exertion of the network's function. Thus, one can distinguish between rapidly diffusing "inactive" states in the cytoplasm and slowly diffusing "active" states on an intracellular surface that switch by nucleotide binding or through protein interactions (Frey et al., 2018). Given a certain configuration of reaction rates, diffusion coefficients, concentrations and other parameters, interactions in such a network can give rise to protein pattern formation.

Various eukaryotic protein networks have been identified that support large-scale pattern formation. For example, during animal cell cytokinesis, the small GTPase Rho and actin self-organize into cortical waves (Bement et al., 2015). Moreover, in budding yeast, a network centered around the GTPase Cdc42 is capable of symmetry breaking (Kozubowski et al., 2008). Furthermore, in the *Caenorhabditis elegans* zygote, mutually antagonistic anterior and posterior Par proteins maintain cell polarity (Goehring et al., 2011). Notably, while Rho and Cdc42 switch between the membrane and cytoplasm dependent on their nucleotide state, reversible membrane binding in the Par system is based on phosphorylation and dephosphorylation of Par proteins.

Similarly, self-organized protein patterns play important roles in bacteria. The most prominent example of intracellular pattern formation in bacteria is the *E. coli* MinCDE

system, which sets the division plane to mid-cell (de Boer et al., 1989) and will be introduced in detail in section 2.3. Other examples include the PomXYZ system regulating cytokinesis in *Myxococcus xanthus* (Schumacher et al., 2017), the broadly conserved ParABS system regulating DNA segregation (Hu et al., 2017) and the FlhF/FlhG system regulating the patterning of flagella (Schuhmacher et al., 2015). All of these systems contain an NTPase of the ParA/MinD family (MinD, PomZ, ParA, FlhG), which reversibly interacts with an intracellular surface in an ATP-dependent manner. Notably, while the MinCDE and FlhF/FlhG systems act on the plasma membrane, the ParABS and PomXYZ systems use nucleoid DNA as a surface for self-organization.

2.3 Self-organized pattern formation by *E. coli* Min proteins

2.3.1 Bacterial cell division

The division of a single cell into two daughter cells is one of the most fundamental processes of all living systems. On a physical level, cell division requires large-scale morphological changes, as the mother cell envelope has to be constricted and ultimately separated (Xiao and Goley, 2016). In animal cells, cytokinesis involves a contractile actomyosin ring, in which actin-associated myosin motors harness chemical energy in the form of ATP to generate the required force for membrane constriction (D'Avino et al., 2015). On the other hand, the precise origin of the constriction force in bacterial cell division has remained unclear and both cytosolic and periplasmic proteins have been implicated in force generation (Xiao and Goley, 2016). Nevertheless, it is well established that, in the vast majority of bacteria, cytokinesis is related to polymerization of the tubulin homologue FtsZ into a ring-like structure at mid-cell (Figure 2.3) (Bi and Lutkenhaus, 1991; Bisson-Filho et al., 2017; Yang et al., 2017). This "Z-ring" then orchestrates assembly of the "divisome", the essential molecular machinery for dividing the cell (Haeusser and Margolin, 2016; Martos et al., 2012) (Figure 2.4).

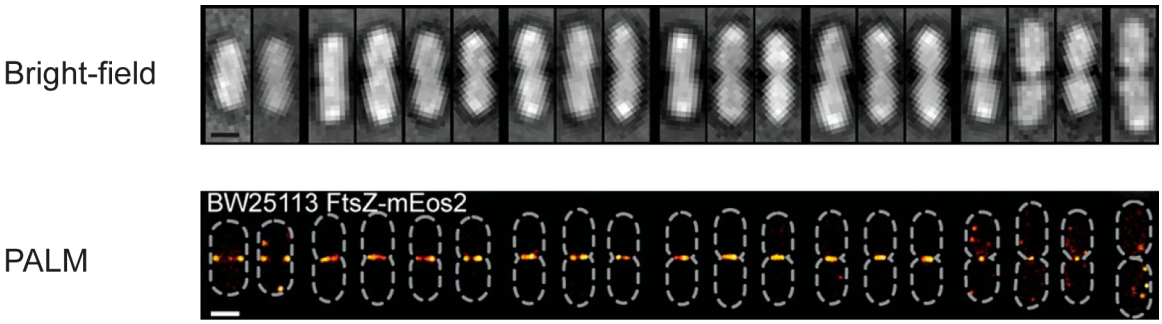

Figure 2.3: FtsZ forms a ring-like structure at mid-cell that is dynamically remodeled during septum closure. Live *E. coli* cells are shown, which were imaged by bright-field microscopy or superresolution photoactivated localization microscopy (PALM) and grouped by measured Z-ring diameter. Dashed lines indicate cell outlines. Adapted from (Coltharp et al., 2016) with permission from PNAS.

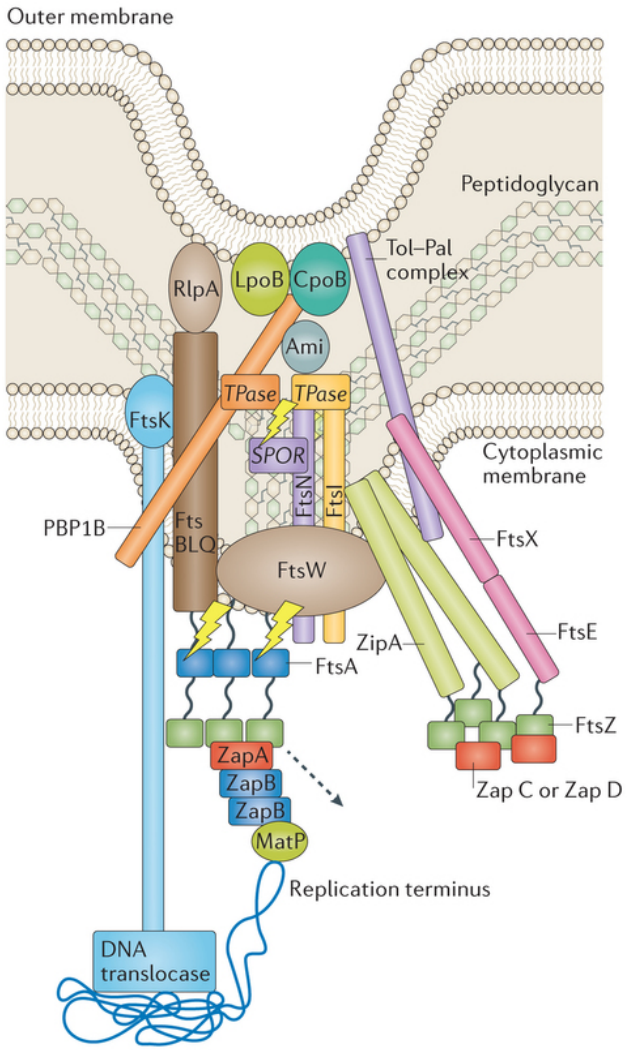

Figure 2.4: Bacterial cytokinesis is orchestrated by a multi-component molecular machinery that involves components in the cytoplasm, periplasm as well as the inner and outer membranes. Yellow bolts indicate regions of putative regulatory signaling. Image adapted from (Haeusser and Margolin, 2016) by permission from Springer Nature: Nature Reviews Microbiology[6], (Haeusser and Margolin, 2016), Copyright 2016.

FtsZ is an essential small GTPase of 40 kDa that, like its eukaryotic homologue, polymerizes into dynamic filaments (Xiao and Goley, 2016). To orchestrate divisome assembly, FtsZ is anchored to the membrane via adaptor proteins, including the peripheral membrane proteins FtsA and the integral membrane protein ZipA (Hale and de Boer, 1997; Pichoff and Lutkenhaus, 2005). These three proteins form the so-called “proto-ring”, which then acts as a scaffold to sequentially recruit further divisome components (Martos et al., 2012).

Importantly, the Z-ring is not a static structure, but is in fact highly dynamic. FtsZ and FtsA have first been found to self-organize into µm-sized chiral vortices on supported membranes *in vitro* (Loose and Mitchison, 2014). Similarly, large-scale treadmilling of FtsZ has recently been observed *in vivo* (Bisson-Filho et al., 2017; Yang et al., 2017). Furthermore, it has been

shown that the FtsZ dynamics on the cytoplasmic side of the inner membrane control the localization and activity of cell wall biogenesis complexes in the periplasm (Bisson-Filho et al., 2017; Yang et al., 2017). In this way, FtsZ guides the progressive and uniform insertion of new cell wall at the narrowing septum during cytokinesis, indicating that FtsZ-directed insertion of peptidoglycan generates force for cytokinesis (Xiao and Goley, 2016). However, it has also been proposed that FtsZ's GTPase activity and polymer mechanics directly generate force (Osawa et al., 2008). In summary, while the contributions of individual processes to constriction force generation are still not comprehensively understood, it is clear that FtsZ plays a central and essential role in bacterial cytokinesis.

2.3.2 Spatial regulation of bacterial cell division

Cytokinesis has to be tightly regulated in space and time to produce daughter cells with defined morphology and molecular content. Accordingly, bacteria have evolved diverse positioning mechanisms for the divisome via regulating Z-ring assembly in a topologically specific fashion. FtsZ polymerization can be regulated positively or negatively at defined intracellular regions. In organisms employing positive regulation, specific proteins recruit and/or stabilize FtsZ and thereby mark the future division site, as has been observed in *Myxococcus xanthus*, *Streptomyces coelicolor* and *Streptococcus pneumoniae* (Fleurie et al., 2014; Treuner-Lange et al., 2013; Willemse et al., 2011). On the other hand, negative regulatory systems in *Escherichia coli*, *Bacillus subtilis*, *Caulobacter crescentus* and other bacteria inhibit FtsZ polymerization anywhere but at the future division site (Bramkamp and van Baarle, 2009; Thanbichler and Shapiro, 2006; Wu and Errington, 2012).

In rod-shaped bacteria including *E. coli* and *B. subtilis*, the Z-ring is positioned at mid-cell by two complementary mechanisms: nucleoid occlusion (NO) and the Min system (Figure 2.5). NO inhibits division near the chromosomes, protecting the latter from bisection during cytokinesis and limiting divisome assembly to nucleoid-free regions in the cell (Bernhardt and de Boer, 2005; Wu and Errington, 2004, 2012). On the other hand, the Min system antagonizes Z-ring assembly at the poles through a concentration gradient of the FtsZ-inhibitor MinC (de Boer et al., 1989). Strikingly, this gradient exhibits a minimum at mid-cell, generating a permissive zone where FtsZ can polymerize. Notably, the Min system even functions in the absence of nucleoid occlusion (Bernhardt and de Boer, 2005). In contrast, loss of the Min system leads to division both at the cell center and near the poles, resulting in chromosomeless "minicells", eponymous for the Min system (Adler et al., 1967; de Boer et al., 1989). Finally, in the absence of both NO and the Min system, a severe filamentation phenotype is caused, likely due to the formation of multiple yet incomplete and thus unproductive Z-rings (Bernhardt and de Boer, 2005; Wu and Errington, 2004).

Min systems can localize the divisome either by oscillatory mechanisms, as is the case in *E. coli* (Figure 2.6 A and Figure 2.7 A), or non-oscillatory mechanisms, as has been observed in *B. subtilis* (Figure 2.6 B) (Lutkenhaus, 2012). The *E. coli* MinCDE system, which is arranged as an operon at the *minB* chromosomal locus (de Boer et al., 1988), is composed of the FtsZ-inhibitor MinC, the peripheral membrane ATPase MinD as well as the latter's activating protein MinE (Bi and Lutkenhaus, 1993; de Boer et al., 1991; de Boer et al., 1989; Hu and

Lutkenhaus, 2001). This system generates a time-averaged MinC concentration gradient via self-organized pole-to-pole oscillations of MinD and MinE (Raskin and de Boer, 1999a, b). Each half-oscillation cycle comprises (1) MinD membrane attachment and growth of a MinD polar zone toward mid-cell, (2) shrinkage of the MinD polar zone mediated by MinE that forms a ring-like structure at the polar zone's rim, and finally (3) MinD and MinE detachment and diffusion to the opposite pole, where the half cycle repeats itself (Lutkenhaus, 2012) (Figure 2.6 A, Figure 2.7 A-C). On time-average, these cell-pole-to-cell-pole oscillations give rise to a non-homogeneous concentration profile of MinD with maxima at the poles and minimum in the cell middle (Loose et al., 2011b) (Figure 2.7 B). MinC interacts with MinD and thereby acts as a passenger of the oscillations (Hu and Lutkenhaus, 1999). Consequently, MinC also displays a time-averaged concentration minimum at mid-cell, where FtsZ assembly is thus permitted to occur (Figure 2.5). Remarkably, the Min system is responsive to cell geometry and adapts its dynamic behavior to changes thereof (Di Ventura and Sourjik, 2011; Wu et al., 2015; Zieske and Schwille, 2014). For example, above a certain cell length and below a critical septum size, a pole-to-pole oscillation splits into two pole-to-middle oscillations (Figure 2.6 A) (Di Ventura and Sourjik, 2011). In this way, Min proteins are partitioned equally into daughter cells to readily regulate divisome assembly within them.

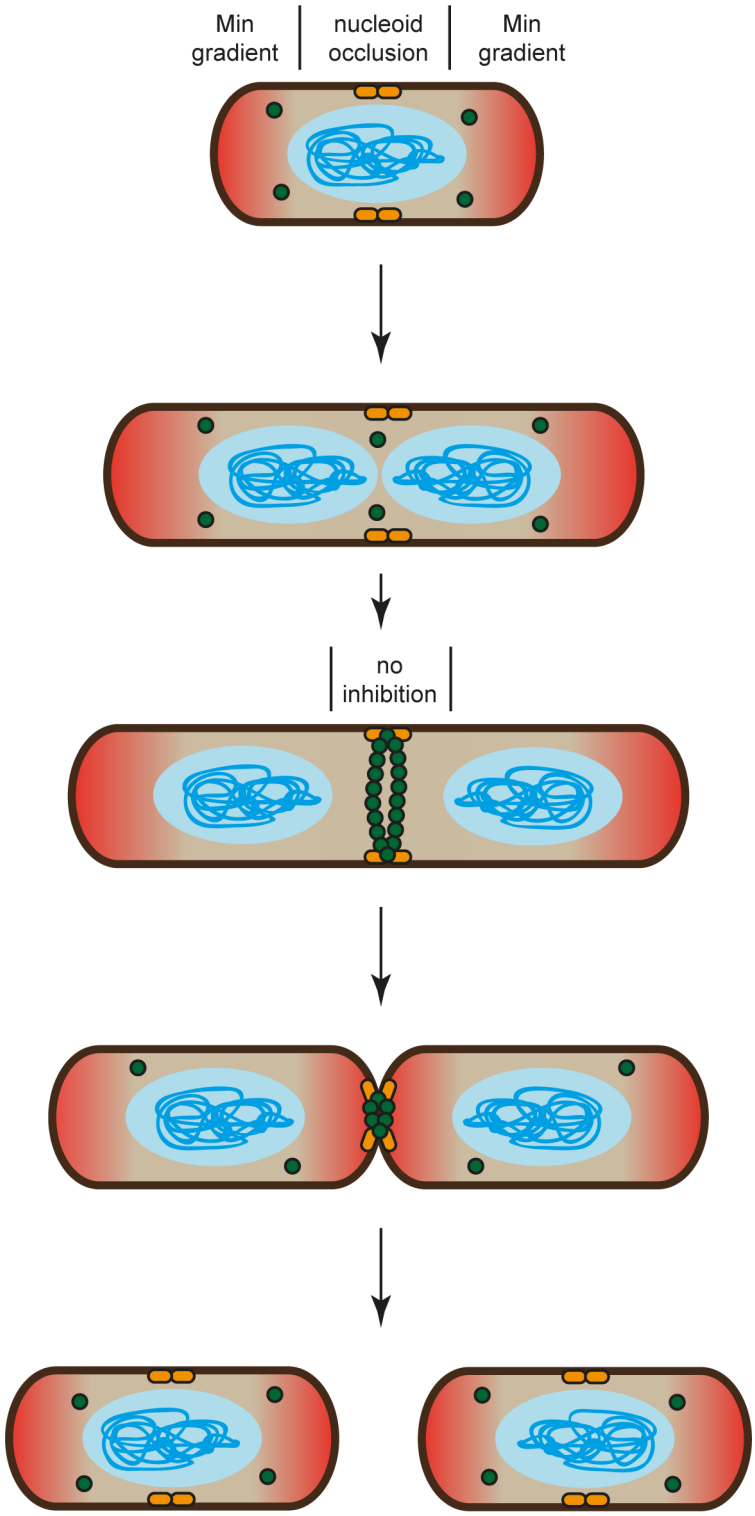

Figure 2.5: Cytokinesis in rod-shaped bacteria is spatially regulated by nucleoid occlusion and the Min system, which both localize assembly of the Z-ring to mid-cell during cell growth. Nucleoid occlusion (blue) inhibits polymerization of FtsZ (green) across or near the chromosomes. The Min gradient (red background) prevents Z-ring assembly at the cell poles. Membrane anchors for FtsZ are shown in orange.

The *B. subtilis* Min system lacks MinE but includes MinJ, which bridges the MinCD complex to DivIVA on the cell membrane (Bramkamp et al., 2008). DivIVA is enriched at regions of high membrane curvature, i.e. at the cell poles and adjacent to the septum (Lenarcic et al., 2009; Ramamurthi and Losick, 2009). Thus, Min proteins inhibit divisome assembly at the mother and nascent daughter cell poles (Figure 2.6 B). As *B. subtilis* Min proteins settle into their localization pattern via recruitment by a "landmark protein" (DivIVA) and not solely by their own interactions, the *B. subtilis* MinCDJ system is not considered a self-organizing system (Lutkenhaus, 2012).

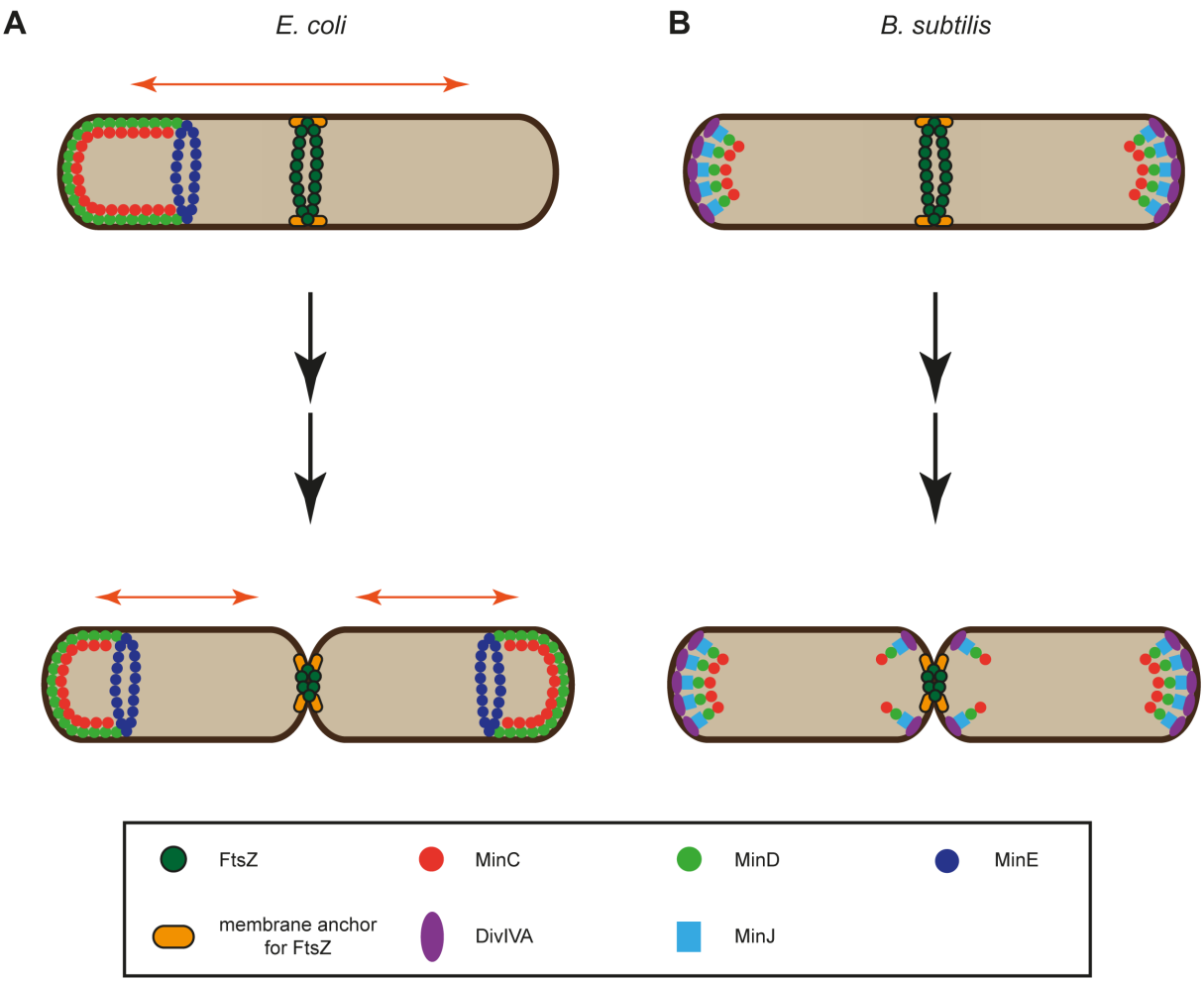

Figure 2.6: The Min systems in *E. coli* and *B. subtilis*. A) In *E. coli*, MinC oscillates under the control of MinD and MinE from pole-to-pole to generate an inhibitory gradient with minimum at mid-cell. During constriction, Min oscillations adapt to septum size and split into a double oscillation to inherit proteins and dynamics into the daughter cells, as indicated by the colored, horizontal arrows. **B)** In *B. subtilis*, MinD and MinC are recruited via MinJ to the landmark protein DivIVA, which preferentially localizes to membrane regions of high negative curvature. Thus, during constriction, the protein complexes also localize to the nascent curved membranes adjacent to the septum to prevent formation of multiple, closely spaced Z-rings and to inherit polar inhibition of division to the daughter cells.

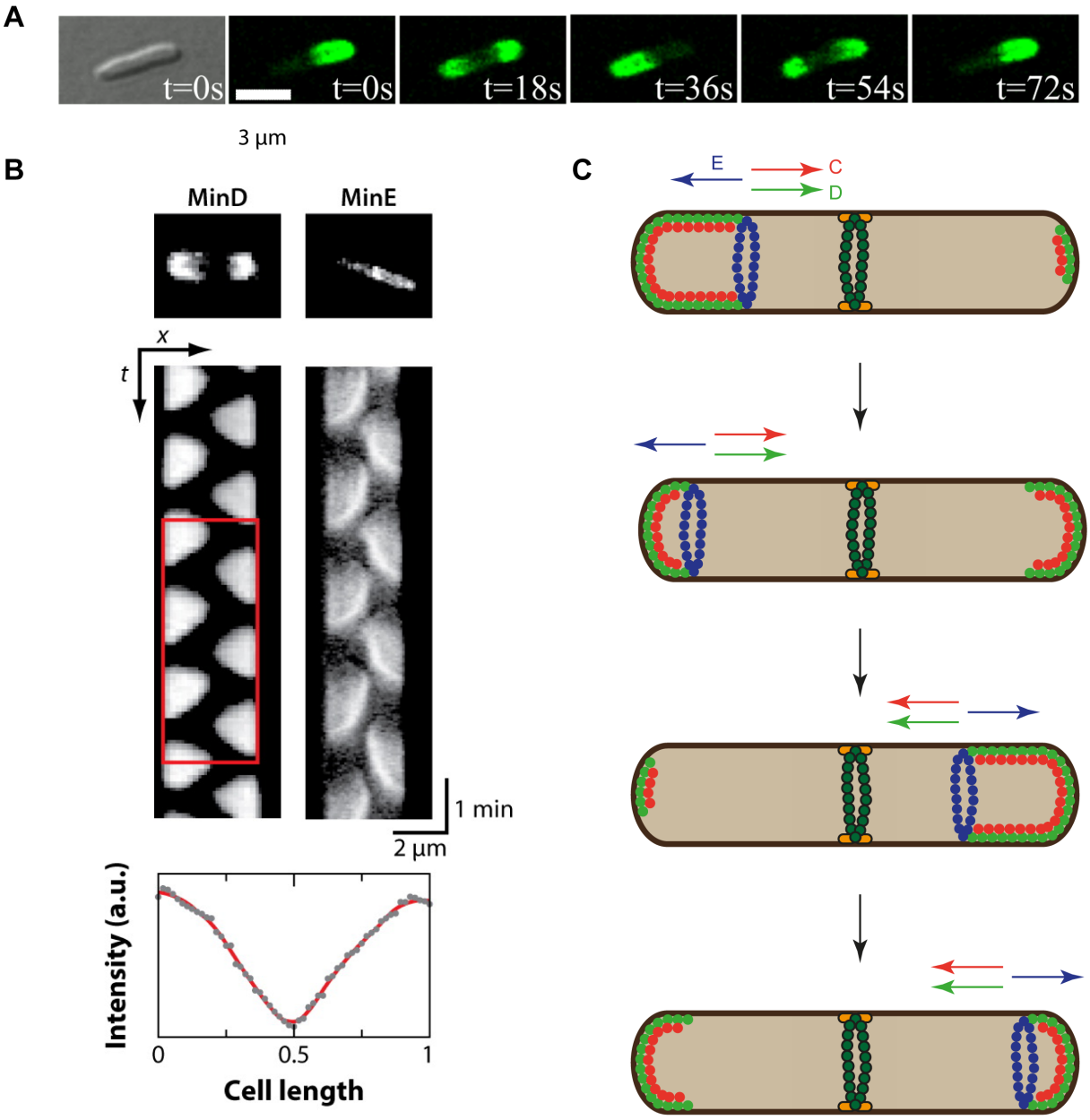

Figure 2.7: Min protein oscillations in *E. coli*. A) Differential interference contrast (DIC) image of an *E. coli* cell, in which time-lapse fluorescence images of GFP-tagged MinD were recorded. Adapted from (Bonny et al., 2013) under the Creative Commons Attribution (CC BY 3.0) License[7]. **B)** Fluorescence images and kymographs of GFP-MinD and MinE-GFP. The bottom panel depicts the time-averaged intensity profile within the red area in the MinD kymograph. Republished with permission of Annual Reviews Inc., from (Loose et al., 2011b), permission conveyed through Copyright Clearance Center, Inc. **C)** Schematic of a Min protein oscillation cycle. MinD forms a cap at the polar membrane, to which it recruits MinC. MinE forms a ring at the rim of the polar zone, detaches MinC and MinD from the membrane and thereby leads to shrinkage of the polar zone toward the pole. MinD and MinC then diffuse through the cytoplasm and form a new polar zone at the opposing pole. The colored arrows indicate the redistribution of MinC, MinD and MinE at the shrinking polar zone. Color scheme for proteins as in Figure 2.6.

2.3.3 The *E. coli* Min system

In this section, the Min system's components are introduced individually (section 2.3.3). Then, the emergent behavior from the interactions of Min proteins with the lipid membrane, as observed by *in vitro* reconstitution, is described (section 2.3.4), followed by a brief introduction to theoretical modeling of Min protein self-organization (section 2.3.5).

2.3.3.1 MinC

MinC directly inhibits FtsZ polymerization to antagonize divisome assembly (Arumugam et al., 2014; Bi and Lutkenhaus, 1993). Accordingly, loss of MinC results in the Min system's eponymous minicell phenotype, analogously to a Min^- strain (de Boer et al., 1988, 1989). In turn, MinC overexpression causes cell filamentation in the presence (de Boer et al., 1989) or absence of MinD and MinE (Hu and Lutkenhaus, 1999).
MinC is a homodimer with monomers composed of two independently folded domains connected via a short, flexible linker, whose length varies between species (Figure 2.8) (Cordell et al., 2001; Hu and Lutkenhaus, 2000). Although the N- and C-terminal domains of MinC display distinct biochemical functionalities, they synergistically inhibit Z-ring formation (Hu and Lutkenhaus, 2000; Shih and Zheng, 2013; Shiomi and Margolin, 2007). The N-terminal domain of MinC disrupts interactions between FtsZ monomers in FtsZ protofilaments (Dajkovic et al., 2008; Hu and Lutkenhaus, 2000; Shen and Lutkenhaus, 2010). In turn, MinC's C-terminal domain interferes with lateral interactions between FtsZ protofilaments (Dajkovic et al., 2008) and is responsible for MinC dimerization and binding of MinD (Cordell et al., 2001; Hu and Lutkenhaus, 2000). Importantly, MinC does not impair FtsZ's GTPase activity but in fact requires it for inhibition (Dajkovic et al., 2008; Hu et al., 1999). Accordingly, MinC was shown to exploit FtsZ's intrinsic turnover dynamics for antagonizing its large-scale assembly (Arumugam et al., 2014).

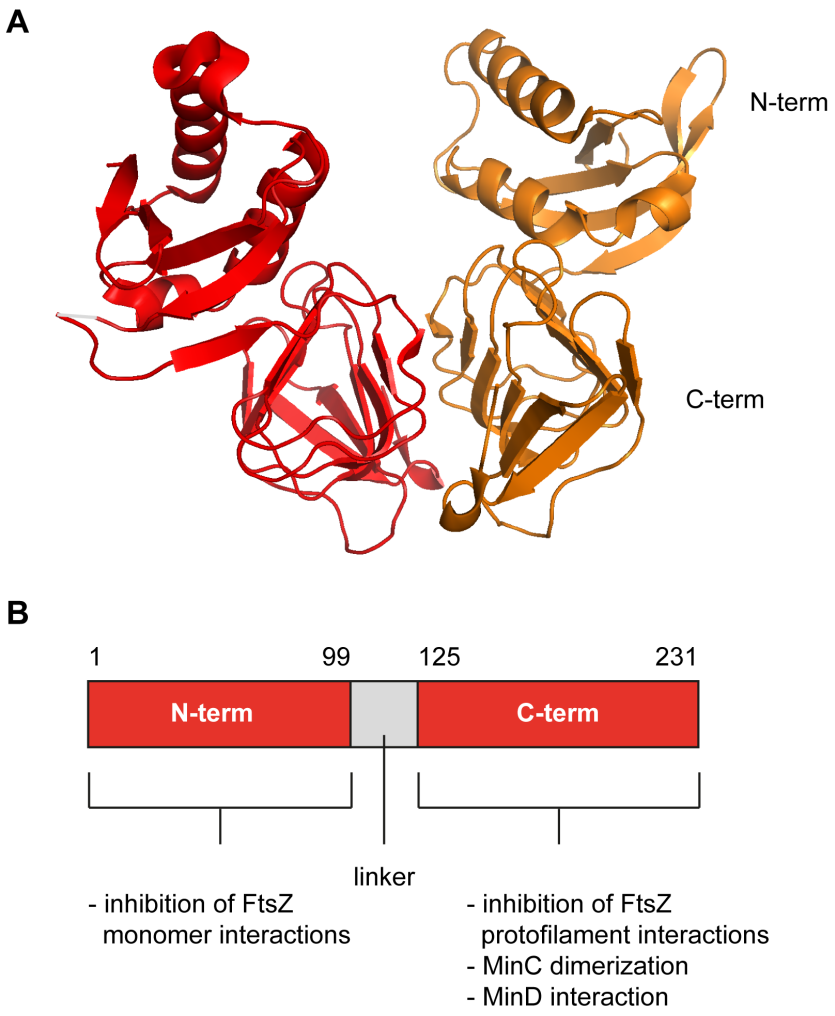

Figure 2.8: MinC structure and function. A) Crystal structure of a MinC dimer from *Thermotoga maritima* (PDB: 1HF2) (Cordell et al., 2001). **B)** *E. coli* MinC domain architecture.

MinC binds to MinD, although it is subsequently displaced by MinE (Lackner et al., 2003). Thus, by following the oscillations of MinD and MinE as a passenger, MinC is distributed according to the MinD gradient and inhibits FtsZ polymerization exclusively at the poles (Hu and Lutkenhaus, 1999; Raskin and de Boer, 1999a). Lastly, it has recently been reported that MinC and MinD form co-polymers under certain conditions *in vitro* (Ghosal et al., 2014). However, their physiological relevance remains controversial (Park et al., 2015).

2.3.3.2 MinD

MinD represents the Min network's central molecular player, as it directly interacts with MinC, MinE and the lipid membrane in an ATP-dependent manner. It is an ATPase of the SIMIBI (Signal recognition particle, MinD and BioD) class, which is itself part of the

superfamily of P-loop NTPases (Bange and Sinning, 2013; Leipe et al., 2002). Within the SIMIBI class, MinD belongs to the MinD/ParA family (Lutkenhaus, 2012). Other members of this family play important roles in chromosome and plasmid segregation (ParA), nitrogen fixation (NifH), regulation of flagella (FlgG) and chemotaxis arrays (ParC) or MinD-independent positioning of the Z-ring (MipZ) (Lutkenhaus, 2012).

An important feature of SIMIBI proteins is their ability to switch between an NTP-bound "on"-state and NDP-bound "off"-state, as found in many pattern-forming biochemical networks (section 2.2.2) (Bange and Sinning, 2013; Lutkenhaus, 2012). For MinD/ParA proteins, the ADP-bound ("off") state is a monomer that can freely diffuse in the cytoplasm. Exchange of ADP for ATP then leads to dimerization. In this "on" state, the proteins gain sufficient affinity to attach to an intracellular surface, such as a lipid membrane or nucleoid DNA. On this surface, active MinD/ParA proteins then recruit effectors, one of which is frequently an ATPase activating protein (AAP) that stimulates their enzymatic activity and consequently detachment as ADP-bound monomers (Lutkenhaus, 2012). This gives rise to a nucleotide-dependent cycle between an inactive, cytoplasmic and active, surface-associated state of the ATPase (Figure 2.9).

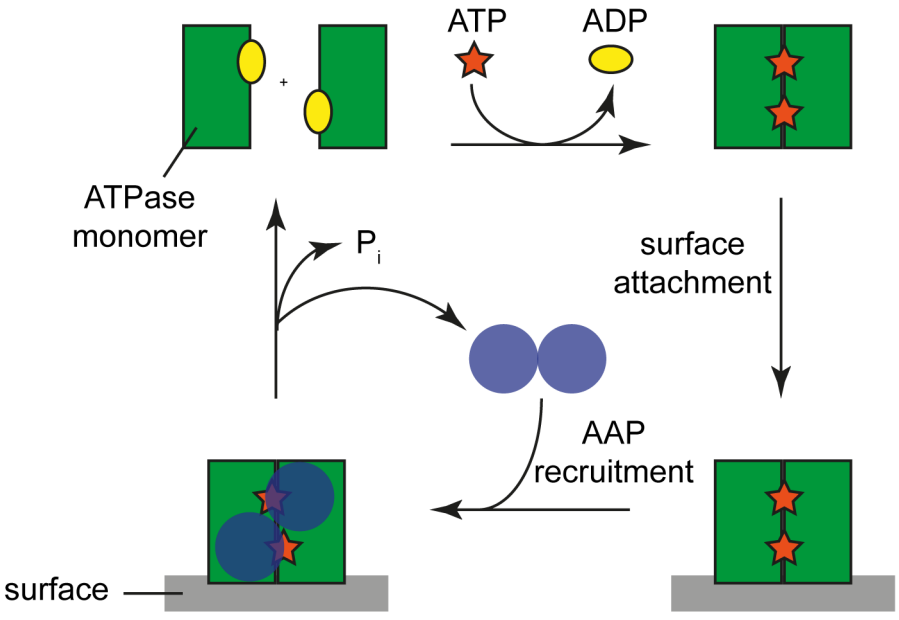

Figure 2.9: ATPases of the MinD/ParA family reversibly interact with an intracellular surface dependent on their nucleotide state. Upon exchanging ADP for ATP, the ATPase (green) dimerizes. This increases its affinity for an intracellular surface (grey) and generates binding sites for effector proteins. One of these effectors is an ATPase activating protein (AAP) (blue) that stimulates the ParA/MinD protein's intrinsically weak ATPase activity to release it from the surface. Thus, ParA/MinD ATPases continuously cycle between the cytoplasm and a surface, driven by ATP binding and AAP-triggered hydrolysis. MinD and ParA bind to the lipid membrane and nucleoid DNA respectively, while MinE and ParB function as their cognate AAPs.

The structural basis for this switch-like behavior of MinD/ParA ATPases can be found in their active sites, which exhibit a hallmark "deviant Walker A motif" (Lutkenhaus and Sundaramoorthy, 2003) (Figure 2.10). This motif contains two conserved lysine residues. The more C-terminal lysine is present in all Walker A sequences and is responsible for binding and hydrolyzing ATP (Lutkenhaus, 2012). On the other hand, the N-terminal, so-called "signature" lysine is unique to the deviant Walker A motif and enables dimerization of the ATPase by binding the γ-phosphate of the ATP attached to the other monomer (Lutkenhaus, 2012; Wu et al., 2011).

An individual *E. coli* MinD monomer is 270 amino acids long and has a molecular mass of around 30 kDa (de Boer et al., 1991). Whereas the active site is located near the N-terminus, MinD interacts with the membrane through a C-terminal, conserved membrane targeting sequence (MTS) that folds into an amphipathic helix (Hu and Lutkenhaus, 2003; Szeto et al., 2003; Szeto et al., 2002) (Figure 2.10). Importantly, the membrane affinity of one copy of the *E. coli* MinD MTS is too weak for binding (Hu and Lutkenhaus, 2003; Lackner et al., 2003). However, the membrane affinity increases sufficiently upon ATP-dependent dimerization, in line with the MinD/ParA switch paradigm (Hu and Lutkenhaus, 2003; Lackner et al., 2003; Lutkenhaus, 2012). Notably, it is experimentally established that MinD membrane interaction is cooperative, although rather weakly with reported Hill coefficients ranging between 1.15 and 2.5 depending on lipid composition and the experimental method used for analyzing membrane binding (Lackner et al., 2003; Mileykovskaya and Dowhan, 2005; Renner and Weibel, 2012). Furthermore, the precise nature of MinD's cooperative membrane binding remains unclear. Although it has been proposed that the membrane plays a role in promoting dimerization of loosely attached MinD monomers (Szeto et al., 2003), that MinD polymerizes into membrane-attached oligomers (Hu et al., 2002; Suefuji et al., 2002) and even that MinE recruits MinD to the membrane (Vecchiarelli et al., 2017), none of the above suggestions has been verified conclusively. Nevertheless, MinD's cooperativity in membrane binding is assumed to be an important source of non-linearity driving pattern formation and a critical part of theoretical models of Min protein self-organization (Frey et al., 2018).

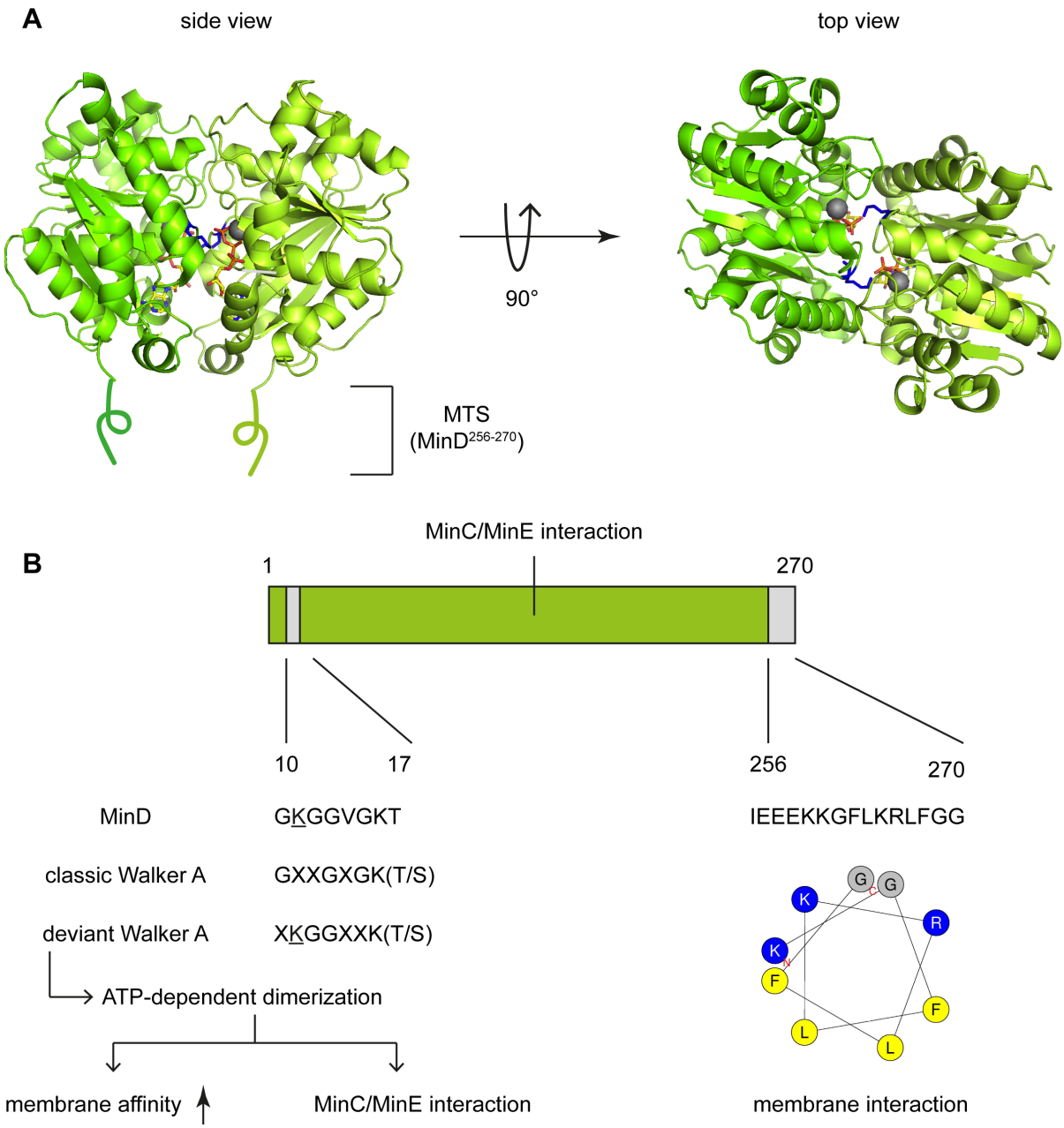

Figure 2.10: MinD structure and function. A) Structure of an ATP-bound MinD dimer from *E. coli* (PDB: 3Q9L) (Wu et al., 2011). ATPs are shown in stick representation and Mg^{2+} ions as grey spheres. MinD's membrane targeting sequence (MTS) is sketched as an extension at the C-terminus. The top view of the dimer illustrates how the signature lysine (K11; blue) mediates dimerization by binding to the γ-phosphate of the ATP on the opposite subunit. **B)** *E. coli* MinD domain architecture including a sequence comparison of classic and deviant Walker A motifs. The amphipathic nature of the MTS is shown via helix wheel representation of residues 261-269 (generated with HeliQuest Version 2).

Besides enabling membrane interaction of MinD, ATP-dependent dimerization also creates overlapping binding sites for MinC and MinE with residues from both subunits complementing each other to build up the interaction interface (Ghosal et al., 2014; Hu et al.,

2003; Ma et al., 2004; Ma et al., 2003). Thus, ATP-dependent-dimerization of MinD allows it to bind to the membrane, where it recruits its biological effector MinC (Lackner et al., 2003). Subsequently, MinE displaces MinC and detaches MinD from the membrane via stimulation of MinD's ATPase activity (Hu and Lutkenhaus, 2001; Lackner et al., 2003). In this way, ATP-dependent control of MinD dimerization, membrane binding and recruitment of MinC and MinE is central for all Min protein interactions (Lackner et al., 2003).

2.3.3.3 MinE

MinE ensures that the MinCD complex inhibits cell division only at the poles and not in the cell middle, a task for which it has historically been referred to as a "topological specificity factor" (de Boer et al., 1989). Biochemically, MinE's core function is the stimulation of MinD's ATPase activity (Hu and Lutkenhaus, 2001). In the absence of MinE and phospholipids, MinD displays only a weak ATPase activity, which is not significantly affected by the addition of either MinE or lipid vesicles alone. However, in the presence of both a lipid membrane and MinE, MinD's ATPase activity is increased by roughly one order of magnitude (Hu and Lutkenhaus, 2001). As MinD has a low membrane affinity in the ADP-bound state, this stimulation of MinD's ATPase activity by MinE promotes release of MinD from the membrane (Lackner et al., 2003).

Loss of MinE results in cell filamentation due to a homogeneous distribution of the MinCD complex over the cytoplasmic membrane (de Boer et al., 1989). In turn, mild overexpression in a WT-background reduces the oscillation period (Hale et al., 2001), whereas more extreme overexpression causes a minicell phenotype due to homogeneous depletion of MinD and MinC from the membrane (de Boer et al., 1989). Notably, MinE assembles into a ring-like structure *in vivo* (Raskin and de Boer, 1997). Although originally believed to be static (Raskin and de Boer, 1997), this so-called "E-ring" is in fact highly dynamic (Hale et al., 2001). Localized at the rim of MinD polar zones, the E-ring moves toward the poles and detaches MinD from the membrane during shrinkage of polar zones (Figure 2.7) (Hale et al., 2001).

MinE forms a homodimer of subunits that are 88 amino acids long (Pichoff et al., 1995) (Figure 2.11 A). Despite its relatively small size, MinE displays an intricate range of structural and functional properties. MinE's N-terminal "anti-MinCD" domain contains a membrane targeting sequence (residues 1-12), which comprises an amphipathic helix (Park et al., 2011; Shih et al., 2011) as well as a patch of cationic residues (Hsieh et al., 2010) (Figure

2.11 B, C). The MTS is followed by the core part of the anti-MinCD domain (residues 13-31), which is directly responsible for binding MinD, detaching it from the membrane via stimulation of ATP hydrolysis and thereby transiently and locally counteracting the inhibitory effect of the MinC-MinD complex toward FtsZ (Figure 2.11 B, D) (Lackner et al., 2003; Park et al., 2011; Zhao et al., 1995).

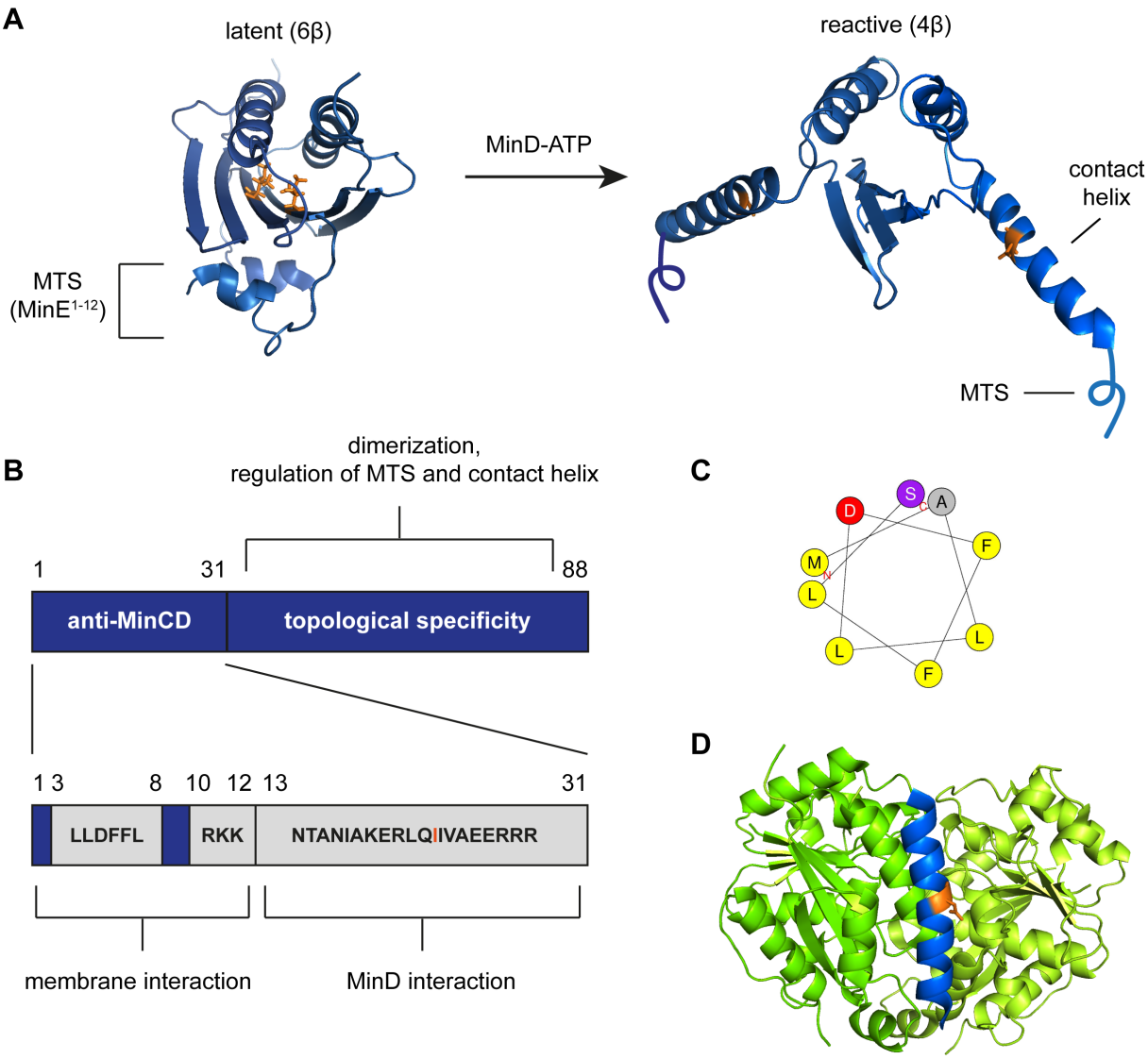

Figure 2.11: MinE structure and function. A) Upon sensing membrane-bound MinD, or through hydrophilic substitutions at residue I24 in the β1-strand, MinE is converted from a "latent" 6β-stranded to a "reactive" 4β-stranded conformation with exposed domains for MinD ATPase stimulation and membrane interaction. Structures correspond to latent MinE from *N. gonorrhoeae* (PDB: 2KXO) (Ghasriani et al., 2010) and reactive MinE from *E. coli* (PDB: 3R9J) (Park et al., 2011) with the I24N mutation highlighted in orange. **B)** *E. coli* MinE domain architecture. MinE's MTS contains a stretch of hydrophobic residues and a cluster of cationic residues. **C)** The amphipathic nature of the MTS is shown via helix wheel representation of residues 1-9 (generated with HeliQuest Version 2). **D)** Reactive MinE binds MinD at its dimer interface via the "contact helix".

The C-terminal part of MinE (residues 32-88) is historically referred to as a "topological specificity domain" (TSD) and is required for faithful divisome placement (Pichoff et al., 1995; Zhao et al., 1995). It was shown to dimerize MinE (Pichoff et al., 1995), but also to sequester the MTS and contact helix in the absence of MinD (Park et al., 2011). Thus, although individual functions have been ascribed to MinE's N- and C-terminal domains, they are not entirely independent, consistent with the observation that mutations in one domain of *Neisseria gonorrhoeae* MinE modulate the structure of the other (Ramos et al., 2006).
Importantly, MinE can switch between two functional states in a MinD-dependent manner, namely a "latent" 6β-stranded conformation and a "reactive" 4β-stranded conformation (Park et al., 2011) (Figure 11 A). In the latent state, the contact helix for MinD interaction is buried in the β1-strand and the MTS masked through hydrophobic tethering to the β-sheet, allowing MinE to freely diffuse in the cytoplasm. On the other hand, in the reactive state, the MTS is released and most of the anti-MinCD domain folds into an α-helix. Via this so-called "contact-helix", MinE interacts with MinD to form the membrane-bound complex, in which ATPase stimulation occurs (Park et al., 2011). Importantly, this structural and functional switch does not occur spontaneously but depends on membrane-bound MinD to trigger MinE's transition from the latent to the reactive state (Park et al., 2017; Park et al., 2011). Very recently, it has been proposed that MinE activation is a multi-step process (Ayed et al., 2017; Park et al., 2017). In this view, the MTS is only loosely anchored to the β-sheet and thus occasionally released in the latent state. By this release, a loop region becomes accessible that can bind, or "sense", membrane-bound MinD to form an "encounter complex" (Ayed et al., 2017; Park et al., 2017; Park et al., 2011). This interaction then nucleates the structural transition of the β1-strand strand to the contact helix, allowing for the formation of the reactive MinDE complex (Ayed et al., 2017; Park et al., 2017).

2.3.3.4 Role of the lipid membrane in pattern formation

Min protein oscillations and gradient formation are emergent phenomena that arise from the ATP-dependent interactions of MinD and MinE with the lipid membrane (Figure 2.12) (Lackner et al., 2003). At the core of this emergent behavior is the cyclic switching of Min proteins between cytoplasmic and membrane-bound states. Thus, the membrane is an essential component for pattern formation, providing a surface for the reversible accumulation of Min proteins as well as for modulating their reaction and diffusion properties. In this way,

it actively participates in pattern formation, analogously to metal surfaces acting as heterogeneous catalysts in chemical reactions (Jakubith et al., 1990). In turn, the cytoplasm is vital for acting as a reservoir, where Min proteins are stored and rapidly redistributed (Frey et al., 2018).

The lipid membrane also plays important roles in generating the non-linear kinetics required for pattern formation. In this regard, MinD membrane interaction is generally accepted to be cooperative, i.e. binding is enhanced with increasing concentrations of already membrane-bound MinD dimers (Lackner et al., 2003; Mileykovskaya et al., 2003; Renner and Weibel, 2012). Moreover, single-molecule experiments have indicated a positive feedback during MinD detachment from the bilayer, based on rapid rebinding of MinE to the membrane-bound protein layer (Loose et al., 2011a). Such rapid rebinding increases the membrane-proximal MinE/MinD ratio during MinD's release from the membrane, which in turn increases the rate of MinD ATPase stimulation and detachment (Loose et al., 2011a).

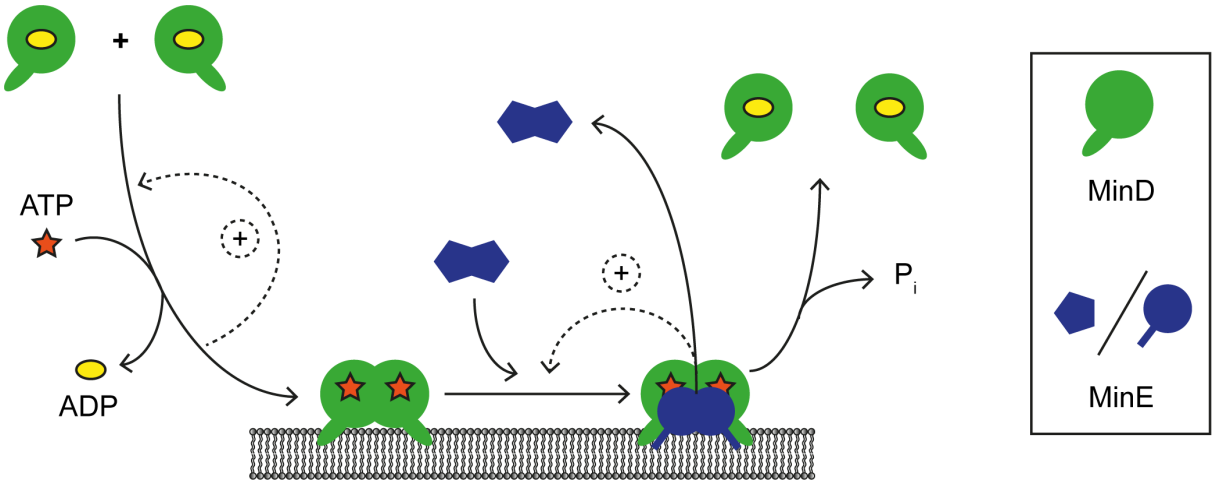

Figure 2.12: Basic scheme of ATP-dependent interactions of MinD, MinE and the lipid membrane. MinD cooperatively interacts with the lipid membrane upon ATP-dependent dimerization. MinE then binds to membrane-bound MinD, whereby it undergoes a conformational change from a latent to a reactive conformation. In the resulting membrane-bound MinD-MinE complex, MinE stimulates MinD's ATPase activity, resulting in detachment of ADP-bound MinD from the membrane. MinE can either detach or rapidly rebind another membrane-bound MinD dimer. Dashed lines indicate proposed positive feedback loops, namely cooperative MinD membrane interaction and rapid rebinding of MinE to another membrane-bound MinD dimer. MinC, which binds MinD before being displaced by MinE, is not shown, as it is not required for pattern formation (Hu and Lutkenhaus, 1999; Hu et al., 2003; Lackner et al., 2003).

Lastly, it is important to note that, with regard to accumulation on the membrane, MinD and MinE generally have antagonistic roles (Frey et al., 2018). Membrane-bound MinD recruits

both MinE and, by means of cooperative attachment, more MinD to the membrane (Lackner et al., 2003). On the other hand, MinE detaches MinD from the membrane (Lackner et al., 2003). Thus, during Min oscillations, MinD-based recruitment and MinE-based detachment alternate in a spatiotemporal fashion (Frey et al., 2018).

2.3.4 *In vitro* reconstitution of Min protein self-organization

2.3.4.1 Benefits of *in vitro* reconstitution for analyzing the Min system

Genetic, biochemical and cell biological studies have systematically uncovered the molecular properties and motifs of Min proteins, as described in the previous section. To analyze the functional roles of these molecular properties in pattern formation, a common approach is to perturb a specific feature by mutagenesis and analyze the resulting effect *in vivo*. However, as a non-linear reaction-diffusion system, the Min system is highly sensitive to even small changes in parameters. Moreover, due to its vital role in divisome positioning, such sensitivity directly affects *E. coli* cell division. Thus, mutations in Min proteins frequently lead to abnormal cell division or its inhibition altogether (Hu and Lutkenhaus, 2001; Park et al., 2011). In turn, division defects give rise to changes in cell morphology that feed back on Min protein dynamics (Wu et al., 2016). Therefore, the patterns emerging in different mutant strains can often not be characterized under the same experimental conditions, impeding direct comparability.

On the other hand, *in vitro* reconstitution of the Min system allows for the precise adjustment, manipulation and reproduction of experimental conditions. Furthermore, the removal of cellular context enables a systematic and broad exploration of the parameter space beyond the limitations posed by cell viability and other boundary conditions. This provides valuable possibilities to investigate a specific parameter's effect on pattern formation via its variation, while keeping the remaining parameters fixed. In the following sections, different cell-free systems for reconstituting Min protein pattern formation are summarized.

2.3.4.2 Reconstitution of Min protein patterns on lipid bilayers *in vitro*

The most simple approach to reconstitute Min protein self-organization *in vitro* is based on a flat supported membrane composed of lipids mimicking the composition of the *E. coli* inner membrane. This supported lipid bilayer (SLB) is topped with a bulk reservoir containing purified Min proteins and ATP along with other buffer components (Loose et al., 2008) (Figure 2.13 A). In this setting, MinD and MinE spontaneously self-organize into traveling surface waves on the membrane (Loose et al., 2008) (Figure 2.13 B). Rotating spirals as well

as so-called “target patterns”, in which waves are emitted from a point-like source, are other prominent features observed *in vitro* (Figure 2.13 B). Remarkably, Min protein patterns are, by their qualitative appearance, similar to the patterns emerging in other prototypical self-organizing systems, such as the Belousov-Zhabotsinky reaction (Figure 2.1) (Zaikin and Zhabotinsky, 1970) or carbon monoxide oxidation patterns on platinum surfaces (Jakubith et al., 1990).

The reconstituted Min waves share both similarities and differences with Min oscillations observed *in vivo* (Loose et al., 2011a; Loose et al., 2008). The most notable difference is that traveling waves are qualitatively distinct from oscillations, which can be viewed as standing waves in a confined space. Furthermore, the traveling waves reconstituted *in vitro* are characterized by a roughly ten times larger length scale compared to stripe patterns formed by Min proteins in filamentous cells *in vivo* (Touhami et al., 2006). This discrepancy in length scale has been suggested to be due to altered effective reaction rates and diffusion coefficients *in vitro* (Loose et al., 2008).

Despite these differences, the temporal periods of the *in vitro* waves and *in vivo* oscillations are in the same range and both depend on the MinE/MinD ratio (Hale et al., 2001; Loose et al., 2008). Moreover, MinE accumulates in a sharp peak at the rear the wave, reminiscent of the E-ring *in vivo* (Figure 2.13 C) (Hale et al., 2001; Loose et al., 2008). Lastly, MinC follows the waves generated by MinD and MinE as a passenger (Loose et al., 2011a). Notably, single-molecule studies have indicated that Min waves propagate by Min proteins binding to the membrane on the leading end and detaching on the trailing end (Loose et al., 2011a). Furthermore, both symmetry breaking and wave propagation have been proposed to depend on MinE’s rapid rebinding to the membrane-bound MinD layer and the resulting positive feedback in MinD detachment (section 2.3.3.4) (Loose et al., 2011a).

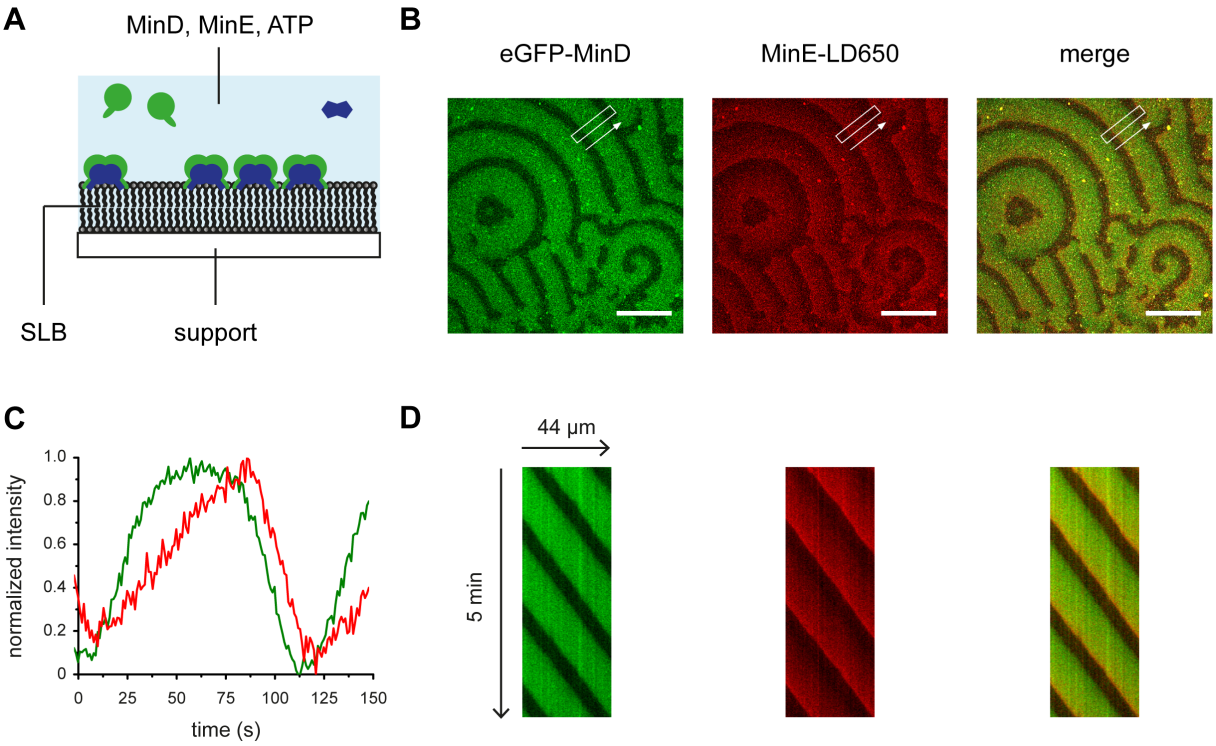

Figure 2.13: *In vitro* reconstitution of Min protein patterns on a supported lipid bilayer (SLB). A) Scheme of the experimental setup: MinD and MinE are added along with ATP into a reaction buffer on top of a flat lipid bilayer, supported by glass or other suitable substrates. **B)** Confocal micrographs of Min protein waves forming on a flat SLB, whose lateral dimensions are much larger than the pattern's wavelength. Scale Bar: 50 µm. **C)** Temporal profile of a Min protein wave; the green and red curves correspond to MinD and MinE respectively. **D)** Kymographs obtained from the rectangular areas in B display a stripe pattern characteristic of traveling waves. Protein concentrations: 1 µM MinD incl. 20 % eGFP-MinD, 1 µM MinE incl. 10 % MinE labeled with the dye LD650 (MinE-LD650).

The emergence of Min protein patterns on a supported lipid bilayer conclusively demonstrated that MinD, MinE, ATP and a lipid membrane are necessary and sufficient for Min protein self-organization (Loose et al., 2008). Furthermore, the reconstituted system enabled the systematic investigation of physicochemical factors on pattern formation. To analyze the effects of protein diffusivity on the patterns, Min proteins have been reconstituted on giant unilamellar vesciles (GUVs), on whose free-standing membrane surface proteins diffuse faster than on SLBs (Martos et al., 2013). This showed that higher diffusion coefficients of Min proteins on membranes are associated with an increased wavelength, suggesting that differences in diffusivities indeed contribute to the higher length scale of Min patterns *in vitro* (Martos et al., 2013). Furthermore, by varying the lipid composition in SLBs, it was found that Min protein patterns do not require specific lipids to form, as had previously been suggested (Vecchiarelli et al., 2014; Zieske and Schwille, 2014). Rather, the patterns are

sensitive to the anionic charge density in the membrane, which also modulates their spatiotemporal properties in combination with the ionic strength in the bulk reservoir above the membrane (Vecchiarelli et al., 2014).

Lastly, using an SLB-coated flow-cell, it was shown that externally applied flow leads to various unusual patterns, while more regular spiral and wave patterns emerge without flow (Ivanov and Mizuuchi, 2010; Vecchiarelli et al., 2016; Vecchiarelli et al., 2014). Moreover, after injecting Min proteins into the flow-cell and then stopping flow, a variety of qualitatively different patterns formed depending on the local concentrations of Min proteins in the bulk phase above the membrane (Vecchiarelli et al., 2016) (Figure 2.14). Most notably, a pattern resembling standing waves, termed "bursts", was observed near the outlet of the flow cell, i.e. where proteins are readily depleted from the bulk (Vecchiarelli et al., 2016).

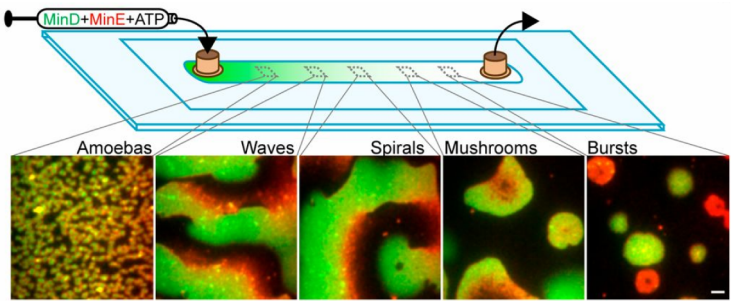

Figure 2.14: Min protein patterns emerging in an SLB-coated flow cell. Inside the flow cell, MinD and MinE form a variety of different patterns depending on the local concentration of Min proteins above the membrane. GFP-MinD and MinE-Alexa647 are shown. Scale Bar: 5 µm. Adapted from (Vecchiarelli et al., 2016) with permission from PNAS.

2.3.4.3 Geometric modulation of reconstituted Min protein patterns

A major difference between the initially reconstituted traveling waves on flat membranes *in vitro* and Min oscillations *in vivo* was the surrounding geometry. The first indication that reconstituted Min protein patterns can "sense" geometry came from experiments, in which Min waves were guided laterally on two-dimensionally confined supported membranes (Schweizer et al., 2012). Similarly, Min waves were aligned via topological cues within a polydimethylsiloxane (PDMS) support (Zieske et al., 2014).

Importantly, pole-to-pole oscillations of Min proteins have been reconstituted *in vitro* using microfabricated, rod-shaped PDMS microcompartments (Zieske and Schwille, 2013) (Figure 2.15 A). These picoliter-sized chambers were not membrane-enclosed in all three dimensions

but contained a buffer-air interface on top (Figure 2.15 A). However, they exhibited a greatly reduced volume-to-surface ratio compared to setups with an extended bulk reservoir above the membrane (Loose et al., 2008; Schweizer et al., 2012; Zieske et al., 2014). To account for the Min system's larger length scale *in vitro*, the dimensions of the chambers were increased approximately tenfold compared to the size of *E. coli* cells (Zieske and Schwille, 2013). Notably, the reconstituted Min oscillations supported formation of a time-averaged gradient of MinD and MinC that localized a chimeric membrane-targeted FtsZ variant (FtsZ-YFP-mts) to the middle of a compartment (Zieske and Schwille, 2014). Furthermore, the reconstituted oscillations were highly sensitive to the geometric boundary conditions, reproducing characteristic protein dynamics observed in round, filamentous or constricting *E. coli* cells (Corbin et al., 2002; Di Ventura and Sourjik, 2011; Fu et al., 2001; Zieske and Schwille, 2013, 2014). Furthermore, systematic variations in geometry have uncovered new geometry-dependent dynamic modes, such as an oscillation along the minor axis for an increased width of the compartment (Zieske and Schwille, 2014).

Later, by applying microfluidic methodologies, the geometry-dependent occurrence of unusual Min protein dynamics has been investigated in PDMS microchambers that were covered with a lipid membrane in all three dimensions (Caspi and Dekker, 2016) (Figure 2.15 B). In this setup, alternative dynamic modes also emerged besides oscillations, most notably traveling waves and rotations (Caspi and Dekker, 2016). Moreover, different dynamic modes were found in chambers of identical geometry. Such co-occurrence and even switching between different modes was also observed *in vivo*, when cells were shaped using a cell-sculpting method (Wu et al., 2015) (Figure 2.15 C), as well as in stochastic simulations (Amiranashvili et al., 2016; Wu et al., 2016), and is indicative of "multistability" of different Min protein patterns. Lastly, Min proteins have also been reconstituted inside lipid droplets (Zieske et al., 2016). Under these conditions, Min proteins rotated or oscillated from side-to-side after an initial time period of homogeneous oscillations between the droplet's lumen and membrane.

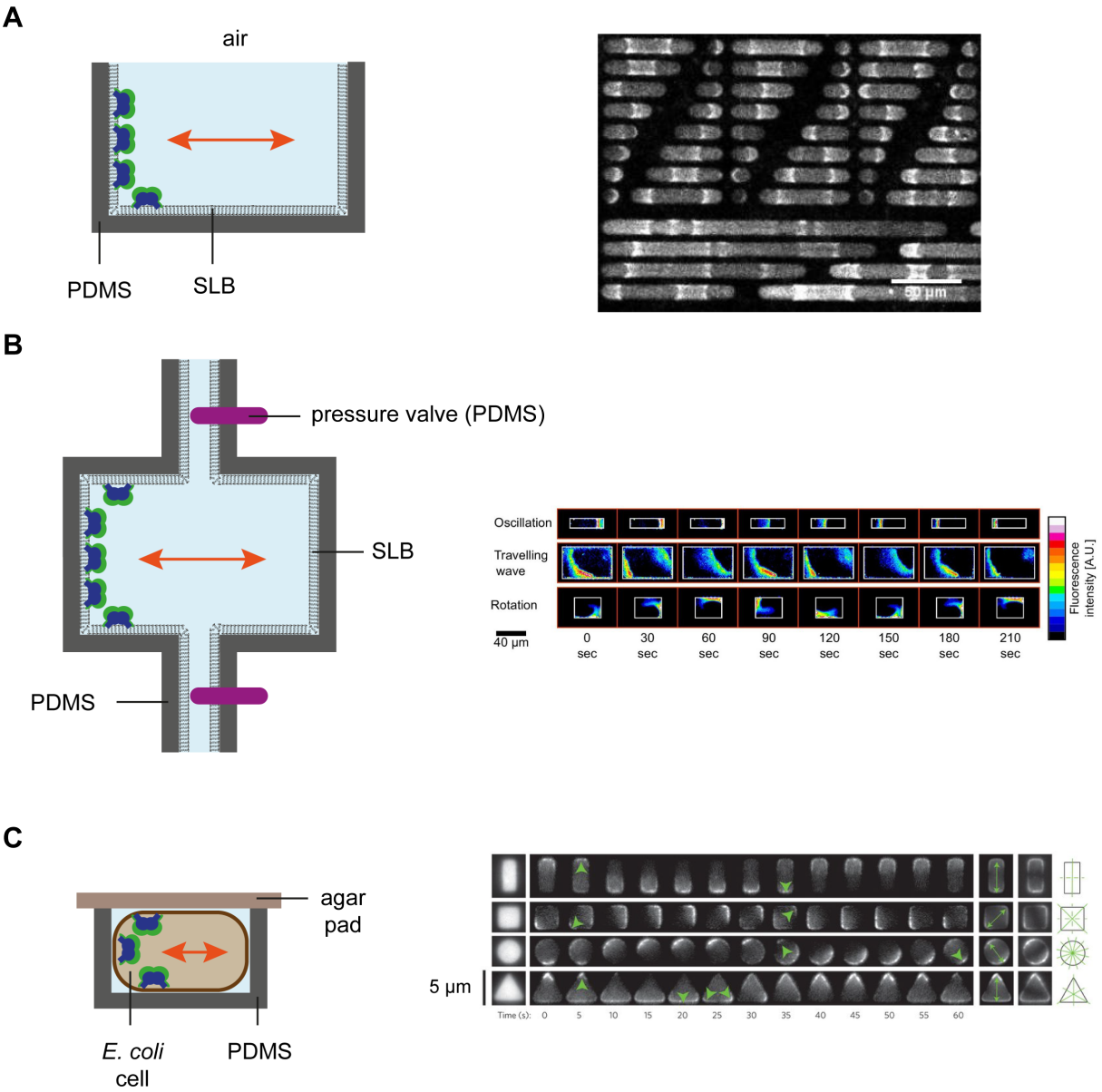

Figure 2.15: Geometric modulation of Min protein oscillations *in vitro* and *in vivo*. Min protein oscillations can be reconstituted in **A)** semi-confined PDMS microchambers, or **B)** pressure-gated microfluidic chambers covered with an SLB on all sides. In both cases, the reconstituted patterns are modulated by chamber length and width, giving rise to a variety of unusual protein dynamics. **C)** Geometric modulation of Min protein dynamics can also be studied *in vivo*, when *E. coli* cells are "sculpted" into pre-defined shapes and cell division and rod-shape maintenance processes are inhibited pharmacologically. The panels on the right are adapted from **A)** (Zieske and Schwille, 2014) under the Creative Commons Attribution (CC BY 4.0) License[8], **B)** (Caspi and Dekker, 2016) under the Creative Commons Attribution (CC BY 4.0) License[8], and **C)** (Wu et al., 2015) by permission from Springer Nature: Nature Nanotechnology[9], (Wu et al., 2015), Copyright 2015.

2.3.5 Mathematical modeling of Min protein self-organization

Since the discovery of Min protein oscillations in *E. coli* (Raskin and de Boer, 1999b), various mathematical models have been developed that recapitulate protein pattern formation (Fange and Elf, 2006; Halatek and Frey, 2012; Howard et al., 2001; Huang et al., 2003; Kruse, 2002; Meinhardt and de Boer, 2001). These models differ in terms of their underlying assumptions, including whether they explicitly consider only membrane-based interactions or also cytosolic processes. The following will focus on the model that forms the theoretical basis for comparison with experimental data within this thesis (section 4.3).

This model is based only on the basic biochemical processes taken to be essential for Min protein pattern formation and is therefore referred to as the "skeleton network" (Figure 2.16) (Denk et al., 2018; Halatek and Frey, 2012; Huang et al., 2003). In the skeleton network, three different types of membrane-related processes can be distinguished, namely 1) *attachment* of MinD to the membrane, 2) *recruitment* of MinD and MinE to already membrane-bound MinD, and finally 3) *detachment* of MinD and MinE from the membrane. Before rebinding to the membrane, MinD exchanges ADP for ATP in the bulk at a finite rate (Figure 2.16). Notably, protein recruitment and detachment generate diffusive fluxes onto and off the membrane respectively. Thus, the membrane and associated protein layer can play the roles of source or sink for proteins, generating local Min protein gradients in the bulk (Frey et al., 2018).

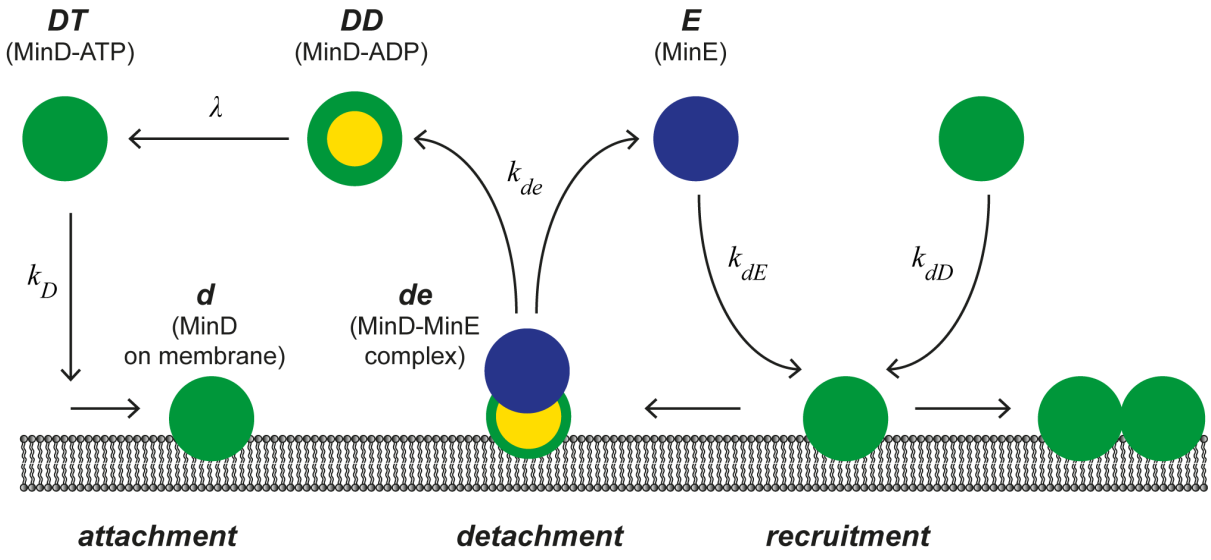

Figure 2.16: Scheme of the "skeleton network". This model is based only on the interactions of MinD, MinE and the lipid membrane assumed to be essential for pattern formation (Halatek and Frey, 2012).

The following reaction-diffusion equations state how the concentrations of MinD and MinE, in different association states, change in time and space, both in the cytosol (eq. 1-3) and on the membrane (eq. 4-5):

$$\partial_t u_{DD} = D_c \nabla_c^2 u_{DD} - \lambda u_{DD} \quad (1)$$
$$\partial_t u_{DT} = D_c \nabla_c^2 u_{DT} + \lambda u_{DD} \quad (2)$$
$$\partial_t u_E = D_c \nabla_c^2 u_E \quad (3)$$

$$\partial_t u_d = D_m \nabla_m^2 u_d + u_{DT}(k_D + k_{dD} u_d) - k_{dE} u_E u_d \quad (4)$$
$$\partial_t u_{de} = D_m \nabla_m^2 u_{de} + k_{dE} u_E u_d - k_{de} u_{de} \quad (5)$$

In these equations, D_c and D_m as well as ∇_c^2 and ∇_m^2 denote the diffusion coefficients of Min proteins as well as operators acting in the cytosol or on the membrane respectively. u_l and u_i correspond to the concentrations of bulk and membrane-bound protein species respectively, as highlighted in Figure 2.16. λ is the rate of nucleotide exchange from ADP to ATP, while k_n denote rate constants for attachment, recruitment and detachment (Figure 2.16). Besides the differential equations above, local particle number conservation is ensured via non-linear reactive boundary conditions stating that the reactions equal the diffusive flux onto and off the membrane (Frey et al., 2018; Halatek and Frey, 2012).

As with other reaction-diffusion systems, the emergence of spatiotemporal patterns depends sensitively on the parameter values in the skeleton model. As several rates in the skeleton network have not yet been measured experimentally, parameter scans are typically performed to analyze under which conditions patterns emerge. In this way, a crucial condition for pattern formation in the skeleton network was revealed, namely that MinE has to be recruited faster to membrane-bound MinD than bulk MinD, while MinD has to be higher in total particle number (Halatek and Frey, 2012).

$$k_{dD} < k_{dE}\,, \quad N_E < N_D \quad (6)$$

Considering the antagonistic roles of MinD and MinE, the above condition enables the spatial separation of membrane zones where either MinD-mediated Min protein recruitment or MinE-mediated detachment dominates. In particular, faster recruitment of MinE allows for a zone, where protein detachment dominates, whereas the higher particle number of MinD

enables a MinE-free zone, allowing recruitment to dominate (Frey et al., 2018; Halatek and Frey, 2012). Min oscillations then arise from an alternating dominance of MinD and MinE.

The skeleton network can reproduce a variety of experimental observations, including the sensitivity of Min patterns to the surrounding geometry (Halatek and Frey, 2012; Wu et al., 2016) and the self-organization of Min proteins into surface waves on flat membranes *in vitro* (Halatek and Frey, 2018). However, it is important to point out that the condition on the relative particle numbers of MinD and MinE (6) is in contrast to *in vitro* experiments, in which patterns have been observed even for MinE/MinD ratios substantially higher than one (Loose et al., 2011a; Loose et al., 2008; Vecchiarelli et al., 2016; Vecchiarelli et al., 2014).

2.4 Aim of this thesis

How are the emergent properties of large-scale patterns determined by the molecular-scale interactions of the underlying components? This intriguing question has inspired both life scientists and physicists to investigate biologically relevant networks and seek principles of self-organization. The *E. coli* Min system is ideally suited toward this end, as it consists of a small number of molecular components, which are relatively well understood on an individual level. Furthermore, experimental assays have been established to systematically investigate Min protein pattern formation (Loose et al., 2008; Zieske and Schwille, 2013). In turn, theoretical models (section 2.3.5) facilitate the interpretation and abstraction of experimental observations. However, despite previous research *in vivo*, *in silico* and to some extent *in vitro*, the molecular determinants of Min protein pattern formation remain poorly understood.

While it is well established that MinD and MinE are necessary and sufficient for pattern formation, it is unclear how specific molecular motifs contribute to self-organization. Although theoretical studies have suggested various parameters that influence Min patterns, the used models were based on different assumptions and conclusions thus varied substantially between them (Bonny et al., 2013; Halatek and Frey, 2012). This motivates a detailed experimental characterization of how Min protein features influence self-organization. Cell-free systems are ideal for this purpose, as they offer controlled and reproducible environments that can be readily manipulated. However, previous studies in this regard were performed under different experimental conditions and with limited parameter variation, which impedes their comparability and has given rise to varying conclusions (Loose et al., 2011a; Vecchiarelli et al., 2016). In short, a systematic analysis on the molecular determinants of Min protein pattern formation is still missing.

This thesis aimed at revealing multi-scale relationships between MinD's and MinE's functional motifs and the emergent properties of Min protein patterns. In particular, it aimed at experimentally determining 1) which features of Min proteins are essential for self-organization, and 2) which essential or non-essential Min protein features serve as modulatory parameters and what exactly their effects are on the characteristics of large-scale Min protein patterns. Addressing these questions also reveals how sensitive the Min system is to molecular changes and, in turn, how robustness may be conferred. Toward these ends, mutant Min proteins were characterized biochemically and their self-organization analyzed by systematic reconstitution on model membranes *in vitro*.

3 Materials and Methods

3.1 Materials

3.1.1 Chemicals and molecular biological reagents

Table 3.1: Chemicals and molecular biological reagents used in this study

Supplier	Material
AppliChem (Darmstadt, Germany)	$CaCl_2$
BD (Franklin Lakes, NJ, USA)	Bacto Agar
Biomol (Hamburg, Germany)	Hepes
BioRad Laboratories (Hercules, CA, USA)	Bradford reagent (Protein Assay Dye Reagent Concentrate), 4x Laemmli sample buffer, Precision Plus Dual Xtra protein standard
Dow Corning (Midland, MI, USA)	PDMS and cross-linking reagent: Sylgard 184 silicon elastomere base and curing agent
Expedeon (San Diego, CA, USA)	InstantBlue Protein Stain
GE Healthcare (Little Chalfont, UK)	Amersham Cy5 mono maleimide
Lumidyne Technologies (New York, NY, USA)	LD650-maleimide
Merck (Darmstadt, Germany)	NaOH, $MgCl_2$, chloroform, ethanol, EDTA, imidazole, β-mercaptoethanol
NEB (Ipswich, MA, USA)	dNTPs, Phusion GC buffer pack
Norland Products (Cranbury, NJ, USA)	Norland Optical Adhesive 63
Roche (Basel, Schweiz)	ATP, cOmplete EDTA-free protease inhibitors
Roth (Karlsruhe, Germany)	HCl, IPTG, KH_2PO_4, K_2HPO_4, KCl, glycerol, tryptone, chloramphenicol
Serva (Heidelberg, Germany)	Kanamycin

Sigma (St. Louis, MO, USA)	DMF, DMSO, NADH, PEP, SDS, ADP, glycerol, glucose, glycine, tetracycline, agarose, ethidium bromide, yeast extract, Trizma Base, acetic acid
Thermo Fisher Scientific (Waltham, MA, USA)	TCEP, GeneRuler 1kb DNA ladder, 6x DNA loading buffer
VWR International (Radnor, PA, USA)	NaCl

3.1.2 Kits and other preparative materials

Table 3.2: Kits and other preparative materials used in this study

Source	**Material**
BioRad Laboratories (Hercules, CA, USA)	Econo-columns, Econo-Pac 10DG desalting columns, Mini-Protean TGX precast 4-20 % or "anykD" protein gels (containing 10 or 12 wells with 50 or 20 µL well volume respectively)
Invitrogen (Carlsbad, CA, USA)	GeneArt Site–Directed Mutagenesis System, GeneArt Seamless Cloning and Assembly Enzyme Mix
Qiagen (Venlo, Niederlande)	QIAprep Spin Miniprep Kit, QIAquick Gel Extraction Kit, Ni-NTA Superflow
Michael Heymann, Frank Siedler, Katja Zieske, Dept. of Cellular and Molecular Biophysics, MPI of Biochemistry (Martinsried, Germany)	Silicon wafers for PDMS microcompartment fabrication

3.1.3 Proteins and lipids

Table 3.3: Commercial proteins and lipids used in this study

Supplier	Material
Avanti Polar Lipids (Alabaster, AL, USA)	*E. coli* polar lipid extract
NEB (Ipswich, MA, USA)	DpnI, Phusion High Fidelity DNA Polymerase
Thermo Fisher Scientific (Waltham, MA, USA)	AccuPrime *Pfx* DNA polymerase, BSA standards
Sigma (St. Louis, MO, USA)	pyruvate kinase / lactate dehydrogenase enzyme mix

3.1.4 Instruments

Table 3.4: Scientific instruments used in this study

Manufacturer	Instrument
Beckman Coulter (Brea, CA, USA)	Centrifuges: Optima MAX-XP and Avanti J-26S XP Rotors: JA-10, JA-25.50, TLA-100
Binder (Tuttlingen, Germany)	Drying and heating chamber: ED53
BioRad Laboratories (Hercules, CA, USA)	SDS-PAGE system
Branson (Danbury, CT, USA)	Sonicator bath 1510
Eppendorf (Hamburg, Germany)	PCR machine: Vapo.protect Mastercycler proS; Centrifuges: 5424 and 5804R, Thermo Mixer C, BioSpectrometer, Research plus pipettes, electroporation system "Eporator" and cuvettes
G. Heinemann Ultraschall- und Labortechnik (Schwäbisch Gmünd, Germany)	Sonifier 250 D
GE Healthcare (Little Chalfont, UK)	Amersham Imager 600

IKA-Werke (Staufen, Germany)	HS 501 digital shaker, Roller 6 digital shaker
Integra Biosciences (Biebertal, Germany)	Pipetboy
Jasco (Hachioji-shi, Tokyo Japan)	V-650 spectrophotometer
Lasos (Jena, Germany)	Argon-Ion laser
Malvern Instruments (Malvern, UK)	Zetasizer Nano
Mettler Toledo (Gießen, Germany)	Scales: PM4800 Deltarange, UMX 2, MS 6002 and XA 205 Dual Range
New Bruinswick Scientific (Edison, NJ, USA)	Incubator shaker: Innova 44
Newport Corporation (Irvine, NJ, USA)	Optical table: Vision IsoStation
PEQLAB (Erlangen, Germany)	Nanodrop 2000, Centrifuge: Perfect Spin Mini
Pfeiffer Vacuum (Asslar, Germany)	Vacuum pump: PK Z40 003
Plasma Technology (Herrenberg, Germany)	Plasma Cleaner: Miniflecto
Sartorius (Göttingen, Germany)	pH meter: PB-11
Scientific Industries (Bohemia, NY, USA)	Vortex-Genie 2
Sharp (Osaka, Japan)	Microwave: Inverter
Tecan (Männedorf, Schweiz)	Plate Reader: infinite M200 Pro
Thermo Fisher Scientific (Waltham, MA, USA)	-80 °C freezer: HeraFreeze HFU T, agarose gel system and imager Ebox VX2
Thinky (Laguna Hills, CA, USA)	Centrifugal Mixer: ARE-250
Vacuubrand (Olching, Germany)	Vacuum pump: RZ6
UVP (Upland, CA, USA)	UV lamp: UVLS-26 EL
Carl Zeiss (Oberkochen, Germany)	Confocal laser scanning microscope: LSM 780, C-Apochromat 40x/1.20 water-immersion objective

3.1.5 Bacterial strains

Table 3.5: Bacterial strains used in this study

Bacterial Strain	Source
E. coli BL21-GOLD(DE3)	Gift from Core Facility, MPI of Biochemistry (Martinsried, Germany)
E. coli XL1-Blue	
E. coli DH5α (One Shot MAX Efficiency DH5α-T1^R competent cells)	Invitrogen (Carlsbad, CA, USA)

3.1.6 Growth media and buffers

Table 3.6: Growth media and buffers used in this study

Buffer	Composition
LB medium	10 g/L tryptone, 5 g/L yeast extract, 5 g/L NaCl; additionally 15 g/L agar for solid medium
TB medium	12 g/L tryptone, 24 g/L yeast extract, 4 mL glycerol, 17 mM KH_2PO_4, 72 mM K_2HPO_4
SOC medium	20 g/L tryptone, 5 g/L yeast extract, 0.5 g/L NaCl, 2.5 mM KCl, 10 mM $MgCl_2$, 20 mM glucose
TAE buffer	40 mM Tris, 20 mM acetic acid, 1 mM EDTA
10x SDS running buffer	250 mM Tris, 1.92 M glycine, 1 % (w/v) SDS
Lysis buffer	50 mM Tris pH 8, 300 mM NaCl, 10 mM imidazole, 10 mM β -mercaptoethanol, cOmplete EDTA-free protease inhibitors; additionally 0.2 mM ADP for MinD purification
Wash buffer	50 mM Tris pH 8, 300 mM NaCl, 20 mM imidazole, 10 mM β-mercaptoethanol, 10 % glycerol
Elution buffer	50 mM Tris pH 8, 300 mM NaCl, 250 mM imidazole, 10 mM β-mercaptoethanol, 10 % glycerol
Storage buffer	50 mM Hepes pH 7.25, 150 mM KCl, 10 % glycerol, 0.1 mM EDTA, 0.2 mM TCEP; additionally 0.2 mM ADP for MinD

SLB buffer	25 mM Tris-HCl pH 7.5, 150 mM KCl
Min buffer	25 mM Tris-HCl pH 7.5, 150 mM KCl, 5 mM $MgCl_2$

3.1.7 Plasmids and oligonucleotides

Plasmids used in this study are summarized in Table 3.7 and have been described previously (Loose et al., 2008; Zieske et al., 2014).

Table 3.7: Plasmids used in this study

Plasmid	Source
pET28a-His-MinD-MinE	Dept. of Cellular and Molecular Biophysics, MPI of Biochemistry (Martinsried, Germany)
pET28a-His-eGFP-MinD	
pET28a-His-MinE	

All oligonucleotides used in this study were synthesized by Eurofins Genomics (Ebersberg) and are summarized in Table 3.8.

Table 3.8: Oligonucleotides used in this study

Oligonucleotide name	Sequence (5'-3')
MinE_K19Q_fwd	ACAGCCAACATTGCACAGGAACGGCTGCAGATT
MinE_K19Q_rev	AATCTGCAGCCGTTCCTGTGCAATGTTGGCTGT
MinE_R21A_fwd	AACATTGCAAAAGAAGCGCTGCAGATTATTGT
MinE_R21A_rev	ACAATAATCTGCAGCGCTTCTTTTGCAATGTT
MinE_L3E_fwd	GGATCCGAATTCGCAGAACTCGATTTCTTTCT
MinE_L3E_rev	AGAAAGAAATCGAGTTCTGCGAATTCGGATCC
MinE_L4E_fwd	TCCGAATTCGCATTAGAAGATTTCTTTCTCTCG
MinE_L4E_rev	CGAGAGAAAGAAATCTTCTAATGCGAATTCGGA
MinE_F6E_fwd	TTCGCATTACTCGATGAATTTCTCTCGCGGAAG
MinE_F6E_rev	CTTCCGCGAGAGAAATTCATCGAGTAATGCGAA
MinE_F7E_fwd	GCATTACTCGATTTCGAACTCTCGCGGAAGAAA
MinE_F7E_rev	TTTCTTCCGCGAGAGTTCGAAATCGAGTAATGC

MinE_Δ(2-12)_fwd_1	CGCGGATCCGAATTCAACACAGCCAACATTGCAAAAGAA
MinE_Δ(2-12)_rev_1	AATGTTGGCTGTGTTGAATTCGGATCCGCGACCCATTTG
MinE_Δ(2-12)_fwd_2	CCGCCTTTGAGTGAGCTGATACCGCTCGCCGCAGCCGAA
MinE_Δ(2-12)_rev_2	CTCACTCAAAGGCGGTAATACGGTTATCCACAGAATCAG
MinE_I24N_fwd	AAGAACGGCTGCAGAACATTGTTGCTGAACGC
MinE_I24N_rev	GCGTTCAGCAACAATGTTCTGCAGCCGTTCTT
MinE_R10G_fwd	GGCTGTGTTTTTCTTCCCCGAGAGAAAGAAATCGA
MinE_R10G_rev	TCGATTTCTTTCTCTCGGGGAAGAAAAACACAGCC
MinE_K11E_fwd	GCAATGTTGGCTGTGTTTTCCTCCCCCGAGAGAAAGAAATC
MinE_K11E_rev	GATTTCTTTCTCTCGGGGGAGGAAAACACAGCCAACATTGC
MinE_K12E_fwd	CAATGTTGGCTGTGTTTTCCTTCCCCGAGAGAAAG
MinE_K12E_rev	CTTTCTCTCGGGGAAGGAAAACACAGCCAACATTG
MinD_L267E_fwd	GGCTTCCTCAAACGCGAATTCGGAGGATAAGTT
MinD_L267E_rev	AACTTATCCTCCGAATTCGCGTTTGAGGAAGCC
eGFP-MinD_L267E_fwd	GGCTTCCTCAAACGCGAATTCGGAGGATAAAAG
eGFP-MinD_L267E_rev	CTTTTATCCTCCGAATTCGCGTTTGAGGAAGCC
MinD_Ins3_fwd	AGAAGAAAGGCTTCCTCGCGAAAATTAAACGCTTGTTCGGAGG
MinD_Ins3_rev	CCTCCGAACAAGCGTTTAATTTTCGCGAGGAAGCCTTTCTTCT

3.2 Methods

3.2.1 Molecular biological methods

3.2.1.1 Generation of MinD and MinE mutant plasmids

Mutations were introduced into pET28a-His-MinE for MinE, pET28a-His-MinD-MinE for MinD and pET28a-His-eGFP-MinD for eGFP-MinD, all of which have been described previously (Loose et al., 2008; Zieske et al., 2014). Note that our His-MinD expression vector (pET28a-His-MinD-MinE) is designed to co-express MinE with His-MinD to counteract the cell division defect conferred by MinD overexpression relative to MinE (de Boer et al., 1989).

Unless otherwise stated, all mutations were introduced using the GeneArt Site–Directed Mutagenesis System (Invitrogen, Carlsbad, CA, USA). The expression plasmid for MinE Δ(2-12) was generated using the GeneArt Seamless Cloning and Assembly Enzyme Mix (Invitrogen, Carlsbad, CA, USA) after prior PCR-based amplification of DNA fragments from pET28a-His-MinE. Plasmids for MinD Ins3, eGFP-MinD Ins3 and MinE C1 (R10G/K11E/K12E) were obtained by PCR-based whole-plasmid amplification with mutagenic primers. For MinE C1, the different mutations were introduced sequentially. All primers are shown in Table 3.8. The presence of the mutations was verified by sequencing (MPI-B sequencing facility).

Plasmids for expression of MinD L267E, eGFP-MinD L267E, MinD Ins3 and eGFP-MinD Ins3 were generated by Andrea Tassinari. Plasmids for expression of MinE C1, MinE L3E/I24N, MinE Δ(2-12)/I24N and MinE L4E/I24N, MinE F6E/I24N, MinE F7E/I24N were generated by Michaela Schaper and Katharina Nakel respectively.

3.2.1.2 PCR

DNA fragments were amplified by polymerase chain reaction (PCR) (Saiki et al., 1988) with Phusion High Fidelity or AccuPrime *Pfx* DNA polymerase. Settings and compositions of PCR reactions were adjusted depending on the used polymerase and DNA fragment of interest. Reactions with Phusion polymerase typically contained 2 U polymerase, 1 mM dNTPs, 2 mM

$MgCl_2$, 50-100 ng of the plasmid template and 0.4 µM forward and reverse primers each in 50 µL total volume of 1x Phusion GC buffer Typically, PCR cycles with Phusion polymerase were performed after initial denaturation for 3 min at 98 °C as follows: 1) Template denaturation for 45 s at 98 °C, 2) Primer annealing for 45 s at a temperature chosen according to the primers' melting temperatures, and 3) extension at 72 °C for 3.5 min. For introducing the R10G mutation into pET28a-His-MinE by whole-plasmid PCR, 18 cycles were performed as above with an annealing temperature of 55 °C. For the remaining whole-plasmid PCRs, 10 cycles were first performed as above with 5 min initial denaturation and annealing temperatures ranging between 50 and 65 °C, but with either the forward or reverse primer in separate reactions. Then, the resulting products were mixed together at equal fractions in 50 µL total volume. After further addition of 1 µL Phusion polymerase (2 U/µL) and incubation for 3 min at 98 °C, 18 more cycles were run as in the first step with 3.5 min and 4 min extension time for MinD and MinE constructs respectively. Whole-plasmid PCRs were followed by digestion of the template DNA with DpnI (15 U) for 1 h at 37 °C and subsequent enzyme deactivation for typically 15 min at 80 °C. For amplifying fragments for the MinE Δ(2-12) expression plasmid, PCRs were performed with AccuPrime polymerase according to the protocol provided by the manufacturer (Invitrogen) with 35 cycles and an annealing temperature of 55 °C. For site-directed mutagenesis with the GeneArt Site–Directed Mutagenesis System, the PCRs were also performed according to the protocol provided by the manufacturer (Invitrogen).

3.2.1.3 Preparation of competent *E. coli* cells

For preparing electrocompetent cells of *E. coli* BL21-GOLD(DE3) or XL1-Blue, cells were grown in 500 mL LB medium containing tetracycline. Upon reaching an OD_{600} of around 0.7, cells were harvested by centrifugation for 15 min at 6000 rpm and 4 °C in a JA-10 rotor. The bacterial pellet was then washed twice by resuspension in 500 mL ice-cold 10 % glycerol and centrifugation for 10 min as above. Finally, cells were resuspended in 10 % glycerol, frozen as 50 µL aliquots in liquid nitrogen and stored at -80 °C. The preparation of competent cells was performed by Beatrix Scheffer.

3.2.1.4 Transformation of competent *E. coli* cells

Transformation of competent cells with plasmid DNA was performed by electroporation or heat shock. In both cases, competent cells were first thawed on ice. For protein expression or plasmid storage, approximately 100 ng plasmid DNA were added to 50 µL electrocompetent *E. coli* BL21-GOLD(DE3) or XL1-Blue cells respectively. Electroporation was then performed at 2500 V, followed by growth in 500 µL SOC medium for 30-60 min at 37 °C while shaking. For constructs resulting from whole-plasmid PCR followed by DpnI digestion, 3 µL of sample were added to 50 µL *E. coli* One Shot MAX Efficiency DH5α-T1^R competent cells. After incubation of the cells on ice for 20 min, heat shock was performed for 1 min at 42 °C. Thereafter, cells were transferred to ice for 2 min and, after addition of 200 µL SOC medium, grown for 1 h at 37 °C while shaking. After transformation, bacteria were plated out on LB plates containing appropriate antibiotics and incubated over night at 37 °C.

3.2.1.5 Agarose gel electrophoresis

DNA fragments were separated according to length by agarose gel electrophoresis (Lee et al., 2012) . For this, DNA samples containing 1x DNA loading buffer were loaded onto gels of 1 % (w/v) agarose in TAE buffer, supplemented with 0.2 µL ethidium bromide per mL of dissolved agarose. A voltage of 120 V was then applied for 45 min and the stained DNA visualized in an Ebox VX2 transilluminator.

3.2.1.6 DNA purification

Plasmid DNA was purified from transformed *E. coli* cultures that were grown over night in 5 mL LB medium supplemented with 50 µg/mL kanamycin (LB-Kan), using the QIAprep Spin Miniprep Kit. DNA fragments separated by agarose gel electrophoresis were extracted and purified with the QIAquick Gel Extraction Kit. DNA concentrations were determined photometrically at 260 nm using a Nanodrop 2000 instrument.

3.2.2 Preparation of model lipid membranes

3.2.2.1 Preparation of SUVs

For preparing small unilamellar vesicles (SUVs) composed of *E. coli* polar lipids, the lipids - stored at –20 °C as 25 mg/mL stocks dissolved in chloroform - were first gently dried in a glass vial with a stream of nitrogen gas followed by the application of vacuum for 30 min. Thereafter, the lipids were resuspended in SLB buffer to a final concentration of 4 mg/mL. The lipids were then incubated at 37 °C for 1 h while vortexing every 20 min to form multilamellar liposomes. Unilamellarity was then achieved by sonication in a sonicator bath until the solution appeared clear, typically around 20 min. The resulting SUVs were then aliquoted and stored as 20 µL aliqiots at –20 °C until further use. Dynamic light scattering using a Zetasizer Nano instrument determined that the average diameter of thawed SUVs was around 70 nm.

3.2.2.2 Preparation of SLBs

Preparation of supported lipid bilayers (SLBs) composed of *E. coli* polar lipids was performed essentially as described previously (Loose et al., 2008). First, a plastic chamber with glass bottom was prepared by gluing a plastic ring on top of a glass cover slide (including a layer of microstructured PDMS in the case of cell-shaped compartments) using Norland Optical Adhesive 63. The glue was cured under a UV lamp at 365 nm for around 10 min. Then, 75 µL SUVs, diluted to 0.5 mg/mL in SLB buffer, were added to the chamber. After additional supplementation with 3 mM $CaCl_2$ to facilitate vesicle rupture, the bilayer was left to form at 37 °C for 20 min. Finally, the SLB was washed ten times with 200 µL SLB buffer to remove non-fused SUVs. The buffer solution was exchanged for Min buffer before self-organization assays.

3.2.3 Protein biochemical techniques

3.2.3.1 Protein expression and purification

Purification of WT or mutant His-MinD, His-eGFP-MinD and His-MinE was carried out essentially as described previously (Loose et al., 2008). Throughout the text, these proteins are referred to simply as MinD, eGFP-MinD and MinE. Sequences of WT Min proteins are shown in section 7.1 within the appendix. Unless otherwise stated, purification steps were performed at 4 °C.

First, *E. coli* BL21-GOLD(DE3) cells were transformed with the respective plasmid and grown in LB-Kan over night at 37 °C and 220 rpm. For storing the strain as a glycerol stock, 200 µL of this culture were added to 5 mL fresh LB-Kan and grown for 4 h at 37 °C and 220 rpm. Then, 500 µL of the bacterial culture were mixed with an equal volume of 100 % glycerol and stored at –80 °C. For protein expression, an overnight bacterial culture, either derived from cells freshly transformed with plasmid or from LB-Kan inoculated with a small sample of the glycerol stock, was added to 800 mL LB-Kan or 500 mL TB-Kan. This expression culture was then grown at 37 °C and 220 rpm until it reached an OD_{600} of around 0.6. Protein expression was then induced by addition of IPTG to a final concentration of 1 mM and the culture grown for another 3-4 h at 220 rpm and 37 °C for MinE and MinD variants, or over night at 16 °C for eGFP-MinD variants. Bacteria were then harvested through centrifugation in a JA-10 rotor for 10 min at 4500 g and 4 °C.

Cell pellets were resuspended in 40 mL lysis buffer and lysed with a tip sonicator (3 min, 30 % amplitude, 30 s pulse on/off each). The lysate was then centrifuged for 45 min at 4 °C and 25000 g in a JA-25.50 rotor to remove any intact cells, membranes or other large debris. Next, the expressed 6xHis-tagged protein was purified using Ni-NTA affinity chromatography (Bornhorst and Falke, 2000). For this, 2 mL Ni-NTA superflow were washed by mixing with 5 mL ddH_2O, pelleting for 3 min at 4 °C and 300 g in an Eppendorf 5804R centrifuge, removing the supernatant, and repeating the procedure once with ddH_2O and twice with lysis buffer. The supernatant of the centrifuged lysate was then added to the washed Ni-NTA superflow and incubated for 1 h while shaking. Thereafter, the suspension was loaded onto a Bio-Rad Econo gravity flow column, which was then washed three times with lysis buffer and wash buffer respectively. Next, the protein was eluted with elution buffer and the peak fractions pooled after qualitative assessment using Bradford reagent. The pooled eluate was

then loaded onto an appropriately equilibrated Bio-Rad 10DG desalting column to exchange the buffer to storage buffer. If aggregation was observed, ultracentrifugation was performed for 30 min at 4 °C and 50000 rpm in a TLA-100 rotor. Purified proteins were stored at –80 °C. Protein concentration and purity were determined with a Bradford assay and SDS-PAGE respectively.
Some MinD and MinE variants were purified by Andrea Tassinari (MinD L267E and Ins3, eGFP-MinD L267E and Ins3) and the MPI-B Core Facility (WT MinD, WT eGFP-MinD, MinD Ins3, WT MinE, MinE K19Q, MinE Δ(2-12)/I24N).

3.2.3.2 Determination of protein concentrations

Protein concentrations were determined photometrically using a Bradford assay (Bradford, 1976). For this, 2 µL of the purified protein or BSA standards of known concentration were mixed with 200 µL 1x Bradford reagent (Bio-Rad). After incubation in a microtiter plate at room temperature for 30 min while shaking, the absorbance at 595 nm was measured using a Tecan infinite M200 Pro plate reader. The concentration of the protein of interest was then estimated based on the BSA standard curve.

3.2.3.3 SDS-PAGE

Sodium dodecyl sulfate polyacrylamide gel electrophoresis (SDS-PAGE) (Laemmli, 1970) was performed using precast Mini-Protean TGX 4-20 % gels, unless noted otherwise. Before loading onto the gels, the protein samples were supplemented with Laemmli sample buffer and denatured at 95 °C for 5 min. For the gels shown in section 7.2, samples were brought to a final concentration of 5 µM in a total volume of 15 µL, including 1x Laemmli sample buffer. For analyzing the protein content in liposome co-sedimentation experiments, the total sample volume for SDS-PAGE was 45 µL, including 1x Laemmli sample buffer. In all cases, 5 µL Bio-Rad Precision Plus Dual Xtra protein standard was used. After loading of samples onto the gel, a voltage of typically 120 V was applied for 60 – 90 min. Gels were then stained with InstantBlue Protein Stain (Expedion) according to the manufacturer's instructions.

3.2.3.4 Protein labeling with chemical dyes

Chemical labeling of MinE at residue C51 was performed with Cy5 mono maleimide or LD650-maleimide following a modified version of the manufacturer's recommended procedure for labeling with Cy dyes (GE Healthcare). First, 0.25 mg of dye were dissolved in anhydrous DMF and added to 500 µL MinE of variable concentration. The labeling reaction was then left to proceed in the dark for 2-3 h at 23 °C while shaking. Thereafter, any aggregates were removed by ultracentrifugation for 30 min at 4 °C and 50000 rpm in a TLA-100 rotor and the labeled protein separated from unbound dye using a Bio-Rad 10DG desalting column. The labeling efficiency (ratio of labeled to total protein) was estimated by absorption spectroscopy using a Jasco V-650 spectrophotometer.

3.2.3.5 ATPase activity assay

MinD's ATPase activity was determined with an ATP/NADH-coupled assay, essentially as described previously (Renner and Weibel, 2012). After ATP hydrolysis, the produced ADP reacts with phosphoenolpyruvate (PEP) to form pyruvate and regenerate ATP in a reaction catalyzed by pyruvate kinase. In a second step, lactate dehydrogenase converts pyruvate to lactate coupled to the oxidation of NADH to NAD^+. Thus, the ATP hydrolysis rate can be determined photometrically by measuring the decrease in NADH absorbance at 340 nm over time. Absorbance measurements were carried out in cuvette format using a Jasco V-650 spectrophotometer. Reactions were performed in a total volume of 150 µL Min buffer with the following components at the specified concentrations: 4 µM MinD, 4 µM MinE, 0.2 mg/mL *E. coli* polar lipid SUVs, 0.5 mM NADH, 2 mM PEP, 24 U/mL pyruvate kinase and 35 U/mL lactate dehydrogenase, 1 mM ATP. The ATP hydrolysis rate in the absence of MinD and MinE was subtracted from the rates observed in the presence of Min proteins.

3.2.3.6 Liposome co-sedimentation assay

Protein binding to lipid vesicles was assessed with a co-sedimentation assay following a modified version of a published protocol (Loose and Mitchison, 2014). First, 5 µM MinD or MinE were incubated with 0.5 mg/mL *E. coli* polar lipid SUVs in Min buffer of 50 µL final volume for 15 min at room temperature. For samples containing MinD, ATP or ADP was also

added to a concentration of 1 mM. After the incubation period, samples were centrifuged for 10 min at 25000 rpm in a TLA-100 rotor to pellet the liposomes. The supernatant was then carefully separated from the pellets, which were subsequently resuspended in Min buffer of the original volume. SDS-PAGE was performed to analyze the protein content in the supernatant and pellet fractions. For determining the percentage of proteins bound to liposomes, band intensities were quantified using FIJI (Schindelin et al., 2012) and the intensity corresponding to the pellet fraction divided by the sum of the intensities for the supernatant and pellet fractions.

3.2.4 Self-organization assays and microscopy

3.2.4.1 Fluorescence microscopy

Confocal fluorescence microscopy was performed with a Zeiss LSM780 laser scanning microscope equipped with a Zeiss C-Apochromat 40x/1.20 water-immersion objective. As in previous studies (Loose et al., 2008), the imaging settings were generally adjusted according to the fluorescence signal available under the given conditions and, therefore, the resulting intensities are not directly comparable in all cases.

3.2.4.2 Image processing and analysis

Image processing and analysis were carried out using the software FIJI (Schindelin et al., 2012). For better visibility of protein patterns in the figures, image brightness and contrast were adjusted. In some cases, when images of widely varying intensity were adjusted equally, micrographs can be displayed outside the dynamic range. Any adjustments were always made after intensity measurements and applied homogeneously for an entire image field or stack.

3.2.4.3 Self-organization assay on flat membranes

Self-organization assays on flat membranes were carried out essentially as described previously (Loose, 2008). First, SLBs composed of *E. coli* polar lipids were prepared on glass, as described in section 3.2.2.2. Then, labeled and unlabeled MinD and MinE of the concentration indicated in the respective figure captions were added in the presence of 2.5 mM ATP into a final volume of 200 µL Min buffer above the SLBs. The reactions were then incubated for up to several hours, allowing ample time for pattern formation.
The outcome of self-organization was analyzed with confocal fluorescence microscopy. For determining the wavelength of Min protein waves, the distance between two wave fronts was measured using FIJI (Schindelin et al., 2012). The wave velocity was determined by recording a time-series and multiplying the frame interval with the number of frames it took a wave front to traverse a distance of specified length. Unless noted otherwise, plotted intensity profiles were individually normalized to a 0-1 range.

3.2.4.4 Self-organization assay in PDMS microcompartments

Self-organization assays in PDMS microcompartments were performed essentially as described previously (Zieske and Schwille, 2013). PDMS chips containing multiple microcompartments were fabricated using a microstructured silicon wafer that served as a template for compartments of defined geometry. Wafers used in this study were designed with AutoCAD and generated using photolithographic techniques (Zieske and Schwille, 2015), which was performed by Katja Zieske or Michael Heymann and Frank Siedler (MPI of Biochemistry).

For microstructure fabrication, PDMS and cross-linking reagent were first mixed at a ratio of 9:1. A small drop of this mixture was then transferred to the template section of the wafer. Immediately thereafter, a glass cover slide was carefully pressed on top, such that the PDMS spread out between the cover slide and the wafer. After curing the PDMS for 3 h at 80 °C, the cover slide, now containing microstructured PDMS, was delicately removed from the wafer with a razor blade. Care was taken not to damage the wafer at any step in the process.

An *E. coli* polar lipid SLB was then formed on plasma cleaned, microstructured PDMS and a self-organization assay started, as described in section 3.2.4.3. Next, Min proteins were trapped inside the compartments by carefully aspirating the buffer reservoir above the chambers, resulting in geometry-modulated Min protein dynamics. Typically, buffer aspiration was carried out once Min proteins had self-organized into surface waves on the SLB. However, in some cases (e.g. for MinE K19Q at 1 μM), buffer aspiration still resulted in Min protein dynamics within the compartments under conditions for which pattern formation was not observed before aspiration. Note that the protein concentrations stated in the text generally refer to the concentrations before buffer aspiration and that, upon aspiration, the resulting concentrations in the compartments are expected to be slightly increased due to prior accumulation of Min proteins on the membrane. Note also, that, when the bottom planes of the compartments were imaged, the dimensions appear slightly smaller than on the top plane due to the compartments' curved walls.

The periodicity of Min oscillations was obtained from kymographs by determining the time interval between the respectively first appearance of two temporally sequential MinD caps at the same pole.

4 Results and discussion

4.1 Modulation of Min protein patterns by MinE's stimulation of MinD's ATPase activity

This section focuses on how Min protein patterns are regulated by MinE's stimulation of MinD's ATPase activity, from here on also referred to as "MinE activity", and by MinE concentration. Parts of the results herein have been published (Kretschmer et al., 2018)[10] and section 4.1.1 as well as portions of section 4.1.3 are thus adapted from, and in part identical to, the manuscript listed below. Section 4.1.2 contains additional, unpublished results.

Reverse and forward engineering of protein pattern formation
Simon Kretschmer, Leon Harrington, and Petra Schwille (2018)
Philosophical Transactions of the Royal Society B *373*: 20170104.
http://dx.doi.org/10.1098/rstb.2017.0104

4.1.1 Modulation of Min protein patterns by MinE activity and concentration

It is generally established that MinE's stimulation of MinD's ATPase rate is a key step for Min protein pattern formation (Hu and Lutkenhaus, 2001). Furthermore, the wavelength and velocity of Min waves were shown to depend on the MinE/MinD concentration ratio (Loose et al., 2008; Vecchiarelli et al., 2016; Vecchiarelli et al., 2014). However, it is unknown how exactly Min protein patterns are affected if the level of ATPase stimulation is decreased.
MinE interacts with MinD via a contact helix formed by residues 13 to 26 (Figure 4.1 A) (Park et al., 2011). Several residues, including K19 and the highly conserved R21, form hydrogen bonds with MinD (Figure 4.1 B) and mutations in these residues can compromise the MinD–MinE interaction (Hu and Lutkenhaus, 2001; Park et al., 2011; Park et al., 2012). To dissect the effects of reduced MinD ATPase stimulation by MinE, we investigated pattern formation by two mutant proteins, MinE K19Q and MinE R21A, that have been shown to be

impaired in MinD ATPase stimulation (Hu and Lutkenhaus, 2001; Park et al., 2012). While MinE R21A was incapable of significant ATPase stimulation, MinE K19Q was reported to stimulate MinD's ATPase rate, albeit at lower levels than the wild-type (WT) (Hu and Lutkenhaus, 2001; Park et al., 2012).

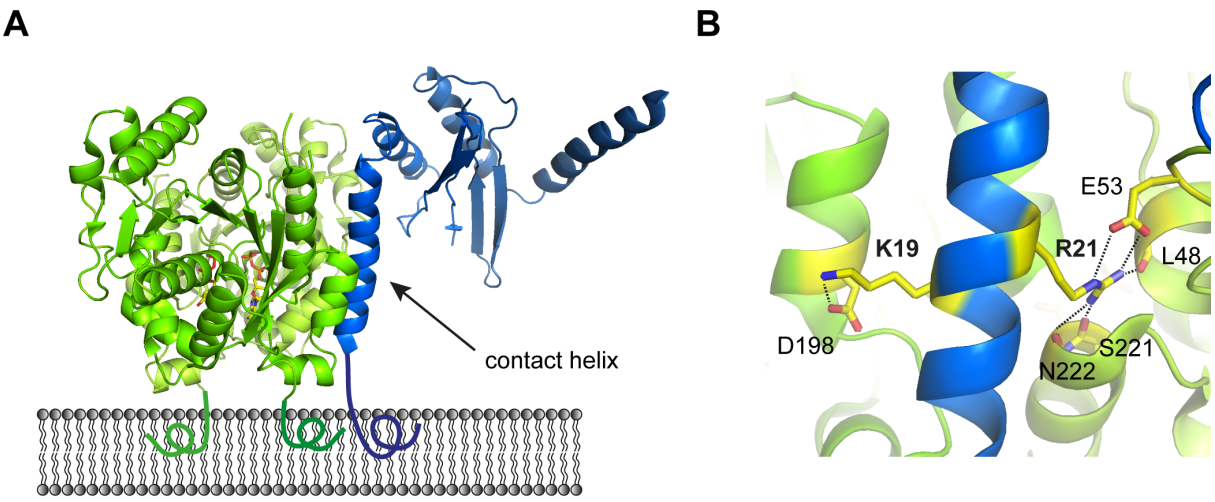

Figure 4.1: Structural aspects of the MinD-MinE interface. A) Crystal structure of the MinD-MinE complex in its presumed membrane-associated state with MinD in green and MinE in blue (PDB: 3R9J), based on (Park et al., 2011). **B)** Residues K19 and R21 in MinE's contact helix interact with MinD via hydrogen bonds, depicted as dashed lines.

We confirmed the effects of these mutations by assaying MinD's ATPase activity in the presence of MinE and liposomes (Figure 4.2 A). We then reconstituted MinE WT or mutant proteins together with MinD on flat SLBs (Figure 4.2 B) and investigated pattern formation by confocal microscopy (Figure 4.2 C).

At low MinE/MinD ratios, where WT MinE supported Min protein self-organization, both MinE K19Q and R21A were incapable of symmetry breaking and pattern formation (Figure 4.2 C). Instead, MinD homogeneously covered the membrane in a protein "carpet", similar to when MinE is absent in the assay (Loose et al., 2008). We then tested whether pattern formation could be rescued at higher MinE mutant levels by increasing the MinE concentration while keeping MinD constant at 1 µM (Figure 4.2 C). MinE R21A was unable to generate Min protein patterns even at high MinE/MinD ratios, consistent with its reported inability to stimulate MinD's enzymatic activity even at elevated concentrations (Park et al., 2012). This confirms that MinD ATPase stimulation by MinE is an essential requirement for pattern formation and explains the high conservation of the R21 residue (Park et al., 2012). In contrast to MinE R21A, Min protein patterns emerged at elevated concentrations of MinE

K19Q (Figure 4.2 C), consistent with the reported rescue of WT-like ATPase stimulation at higher mutant concentrations (Hu and Lutkenhaus, 2001). Strikingly, while the mutant protein patterns required a higher MinE/MinD ratio, they also tolerated a higher excess of MinE relative to MinD. This emergence of Min protein patterns in a limited concentration range can be understood by considering MinE's functional role of antagonizing MinD accumulation on the membrane. When MinE's activity or concentration is too low, MinE's antagonism toward MinD is too weak to allow symmetry breaking, which results in a homogeneous distribution of MinD on the membrane. In turn, if MinE's antagonistic activity is too strong, MinD cannot accumulate effectively on the bilayer, resulting in uniform depletion of MinD from the membrane.

Finally, we compared the wavelength and velocity of the wave patterns formed by WT MinE and MinE K19Q (Figure 4.2 D, E). At relatively low MinE concentrations, the K19Q mutant displayed a significantly higher wavelength and lower velocity than WT MinE (Figure 4.2 D, E), consistent with a slower oscillation period observed for this mutant *in vivo* (Hu and Lutkenhaus, 2001). With increasing MinE concentration, the wavelength decreased and the velocity increased for both proteins (Figure 4.2 D, E), in agreement with earlier studies of WT MinE (Loose et al., 2008). In this way, the wave properties displayed by WT MinE at low concentrations could be rescued by elevating the mutant's concentration. While the K19Q mutant stimulated MinD's ATPase activity to around 50 % of the WT's level at the tested concentrations (Figure 4.2 A), the mutant concentration had to be increased by roughly one order of magnitude to rescue the behaviour observed with lower concentrations of WT MinE on SLBs (Figure 4.2 C-E). This can be explained with the observation that MinE's stimulation of MinD's ATPase activity follows a higher-order concentration dependency (Vecchiarelli et al., 2016).

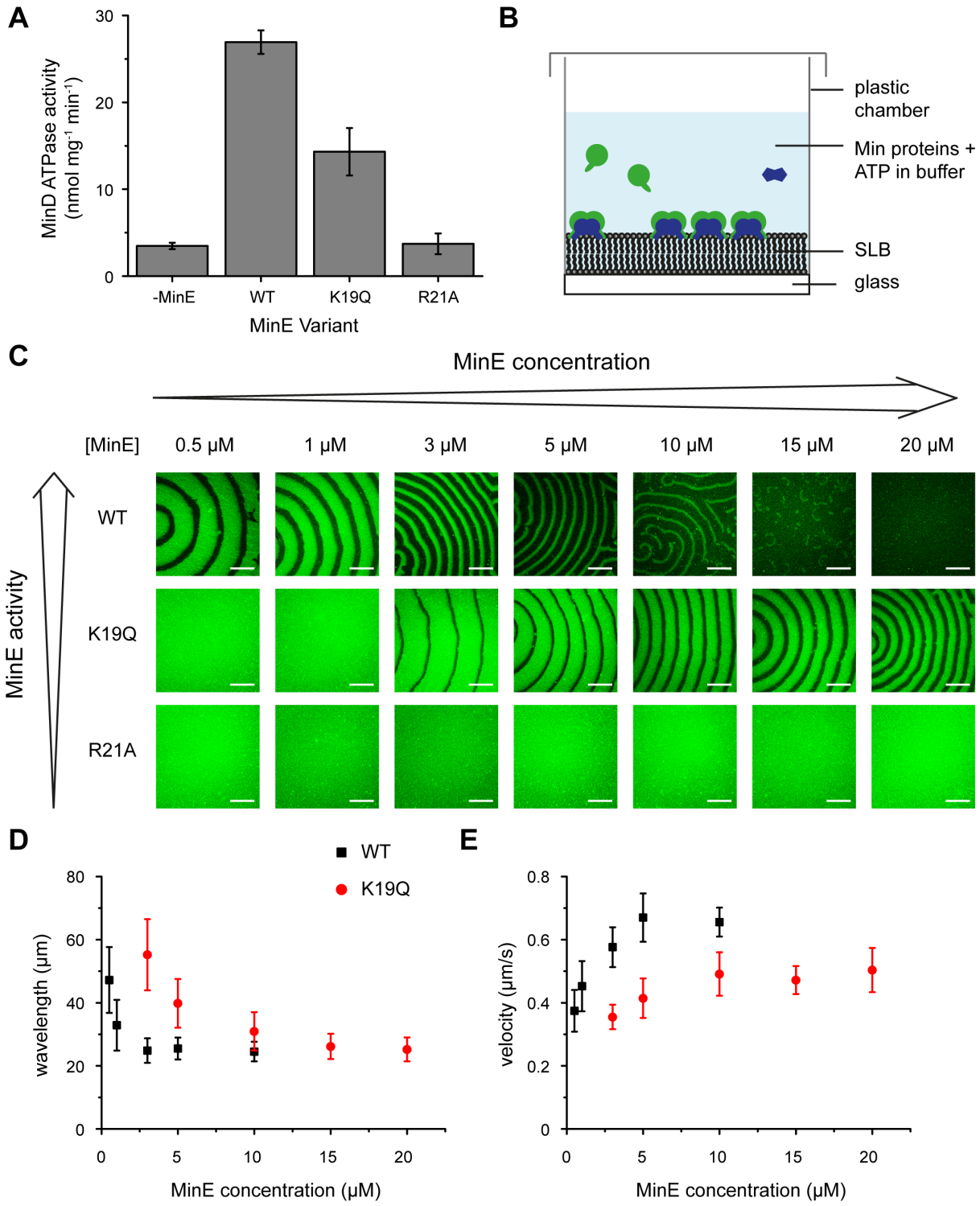

Figure 4.2: Modulation of large-scale Min protein patterns on flat membranes by MinE activity and concentration. A) ATPase stimulation assay with WT MinE and MinE K19Q and R21A using 4 µM MinD, 4 µM MinE and 0.2 mg/mL small unilamellar vesicles made of *E. coli* polar lipids. Error bars represent standard deviations (N=3). **B)** Schematic of the self-organization assay on flat supported lipid bilayers. **C)** Confocal images of the self-organization assay at different MinE concentrations with MinD constant at 1 µM with 20 % eGFP-MinD. Scale Bar: 50 µm. Dependence of the mean **D)** wavelength and **E)** velocity of WT and K19Q waves on MinE concentration (MinD at 1 µM). Error bars represent standard deviations (N ≥ 7 waves from three independent experiments).

4.1.2 Additional results

4.1.2.1 Wave profiles for a MinE mutant impaired in MinD ATPase stimulation

Besides characterizing the concentration range and spatiotemporal properties of the patterns emerging for a MinE mutant (MinE K19Q) with reduced capacity to stimulate MinD's ATPase activity, we also investigated the protein distribution within the mutant waves. In particular, we tested if the MinE mutant could still accumulate at the rear of Min waves. For this, labeled MinD and labeled WT or mutant MinE were co-reconstituted on flat membranes to analyze the MinD and MinE profiles of the resulting waves (Figure 4.3).

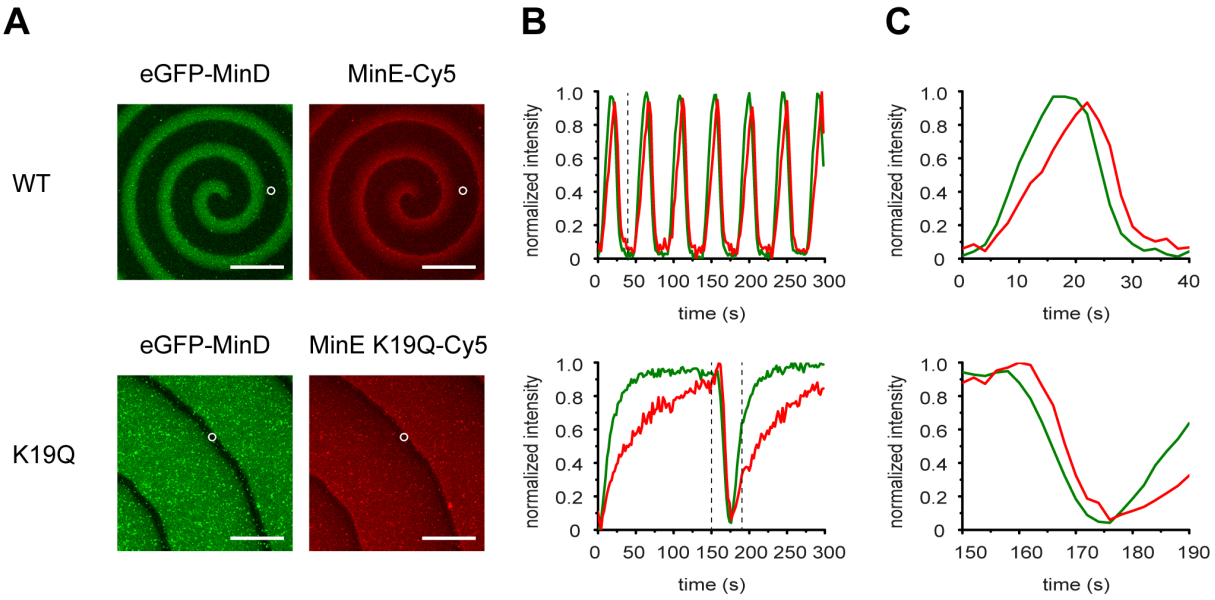

Figure 4.3: Wave profile for a MinE mutant with reduced capacity to stimulate MinD's ATPase activity. **A)** Fluorescence micrographs, and **B)** normalized temporal wave profiles measured in the area indicated in the micrographs for 5 min, and **C)** an excerpt of 40 s highlighting the shift of the MinD and MinE curves, are shown for WT MinE and MinE K19Q. Protein concentrations: 1 µM MinD incl. 20 % eGFP-MinD and 3 µM WT or mutant MinE incl. 10 % WT or mutant MinE-Cy5. Scale Bar: 50 µm.

Our analysis showed that, although different in their temporal scales, the profiles of the WT and K19Q mutant waves were similar on a qualitative level. In particular, the intensity of both MinE variants increased toward a peak at the wave's rear, in contrast to the MinD profiles, which exhibited a more plateau-like shape. Furthermore, MinE's subsequent decrease in intensity lagged behind that of MinD (Figure 4.3). Thus, the characteristic features of MinE's wave profile were retained when the degree of MinD ATPase stimulation was decreased.

4.1.2.2 Modulation of Min oscillations in cell-shaped microcompartments by MinE activity and concentration

The observed modulation of Min patterns on flat membranes by MinE activity and concentration (section 4.1.1) suggests that these two parameters may also regulate Min oscillations in cell-like geometry. Previous *in vivo* experiments, in which MinE was overexpressed with respect to MinD showed that the oscillation period decreases with increasing MinE concentration (Hale et al., 2001). In turn, reducing MinE's capacity to stimulate MinD's ATPase rate with the K19Q mutation resulted in a longer oscillation period *in vivo* (Hu and Lutkenhaus, 2001). Combined, these two studies indicate that the Min oscillation period in cellular geometry decreases with MinE concentration and activity. However, the underlying data cannot be compared directly between the two studies because varying both parameters resulted in different cell morphologies, which also affects the oscillation period (Bonny et al., 2013; Fu et al., 2001). Furthermore, it has remained unknown how exactly MinE activity and concentration complement each other in setting the oscillation period. For instance, it was interesting to test if a reduction in activity can be compensated by an increase in concentration, as we observed on flat membranes (section 4.1.1). Therefore, to systematically investigate how MinE concentration and activity act together in determining the Min oscillation period, we reconstituted MinD at a fixed concentration together with WT MinE or MinE K19Q of varying concentration in cell-shaped microcompartments (Figure 4.4 A, B).

In our reconstitution experiments, both MinE variants showed oscillation-type dynamics at MinE/MinD ratios of 1, 3 and 10 (Figure 4.4 B). At 1 µM MinE K19Q, the dynamics only occurred in a small number of compartments and did not qualitatively resemble the characteristic oscillations, as observed in kymographs along the compartment length (Figure 4.4 B). Instead, MinD was mostly homogeneously distributed, consistent with the absence of wave patterns on flat membranes at this concentration (section 4.1.1), and only transiently depleted at one of the two poles (Figure 4.4 B). However, as this pattern appeared to have some regularity, we treated it as an oscillation and measured its periodicity. At higher mutant concentrations, the dynamics were characterized by more typical oscillation-type kymographs (Figure 4.4 B).

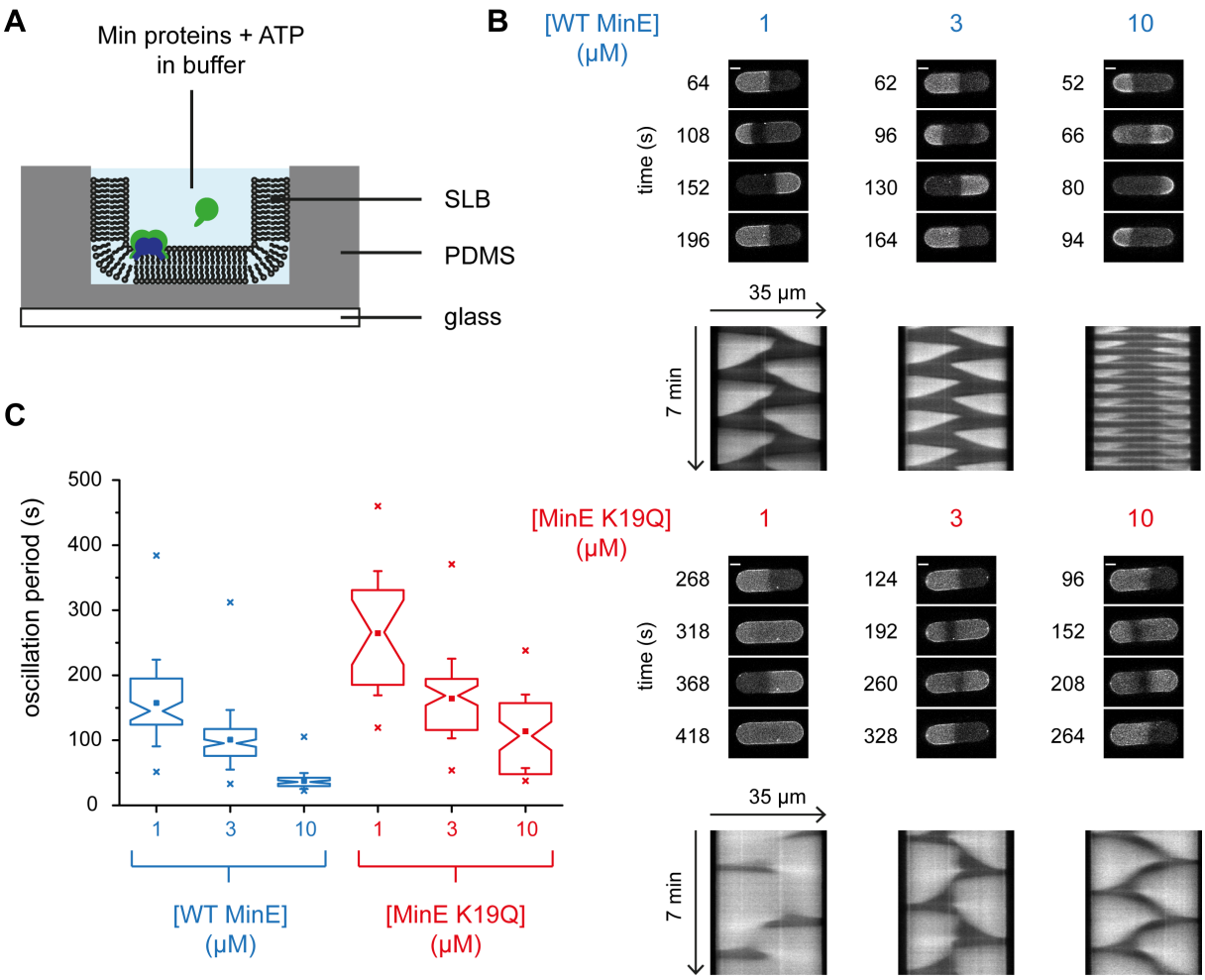

Figure 4.4: Modulation of the Min oscillation period by MinE activity and concentration. A) Schematic of the self-organization assay using volume-limited PDMS microcompartments to mimic the rod-like shape of *E. coli* cells. **B)** Examples of time-lapse images for one oscillation cycle and kymographs along the compartment length for varying concentrations of WT MinE or MinE K19Q with MinD at 1 µM incl. 20 % eGFP-MinD. The compartments were around 35 µm long, 10 µm wide and 10 µm deep. Scale Bar: 5 µm. **C)** Box plot showing 95 % confidence interval notches of the median oscillation period for different concentrations of WT MinE and MinE K19Q. Boxes, filled squares, whiskers, and crosses indicate the interquartile range, mean, one standard deviation and maximum/minimum values respectively. The narrowest point of the box corresponds to the median. If notches of two boxes do not overlap, their medians can be viewed as different with 95 % confidence (McGill et al., 1978). N = 63, 133, 61 compartments for 1, 3, 10 µM WT MinE and 21, 68, 62 compartments for 1, 3, 10 µM MinE K19Q respectively, from three independent experiments.

In our reconstituted system, the detailed characteristics of the oscillations varied between compartments even under the same conditions, which also resulted in a relatively broad distribution of oscillation periods (Figure 4.4 C). This could be due to two processes that are difficult to control in the reconstitution protocol (Zieske and Schwille, 2013). First, variable amounts of protein may be encapsulated upon aspiration of the buffer. Second, as previously

noted (Zieske and Schwille, 2014), buffer evaporation increases the oscillation period during the experiment, and the levels of evaporation are likely different between compartments.

Despite the broad distribution of oscillation periods for a given concentration, we observed a decrease in the median oscillation period when increasing the concentration of both WT MinE and MinE K19Q (Figure 4.4 C), consistent with *in vivo* observations (Hale et al., 2001). Furthermore, at low concentrations, the median oscillation period was higher for MinE K19Q compared to the WT, as observed *in vivo* (Hu and Lutkenhaus, 2001). Strikingly, increasing the mutant concentration resulted in a median oscillation period resembling the one observed for the WT at lower concentrations (Figure 4.4 C), showing a similar rescue effect as observed on flat membranes (section 4.1.1).

Lastly, it is interesting to note that for the WT, not only the oscillation period but also the type of dynamic behavior appeared sensitive to concentration. Although in general, different dynamics could sometimes be observed transiently or unsystematically, we reproducibly observed that, at 10 µM MinE, pole-to-pole oscillations (Figure 4.4) and traveling waves (Figure 4.5) appeared to co-exist at approximately equal fractions. Furthermore, these two modes frequently switched between each other within the same compartment (Figure 4.5). Although motivating a more detailed characterization at various concentrations, this observation already indicates that Min protein concentrations modulate the system's dynamic behavior in cell-like geometry *in vitro*.

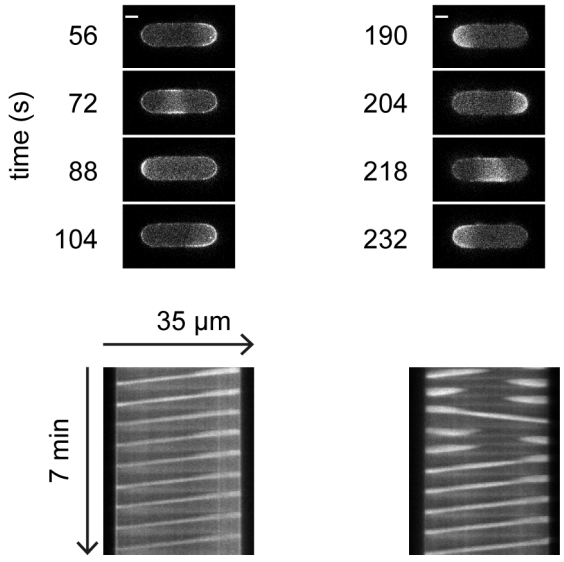

Figure 4.5: Traveling wave dynamics co-exist with pole-to-pole oscillations at elevated concentrations of WT MinE. Examples of traveling wave dynamics alone (left) or in combination (right) with pole-to-pole oscillations, at 10 µM WT MinE and 1 µM MinD incl. 20 % eGFP-MinD. Compartment dimensions as in Figure 4.4. Scale Bar: 5 µm.

4.1.3 Discussion

In this section, we dissected the effects of reduced MinD ATPase stimulation by MinE on reconstituted Min protein patterns. For this, we analyzed MinE mutants that had previously been reported to be impaired in this process. Reconstitution experiments on flat lipid bilayers demonstrated that MinD ATPase stimulation by MinE is strictly required for pattern formation. Furthermore, a MinE mutant with reduced activity required higher concentrations to form patterns. Moreover, while the mutant retained the capacity to accumulate at the rear of Min waves, their wavelength and velocity on flat membranes as well as the periodicity of Min oscillations in cell-shaped microcompartments were altered compared to WT patterns at low MinE concentrations. Strikingly, an increase in mutant concentration compensated for the reduced activity and rescued the behavior observed for the WT at low concentration, consistent with the concentration-dependent rescue of WT-like ATPase stimulation previously reported for the mutant (Hu and Lutkenhaus, 2001). Thus, MinE activity and concentration regulate the spatial and temporal properties of Min protein patterns in a complementary fashion.

Hypothetically, the combined regulation of Min protein dynamics by MinE activity and concentration could also modulate the Min system *in vivo*. For example, during evolution, mutations changing MinE's activity may broadly alter the Min system's behavior, e.g. by allowing for pattern formation under different cellular conditions. On the other hand, more subtle changes in expression may fine-tune the characteristics of Min protein patterns.

Interestingly, in cell-shaped microcompartments, a co-existence of pole-to-pole oscillations and traveling waves was observed at elevated concentrations of WT MinE. Notably, traveling waves have previously been observed *in vivo* within elongated cells, when both MinD and MinE were overexpressed (Bonny et al., 2013; Sliusarenko et al., 2011). Furthermore, the co-occurrence and switching of different dynamic modes under the same conditions is known as "multistability" and has been observed *in vivo* and predicted theoretically (Amiranashvili et al., 2016; Wu et al., 2016). Additionally, stochastic simulations have suggested a dependence of the Min system's multistable behavior on Min protein concentrations, a behavior termed "concentration sensing" (Amiranashvili et al., 2016). In the future, it would be interesting to further investigate this phenomenon experimentally and e.g. determine the relative fractions of different dynamics at varying absolute and relative MinD and MinE concentrations, ideally in combination with other factors including mutations and compartment geometry.

Lastly, in the context of synthetic biology, our characterization here serves as a guide for externally controlling Min protein pattern formation *in situ* by reversibly changing MinE's activity or effective concentration. In particular, by shifting MinE's activity or effective concentration beyond the thresholds compatible with Min protein patterns, their assembly or disassembly can be reversibly controlled. Recently, this concept has successfully been implemented by optically controlling the interaction of a photoswitchable MinE peptide with MinD (Glock et al., 2018).

4.2 Modulation of Min protein patterns by MinE's membrane affinity

This section focuses on how Min protein patterns are influenced by MinE's interaction with the lipid bilayer via its N-terminal membrane targeting sequence (MTS). Parts of the results herein have been published (Kretschmer et al., 2017)[11] and section 4.2.1 as well as portions of section 4.2.3 are thus adapted from, and in part identical to, the manuscript listed below. Supporting information for section 4.2.1 is shown in section 7.3 within the appendix. Section 4.2.2 contains additional, unpublished results.

Large-scale modulation of reconstituted Min protein patterns and gradients by defined mutations in MinE's membrane targeting sequence
Simon Kretschmer, Katja Zieske, and Petra Schwille (2017)
PLoS ONE *12(6)*: e0179582, https://doi.org/10.1371/journal.pone.0179582

4.2.1 Large-scale modulation of reconstituted Min protein patterns and gradients by defined mutations in MinE's membrane targeting sequence

Despite previous studies on MinE's MTS, its precise role in pattern and gradient formation has remained ambiguous. While it was suggested theoretically that MinE membrane interaction is important for robust pattern formation (Bonny et al., 2013; Schweizer et al., 2012), many mathematical models display regular Min protein dynamics even in its absence (Amiranashvili et al., 2016; Halatek and Frey, 2012; Huang et al., 2003). On the other hand, *in vivo* experiments showed that mutations in MinE's MTS are associated with severe cell division defects (Park et al., 2011). Furthermore, previous *in vitro* data suggested that mutations lead to either disordered patterns or traveling waves with altered characteristics on flat membranes, dependent on the mutation (Loose et al., 2011a; Vecchiarelli et al., 2016). Additionally, it was recently observed that pole-to-pole oscillations in cell-shaped microcompartments are compromised upon a deletion in MinE's MTS (Zieske and Schwille, 2014). While these experimental studies indicate an important role of MinE's MTS, its precise role is still unclear due to the discrepancy of theoretical predictions and the range of apparently contradictory effects described *in vitro*. Thus, important questions remain: Is MinE

membrane interaction indispensable for pattern and gradient formation or does it serve a modulatory role? If regular pole-to-pole oscillations are compromised, which other modes may emerge in cell-like geometry and how do they affect functional gradient formation? Finally, how stable is the Min-based positioning system against biochemical variations, i.e. can relatively simple biochemical changes like single mutations result in a large-scale remodeling of the Min oscillator, and if so, how?

Previous conclusions on the role of MinE's MTS in pattern and gradient formation were based on *in vitro* experiments with only one mutant at a particular concentration in a given geometric setup that was different in each case (Loose et al., 2011a; Vecchiarelli et al., 2016; Zieske and Schwille, 2014). However, emergent behaviors in reaction-diffusion systems are generally sensitive to changes in parameter values and typically depend on the interplay of various factors. Thus, the different results regarding MinE membrane interaction are hard to compare and general conclusions difficult to draw. Therefore, here, we investigate MinE's membrane interaction while systematically and comprehensively exploring variations in protein sequence, concentration and assay geometry, with regard to pattern and gradient formation.

4.2.1.1 MinE membrane interaction shifts the lower limit of the concentration-dependent length scale of Min protein patterns

Membrane interaction of MinE has been suggested to be mediated both by conserved hydrophobic residues (L3, L4, F6, F7, L8), which are inserted into the core of the lipid bilayer, as well as a cluster of cationic residues (R10, K11, K12), apparently interacting electrostatically with anionic lipid head groups (Hsieh et al., 2010; Park et al., 2011; Shih et al., 2011). While an initial reconstitution study of a mutant with impaired electrostatic interactions (MinE R10G/K11E/K12E) appeared unable to self-organize into planar surface waves (Loose et al., 2011a), a mutant that lacked hydrophobic residues but left some of the cationic residues intact ($MinE^{11-88}$) formed surface waves (Vecchiarelli et al., 2016). This discrepancy still left doubts whether or not MinE membrane interaction was required for wave formation. Therefore, we engineered a MinE mutant lacking the entire MTS (MinE Δ(2-12)) and thus, being impaired in both hydrophobic and electrostatic interactions.

Strikingly, MinE Δ(2-12) still supported self-organization into regular spiral and traveling waves, when reconstituted with MinD and ATP on a supported lipid bilayer (SLB) (Figure

4.6 A). This demonstrates that MinE membrane interaction is dispensable for pattern formation *per se*, consistent with mathematical models that do not require the incorporation of MinE membrane interaction (Halatek and Frey, 2012, 2014).

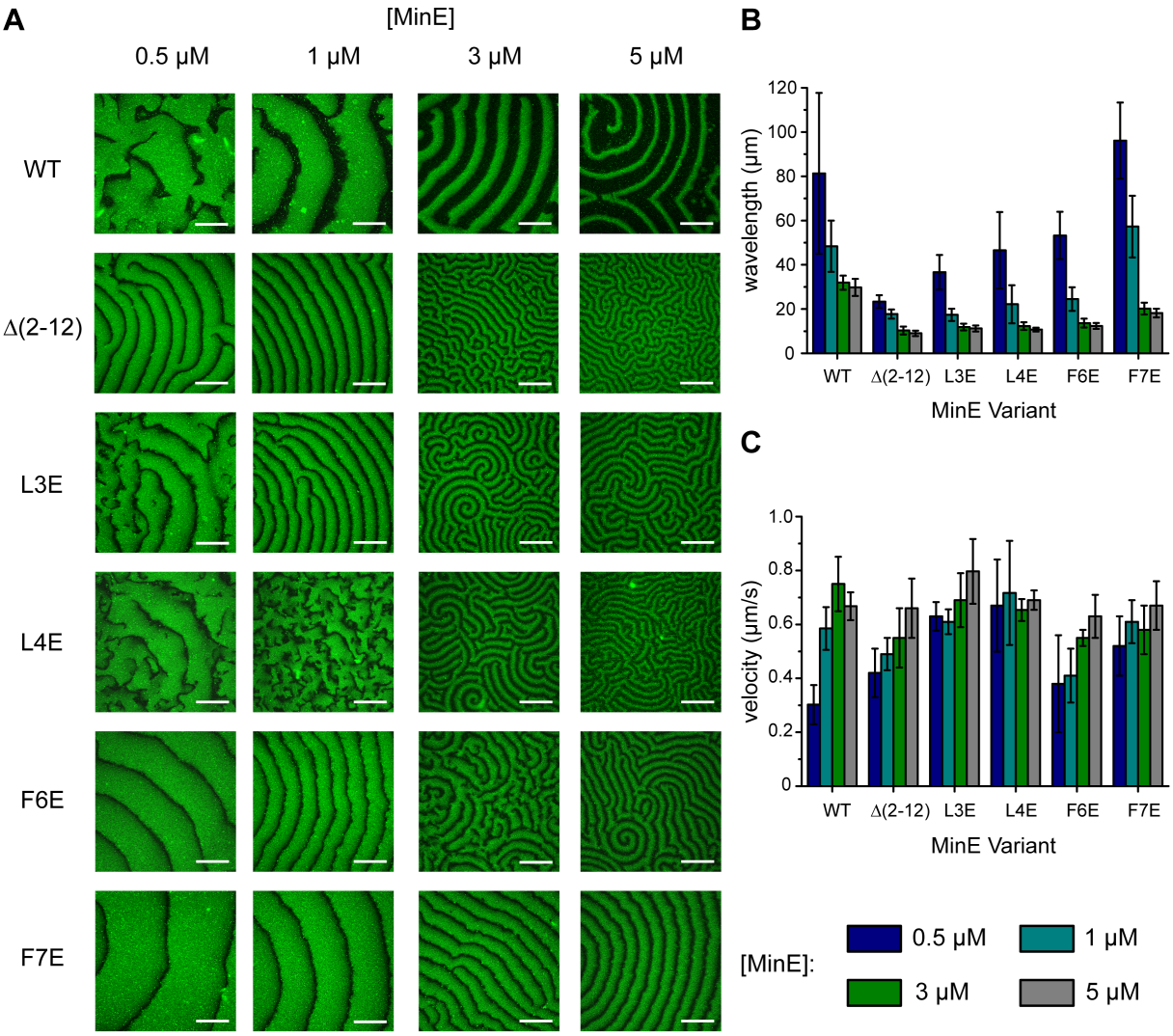

Figure 4.6: Truncation or mutation of MinE's membrane targeting sequence decreases the lower limit of the length scale of Min protein patterns. A) Confocal images of self-organized WT and Δ(2-12), L3E, L4E, F6E, F7E mutant waves on flat membranes. WT MinE and mutant proteins were titrated from 0.5 to 5 µM (MinD at 1 µM with 20 % eGFP-MinD). Scale Bar: 50 µm. Dependence of the mean **B)** wavelength and **C)** velocity of WT and mutant waves on MinE concentration (MinD at 1 µM). Error bars represent standard deviation ($N \geq 3$) from at least three independent experiments.

Remarkably, we observed a reduced length scale of wave patterns for MinE Δ(2-12) compared to WT MinE (Figure 4.6 A, B). A similar effect has been reported for MinE$^{11\text{-}88}$ in an SLB-coated flow cell (Vecchiarelli et al., 2016). However, the severity of the reported change was still unclear, as the wavelength of Min patterns is known to also depend on the

MinE/MinD ratio (Loose et al., 2008). Therefore, we systematically varied the MinE/MinD ratio and measured the wavelength of the truncation mutant. With this approach, we determined that the wavelength of MinE Δ(2-12) could be reduced to as low as roughly 10 µm, compared to around 30 µm for the WT (Figure 4.6 A, B). On the other hand, the velocity of the mutant waves saturated on a similar level compared to WT MinE. Vecchiarelli et al. reported an increased wave velocity for $MinE^{11-88}$ compared to WT MinE at one tested concentration in their flow-cell setup (Vecchiarelli et al., 2016). These results are not directly comparable due to potential effects of flow as well as the unknown local concentrations within the flow cell that give rise to the patterns. However, despite these differences, the reported mutant velocity is in the same range as the maximum velocity for all of our mutant proteins, suggesting a general agreement. In summary, impairing MinE membrane interaction via truncation strongly reduced the lower limit of the concentration-dependent wavelength, allowing Min protein waves to assume small length scales impossible to obtain with the WT even at increased MinE concentrations (Figure 4.6 A, B).

To further investigate the effects of reduced membrane affinity on Min patterns, we focused on hydrophobic membrane interactions of specific amino acids in the MTS. For this, we analyzed Min protein patterns of MinE mutants with single hydrophobic residue mutations. Specifically, residues L3, L4, F6 or F7 were substituted by glutamate to disrupt the amphipathicity of the MTS. *In vivo* experiments showed that these mutants are impaired in membrane interaction (Park et al., 2011), which we corroborated *in vitro* using a liposome co-sedimentation assay (Appendix, Figure 7.5). Strikingly, although the patterns varied slightly between the different mutants at a given concentration, we observed that the characteristic reduction in the lower limit of the wavelength was observed for all mutants, similar to the truncation mutant (Figure 4.6 A, B). Taken together, our results demonstrate that MinE's MTS defines the lower limit of the concentration-dependent wavelength, and that mutations of even single hydrophobic residues can dramatically reduce the length scale of Min protein patterns.

4.2.1.2 MinE membrane interaction restrains MinE's capacity to stimulate MinD's ATPase activity

The length scale of Min protein patterns represents an emergent property of a self-organizing system. As changes in such observables often depend directly or indirectly on different

parameters, we investigated how mutations in the MTS affect MinE's core function of stimulating MinD's ATPase activity, which is directly responsible for triggering MinD detachment from the membrane (Hu and Lutkenhaus, 2001; Lackner et al., 2003). For this, we performed MinD ATPase stimulation assays in the presence of liposomes with the truncation mutant and all four mutants with individual substitutions of hydrophobic residues.

Strikingly, we observed that all five mutants stimulated MinD's ATPase activity to a significantly higher level than the WT (Figure 4.7). This previously unknown increase in ATPase stimulation by single mutations in the MTS's hydrophobic residues is consistent with the increased MinD ATPase stimulation reported for MinE R10G/K11E/K12E, which is impaired in electrostatic membrane interaction (Hsieh et al., 2010). On the other hand, Vecchiarelli et al. observed only a slight, non-significant difference in the ATPase stimulation for $MinE^{11-88}$ (Vecchiarelli et al., 2016). However, these experiments were performed at different concentrations and temperature as well as in a different assay from ours, impeding direct comparability. Mechanistically, the effectively higher ATPase rate could be due to faster MinE detachment following stimulation of one MinD dimer's ATPase activity and thus shorter delay before binding the next one.

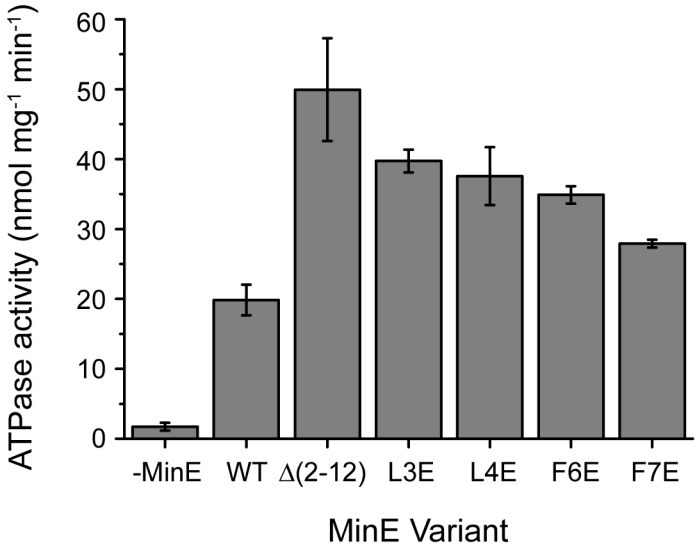

Figure 4.7: Mutation or truncation of MinE's membrane targeting sequence causes higher bulk stimulation of MinD's ATPase activity, indicating increased antagonistic potential of MinE in the absence of its membrane interaction. ATPase stimulation assay with WT MinE or MinE Δ(2-12), L3E, L4E, F6E, F7E using 4 µM MinD, 4 µM MinE and 0.2 mg/mL small unilamellar vesicles made of *E. coli* polar lipids. Error bars represent standard deviation from three independent experiments.

In conclusion, membrane interaction appears to restrain MinE's capacity to stimulate MinD's ATPase activity and thereby also to antagonize MinD accumulation on the membrane. Conversely, mutations in MinE's MTS alleviate this restraint. Thus, the increased ATPase stimulation observed with the mutants indicates a more efficient detachment of MinD from the membrane, which may explain the shorter wavelength of the mutant patterns.

4.2.1.3 MinE membrane interaction shapes the Min gradient by adapting Min protein dynamics to cell-like geometry

As impaired MinE membrane interaction reduced the length scale of Min waves while still supporting pattern formation, the role of MinE membrane binding in Min oscillation and gradient formation was an outstanding question. A previous study with a mutant lacking the MTS's hydrophobic patch indicated that regular pole-to-pole oscillations in cell-like geometry are compromised without MinE membrane binding (Zieske and Schwille, 2014). However, it has remained unclear which specific dynamic modes can emerge in the absence of MinE membrane interaction and in particular, how each of them affects gradient formation. Furthermore, it was unclear how sensitive the Min oscillator is to single mutations in the membrane targeting sequence. Therefore, we reconstituted MinE L3E together with MinD and ATP under physiological conditions in cell-shaped compartments.

Remarkably, in contrast to the typical pole-to-pole oscillations for WT MinE or the irregular dynamics reported previously (Zieske and Schwille, 2014), the L3E mutant supported a rich diversity of dynamic modes (Figure 4.8). Notably, these modes emerged in different compartments under the same experimental conditions and occasionally even alternated within the same compartment. This diversity of *in vitro* Min protein dynamics supports the notion of multistability, previously reported *in vivo* and *in silico* (Amiranashvili et al., 2016; Wu et al., 2016).

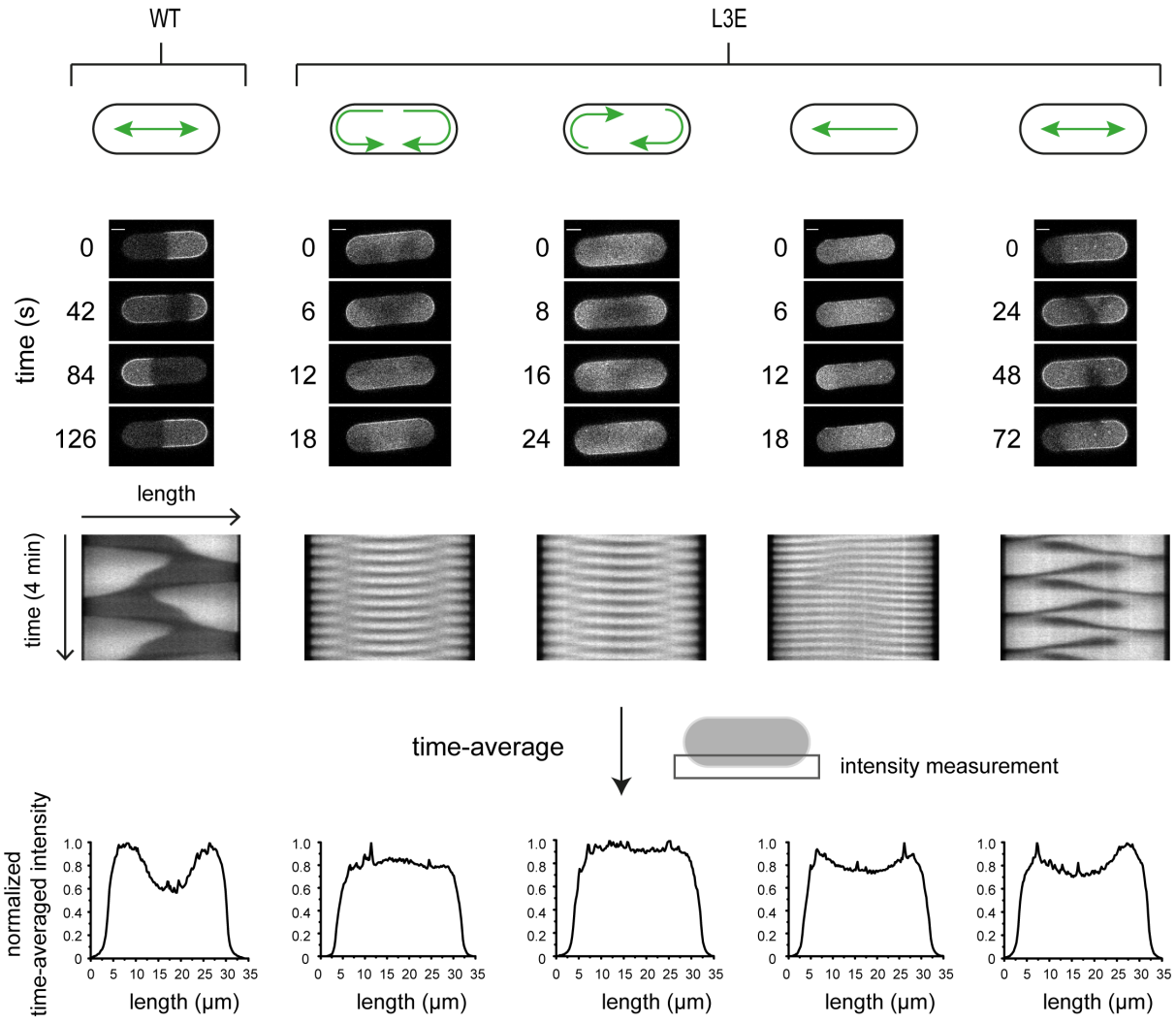

Figure 4.8: Mutation of MinE's membrane targeting sequence leads to unusual dynamics and defects in gradient formation in cell-shaped compartments. WT and L3E panels show representative time-lapse images, kymographs along the compartment length as well as the time-averaged fluorescence intensity, which was measured along a compartment edge. The L3E mutant exhibited diverse dynamical modes observed in different compartments under the same experimental conditions. These mutant dynamics comprised (from left to right) bi- or unidirectional rotations, traveling waves and irregular pole-to-pole oscillations. All images at 1 µM MinD with 20 % eGFP-MinD and 1 µM MinE. Scale Bar: 5 µm. The compartments were 35 µm long, 10 µm wide and 10 µm deep.

We observed four major types of defined dynamics for the L3E mutant. Besides pole-to-pole oscillations, which appeared irregular compared to WT oscillations, traveling waves as well as striking rotational modes emerged (Figure 4.8). In the rotational dynamics, MinD either split into two concurrent and bidirectional rotations via both poles or performed unidirectional rotations around the entire compartment periphery. Interestingly, bidirectional rotations appeared like a short-axis oscillation in kymographs along the compartment width (Appendix, Figure 7.6). Importantly, WT oscillations produced a clear gradient with a depth of up to

50 %. In contrast, the rotational modes observed with MinE L3E did not display a time-averaged gradient. Moreover, the traveling waves and oscillations displayed by MinE L3E formed weaker gradients with a depth of up to only around 70 % (Figure 4.8). Thus, the different dynamic modes observed for MinE L3E either completely abolished or substantially compromised gradient formation. This indicates that MinE's MTS mediates functional gradient formation by selecting regular pole-to-pole oscillations and suppressing alternative dynamics under physiological conditions in cell-like geometry.

To confirm that unusual dynamics also emerge for other mutations in the MTS, we reconstituted MinE Δ(2-12) and F6E mutant dynamics in cell-shaped microcompartments (Appendix, Figure 7.7 and Figure 7.8). We observed similarly unusual dynamics with the most notable difference being the observed fraction of the respective modes (Appendix, Figures 7.7 – 7.9).

Taken together, our results demonstrate that MinE's capacity to interact with the membrane plays a key role in selecting the modes of Min protein dynamics and thereby adapting the Min oscillator for gradient formation in cell-like geometry. Intriguingly, a rich diversity of dynamic modes can emerge even without MinE membrane interaction. Finally, even a single mutation in MinE's MTS causes a large-scale remodeling of the Min oscillator.

4.2.2 Additional results

4.2.2.1 Reevaluation of pattern formation by MinE C1

Previously, a MinE mutant with substitutions in a cluster of cationic residues in the MTS - MinE R10G/K11E/K12E, also termed "MinE C1" (Hsieh et al., 2010) - was reported to form only unsynchronized waves (Loose et al., 2011a). In retrospect, this result is surprising as other MinE mutants lacking some or all of these residues formed regular wave patterns (section 4.2.1.1) (Vecchiarelli et al., 2016). Besides protein properties, Min protein concentrations are another important factor influencing Min waves, which generally tend to appear irregular at low MinE/MinD ratios (see also section 4.3.1.2). Therefore, and because MinE C1 was previously only analyzed at one particular MinE/MinD ratio, we hypothesized that regular wave formation would occur at higher concentrations of this mutant. To test this notion, we reconstituted MinE C1 with MinD on flat membranes and systematically increased the MinE/MinD ratio (Figure 4.9).

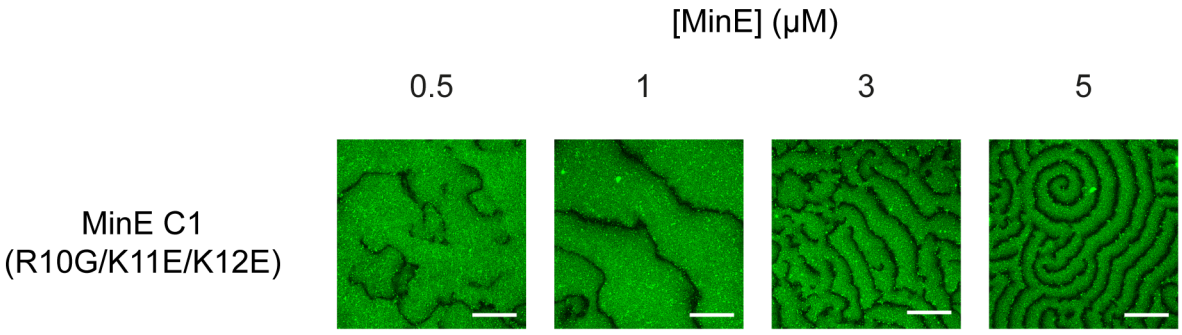

Figure 4.9: MinE C1 forms regular wave patterns at high MinE/MinD concentration ratios. Confocal images of Min protein patterns formed at different concentrations of MinE C1 with MinD at 1 µM incl. 20 % eGFP-MinD on a flat SLB. Scale Bar: 50 µm**.**

While patterns appeared irregular at low concentrations, we found that regular spiral and traveling wave patterns indeed formed for increased concentrations of the C1 mutant (Figure 4.9). The requirement for higher concentrations of MinE C1 may be due to the observation that, besides its defect in membrane interaction, the mutant also has a lower affinity for MinD (Hsieh et al., 2010), as was previously suggested (Halatek and Frey, 2012). In summary, consistent with the results gained with other MTS mutants (section 4.2.1.1), our reevaluation of MinE C1 confirms that regular wave patterns can still form when MinE membrane interaction is impaired.

4.2.2.2 Wave profiles for a MinE mutant impaired in membrane interaction

It has been reported that MinE membrane interaction regulates the MinD and MinE distributions within Min waves (Vecchiarelli et al., 2016). In particular, analysis of wave profiles for MinE$^{11-88}$ suggested that the characteristic accumulation of MinE at the rear of the waves and its "lingering" after initiating MinD detachment are impaired in the absence of MinE's MTS (Vecchiarelli et al., 2016). We sought to independently confirm this result and therefore co-reconstituted labeled MinD with labeled WT MinE or MinE Δ(2-12) on flat membranes (Figure 4.10).

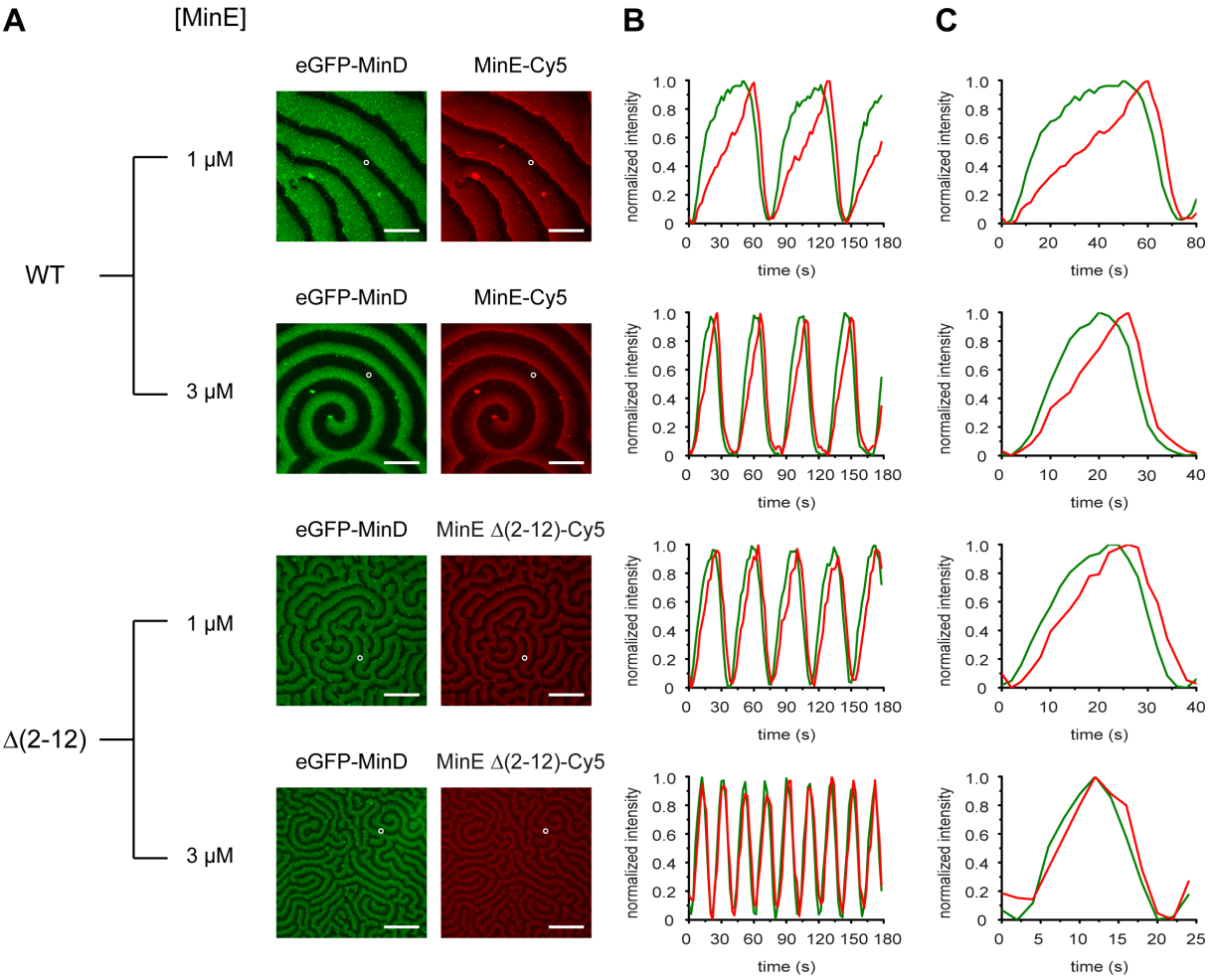

Figure 4.10: Wave profiles in the presence and absence of MinE's N-terminal membrane targeting sequence. A) Fluorescence micrographs, and **B)** normalized temporal wave profiles measured in the area indicated in the micrographs for 3 min, and **C)** separately normalized profiles for one wave only are shown for WT MinE and MinE Δ(2-12). Protein concentrations: 1 µM MinD incl. 20 % eGFP-MinD and 1 or 3 µM WT or mutant MinE incl. 10 % WT or mutant MinE-Cy5. Scale Bar: 50 µm.

As the effects of deleting MinE's MTS, particularly the reduction of the wavelength of Min patterns, were most apparent at high MinE/MinD ratios (section 4.2.1.1), we tested MinE concentrations of 1 μM and 3 μM while keeping MinD fixed at 1 μM (Figure 4.10). For WT MinE, a clear difference between the MinD and MinE profiles was observed at both concentrations. In particular, whereas the MinD profile appeared relatively symmetrical, MinE accumulated toward a clear peak at the rear of the wave, which was followed by a steep decrease in intensity (Figure 4.10), consistent with previous observations (Loose et al., 2008). In contrast, for MinE Δ(2-12), the MinD and MinE profiles within a wave appeared more similar. Nevertheless, both WT MinE and MinE Δ(2-12) lagged behind MinD during the increase as well as decrease in intensity. Notably, while the lag of MinE Δ(2-12) with respect to MinD was clearly observable at 1 μM, the shift of the profiles was less apparent for the shorter waves emerging at 3 μM MinE Δ(2-12) (Figure 4.10). This can give the impression that MinD and MinE detach from the membrane-bound protein layer simultaneously, especially when displaying multiple waves in the same plot. In this respect, our observations are similar to previously published experiments (Vecchiarelli et al., 2016). However, we show that the temporal lag of MinE with respect to MinD during wave propagation is not completely diminished, although the WT MinE profiles exhibited a more unique shape and clearer peak at the waves' rear compared to the MinD profiles in the same waves.

These results are interesting with respect to the notion that MinE accumulates during wave propagation by "rapid rebinding" of detached MinE to the MinD layer on the membrane (Loose et al., 2011a). In this view, a single MinE processively binds multiple MinD dimers by cycling between them via the bulk, allowing MinE to effectively remain within the membrane-bound protein layer during wave propagation. Moreover, rapid rebinding was proposed to be responsible for the lag of MinE detachment with respect to MinD (Loose et al., 2011a). Our observations of higher similarity between the MinD and MinE profiles within a wave, indicating efficient MinD-dependent accumulation of MinE, as well as the retained lag in detachment suggest that rapid rebinding is not compromised when MinE membrane interaction is impaired, but that it may even be enhanced. This would also be consistent with the increased stimulation of MinD's ATPase activity for MinE mutants impaired in membrane binding, as these mutants would not stay bound to the membrane upon MinD detachment and would therefore be available faster than the WT for binding the next membrane-bound MinD dimer from the bulk (section 4.2.1.2) (Ayed et al., 2017). In the future, it would be interesting to directly investigate rapid rebinding for the WT and mutant proteins by single-molecule experiments (Loose et al., 2011a).

4.2.3 Discussion

Here, we experimentally investigated the role of MinE membrane interaction in pattern formation. For this, we analyzed a MinE mutant lacking the N-terminal membrane targeting sequence as well as mutants with individual amino acid substitutions that were previously reported to be impaired in membrane binding (Hsieh et al., 2010; Park et al., 2011).
Our characterization of different mutants resolved the question if pattern formation can occur in the absence of MinE membrane interaction, which had remained ambiguous from previous theoretical and experimental studies (Bonny et al., 2013; Halatek and Frey, 2012, 2014; Loose et al., 2011a; Vecchiarelli et al., 2016). In particular, in previous studies, a mutant lacking most of the MTS ($MinE^{11-88}$) supported regular self-organization into traveling waves (Vecchiarelli et al., 2016), whereas a MinE mutant impaired in electrostatic membrane interaction (MinE C1) displayed only unsynchronized wave patterns (Loose et al., 2011a). By reevaluating pattern formation with MinE C1, we found that this mutant is capable of supporting regular wave formation at a higher MinE concentration than employed in the previous study. Strikingly, we also observed Min protein patterns with all other mutants, including the truncation mutant lacking the entire MTS. Thus, we unambiguously demonstrate that regular Min protein patterns can form even in the absence of MinE's MTS.

Moreover, our results reveal that MinE membrane affinity is an important modulatory parameter for large-scale Min protein patterns. Most strikingly, we found that the length scale of Min protein patterns is reduced in the absence of MinE membrane interaction. Specifically, the lower limit of the range of wavelengths obtainable at varying MinE/MinD ratios was reduced for mutants impaired in membrane interaction, such that the mutant patterns could assume length scales below those for even elevated WT concentrations (Figure 4.11). Thus, increasing the concentration of the MinE mutants did not rescue the WT behavior, but exacerbated the effects of the mutations, both with regard to the length scale and wave profiles. Accordingly, we observed that the effective ATPase rate in the Min system, an observable known to depend on MinE concentration (Hu and Lutkenhaus, 2001), is increased in the absence of MinE membrane interaction. A recent study independently confirmed this result and additionally revealed that specifically MinE's maximum stimulatory capacity, observed at high concentrations, is increased compared to the WT (Ayed et al., 2017). This is an important difference to the previously discussed case of a mutant impaired in ATPase stimulation (MinE K19Q), which has a maximum stimulatory capacity similar to the WT (Hu

and Lutkenhaus, 2001) and thus showed concentration-dependent rescue behavior *in vitro* (section 4.1.1). Taken together, these results suggest that the MTS restrains MinE's stimulation of MinD's ATPase activity, and thus MinD's accumulation on the membrane, and that alleviating this restraint is associated with large-scale changes in self-organization.

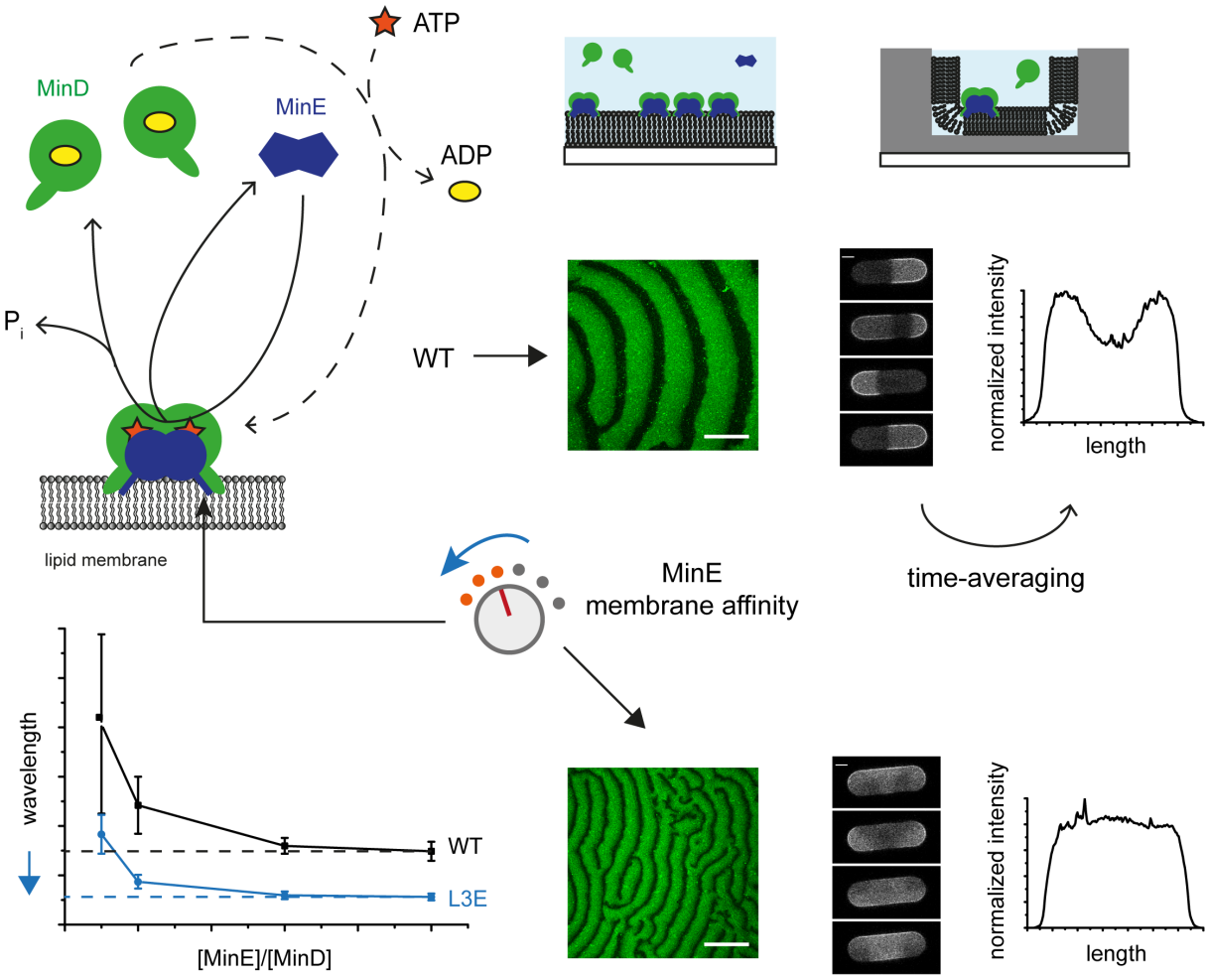

Figure 4.11: Large-scale modulation of the Min oscillator by reducing MinE's membrane affinity. Biochemical alterations, such as single mutations, in MinE's membrane targeting sequence cause a marked reduction in the lower limit of the length scale of Min protein patterns along with unusual dynamic modes in cell-like geometry. Thus, the Min oscillator is both highly versatile and sensitive to biochemical changes. Scale Bars: 50 µm (left) and 5 µm (right). P_i: inorganic phosphate. Units and values on graphs are left out for simplicity (see Figures 4.6 and 4.8 for data).

Besides the effects of mutations in MinE's MTS described above, a variety of unusual dynamic modes deficient in gradient formation emerged in cell-shaped compartments. In particular, striking rotational modes, traveling waves and irregular pole-to-pole oscillations were observed. This altered dynamic behavior could result from differences in interaction

rates as well as related effective parameters, such as the Min system's ATPase rate or the emergent length scale of Min protein patterns, in combination with compartment geometry (Wu et al., 2016). Although an unambiguous cause is challenging to determine due to the interdependence of these different parameters, it is striking that various forms of unusual dynamic modes have been observed for WT Min proteins in a geometry-dependent manner *in vitro* (Caspi and Dekker, 2016; Zieske and Schwille, 2014). Most notably, while pole-to-pole oscillations were predominantly found in small and narrow chambers that were fully confined, rotations and traveling waves frequently occurred when the width and length of the chambers was increased (Caspi and Dekker, 2016). This observation of similar dynamics for both reduced wavelengths of Min protein patterns and increased system sizes suggests that both factors act together in selecting an appropriate behavior in cell-like geometry. Thus, it is possible that MinE membrane interaction adapts the length sale of Min protein patterns for robust oscillation and gradient formation in a particular geometry. In the future, it would be interesting to further investigate this notion and test whether the mutants support a stable oscillatory behavior and regular gradient formation in compartments that are smaller than the ones used here. Thus, by systematically varying multiple parameters, new insights could be gained on the interplay between geometry, kinetic rates and the emergent properties of Min protein patterns.

Lastly, our results highlight that the spatiotemporal properties of Min patterns, as well as gradient formation, are remarkably sensitive to changes in MinE's MTS, as even single mutations had drastic effects. Interestingly, such sensitivity is not unusual in dynamic biochemical networks, as recently exemplified in a reconstituted Ras signaling network (Coyle and Lim, 2016). Moreover, while the observed sensitivity makes the Min system vulnerable, it may also provide benefits, e.g. by facilitating the evolutionary adaptation of the Min system to different cellular conditions. For example, mutations in the MTS may hypothetically adapt the Min system to altered cell morphologies in the course of evolution.

4.3 Modulation of Min protein patterns by MinE's conformational switch

This section focuses on the role of MinE's conformational switch in pattern formation, which we addressed with a combined theoretical and experimental approach. The research described here was performed in close collaboration with Erwin Frey, Jacob Halatek and Jonas Denk (LMU Munich), who performed all mathematical modeling reported in this section. Parts of the results herein have been published (Denk et al., 2018)[12] and sections 4.3.1 and 4.3.3, including figures, are thus based on the manuscript listed below. Supporting information regarding mathematical modeling is shown in section 7.4 within the appendix. Section 4.3.2 contains additional, unpublished results.

MinE conformational switching confers robustness on self-organized Min protein patterns

Jonas Denk*, Simon Kretschmer*, Jacob Halatek*, Caroline Hartl, Petra Schwille, and Erwin Frey (2018)

(* J.D., S.K. and J.H. contributed equally to this work)

Proceedings of the National Academy of Sciences of the United States of America

PNAS 201719801; published ahead of print April 16, 2018.

https://doi.org/10.1073/pnas.1719801115

4.3.1 MinE conformational switching confers robustness on self-organized Min protein patterns

The Min system provides an attractive basis for theoretically studying protein pattern formation, as its components are known, reasonably well understood and experimentally accessible. Accordingly, various mathematical models of Min protein pattern formation have been developed (Halatek and Frey, 2012; Howard et al., 2001; Huang et al., 2003; Kruse, 2002; Meinhardt and de Boer, 2001; Wu et al., 2016). Among these different models, the so-called "skeleton network" is a particularly useful framework, as its underlying interactions are generally accepted and it incorporates only the processes taken to be essential for pattern formation (section 2.3.5) (Frey et al., 2018; Halatek and Frey, 2012; Huang et al., 2003). In

this model, MinD attaches to the membrane and then recruits further MinD as well as MinE. After formation of a MinDE complex, MinE's stimulation of MinD's ATPase activity leads to detachment of both MinD and MinE. MinD then substitutes ATP for ADP and rebinds to the membrane. This reaction network reproduces a variety of experimental observations, such as the Min system's responsiveness to geometry (Halatek and Frey, 2012; Wu et al., 2016) and the formation of surface waves on flat membranes *in vitro* (Halatek and Frey, 2018). Nevertheless, a striking discrepancy between models based on the skeleton network and prior experiments is that Min patterns can only form if MinD is present in excess of MinE (Halatek and Frey, 2012; Huang et al., 2003) (section 2.3.5). This condition is in conflict with experimental studies that show pattern formation even if MinE is substantially more abundant than MinD (Loose et al., 2011a; Loose et al., 2008; Vecchiarelli et al., 2016; Vecchiarelli et al., 2014). In turn, this discrepancy raises the question if the skeleton network can be extended, based on biochemical data on Min protein interactions, to reproduce Min patterns that are more robust to changes in the MinE/MinD ratio, in particular to show patterns also when MinE is present in excess of MinD. Addressing this question by the example of the Min system may also uncover general principles of robust pattern formation.

A plausible candidate for extending the skeleton network is MinE's conformational switch, which has been discovered only relatively recently (Park et al., 2011). Essentially, MinE can exist in a "latent" 6β-conformation with sequestered contact helix and masked MTS as well as a "reactive" 4β-conformation, in which the β1-strand folds into the contact helix for MinD interaction and the MTS is released (Figure 2.11 in section 2.3.3.3) (Park et al., 2017; Park et al., 2011). Instead of these two conformations being in equilibrium, MinE is assumed to switch from the latent to the reactive state upon "sensing" membrane-bound MinD (Park et al., 2017; Park et al., 2011). In this view, latent MinE first forms a so-called "encounter complex" with membrane-bound MinD, in which only the surface-exposed residues in the 6β-conformation (residues 14-21) participate in the interaction (Ayed et al., 2017; Park et al., 2017; Park et al., 2011). This relatively weak interaction is then believed to nucleate the formation of MinE's contact helix and thereby trigger the switch to the 4β-conformation (Ayed et al., 2017; Park et al., 2017; Park et al., 2011). In the resulting membrane-bound MinDE complex, the two proteins interact via a more extensive interface, involving residues 14-26 in MinE, than in the encounter complex (Ayed et al., 2017; Park et al., 2011). After stimulation of MinD's ATPase activity, the complex disintegrates.

Whereas formation of MinE's contact helix appears to be strictly dependent on MinD, it has been proposed that the 6β-conformation is flexible enough to allow for occasional,

spontaneous release of the MTS (Ayed et al., 2017; Park et al., 2017). However, it is unclear if the primary role of this process is related to membrane binding or the switch to the reactive state, as the release of the MTS also facilitates the accessibility of residues implied in forming the encounter complex with MinD (Ayed et al., 2017). Furthermore, MinE's reversal from the reactive to the latent form after stimulating MinD's ATPase activity has not been characterized yet, although it is plausible that it is also a multi-step process.

Despite structural, biochemical and genetic studies on MinE's conformational switch (Ayed et al., 2017; Park et al., 2017; Park et al., 2011; Zheng et al., 2014), its functional role in Min protein pattern formation has remained unclear. Thus, we addressed its role through a combined theoretical and experimental approach. On the one hand, theoretical predictions were made based on systematic extensions of the skeleton model to disentangle the switch's functional aspects, i.e. MinD and membrane interaction. On the other hand, we performed reconstitution experiments with MinE mutants impaired in conformational switching and membrane interaction.

4.3.1.1 Theoretical analysis of the role of MinE's conformational switch in Min protein pattern formation

First, the role of MinE's reactive and latent states with regard to its interaction with MinD, independent of membrane binding was analyzed. For this, the skeleton model was extended assuming that, upon disintegration of the MinDE complex, (reactive) MinE switches rapidly, yet not instantaneously, to the latent state (Figure 4.12 B) (Appendix, section 7.4.1). The reactive and latent states are characterized by high and low recruitment rates to membrane-bound MinD respectively. This choice of different recruitment rates reflects that latent MinE first has to form the encounter complex and undergo the conversion from the 6β- to the 4β-conformation before forming a functional MinDE complex. On the other hand, as reactive MinE is already folded in the 4β-conformation, this multi-step recruitment process is reduced to a single step, resulting in an effectively increased interaction rate. Moreover, the affinity for MinD would be expected to be higher in the reactive compared to the latent form due to the larger interaction interface.

To theoretically analyze pattern formation in the original and extended skeleton networks, linear stability analysis was performed. With this mathematical method, one basically tests if small perturbations to a steady state, such as a homogeneous protein distribution, are

suppressed or amplified. In the latter case, the analyzed parameter set would be permissive of pattern formation. Accordingly, by performing extensive parameter scans, it is possible to identify parameter regimes compatible with pattern formation (Denk et al., 2018).

The linear stability analysis performed here, covering a broad range of recruitment rates, showed that the extension with the reactive-latent switch strongly increased the concentration range allowing for pattern formation compared to the original skeleton network. Notably, incorporating the switch supported pattern formation also above a MinE/MinD ratio of one, in contrast to the skeleton network (Figure 4.12 A, B).

Another interesting aspect of MinE's conformational switch is that the MTS is stably exposed in the reactive state (Park et al., 2011). Therefore, MinE could hypothetically stay bound to the membrane after MinD detachment and eventually reassociate with another membrane-bound MinD molecule. To theoretically analyze the effects of such persistent membrane binding on the robustness of Min protein patterns against variations in protein concentration, the skeleton network was extended accordingly (Figure 4.12 C) (Appendix, section 7.4.2). Depending on the parameter values, two scenarios were obtained by linear stability analysis. If free membrane-bound MinE is more likely to detach than reassociate with MinD, the maximal MinE/MinD ratio allowing for pattern formation increases with slower detachment of persistently bound MinE. In this case, MinE is effectively sequestered from binding another MinD via the bulk and therefore depletes it from the membrane less efficiently. However, reassociation could also be fast compared to detachment and potentially also compared to MinE recruitment from the bulk. In this case, the maximal MinE/MinD ratio compatible with pattern formation decreases for smaller detachment rates of persistently bound MinE, as MinE removes MinD from the membrane more efficiently (Figure 4.12 C).

As certain MinE variants, including those locked in the 4β-conformation, can attach to the membrane independently of MinD (Park et al., 2011), and because of the proposed, spontaneous MTS release for WT MinE (Ayed et al., 2017; Park et al., 2017), potential effects of direct MinE membrane attachment on pattern robustness were also investigated. An accordingly extended skeleton network showed qualitatively similar effects as for persistent membrane binding, such that both scenarios described above were retained (Figure 4.12 D). Only for very fast direct MinE membrane attachment in the sequestration scenario, the effect on the concentration range allowing for pattern formation was reversed. However, in this case, the rate of membrane binding was two orders of magnitude higher for MinE than for MinD, which is unrealistic considering that the MTSs of MinD and MinE are of roughly equal structure and length (Park et al., 2011).

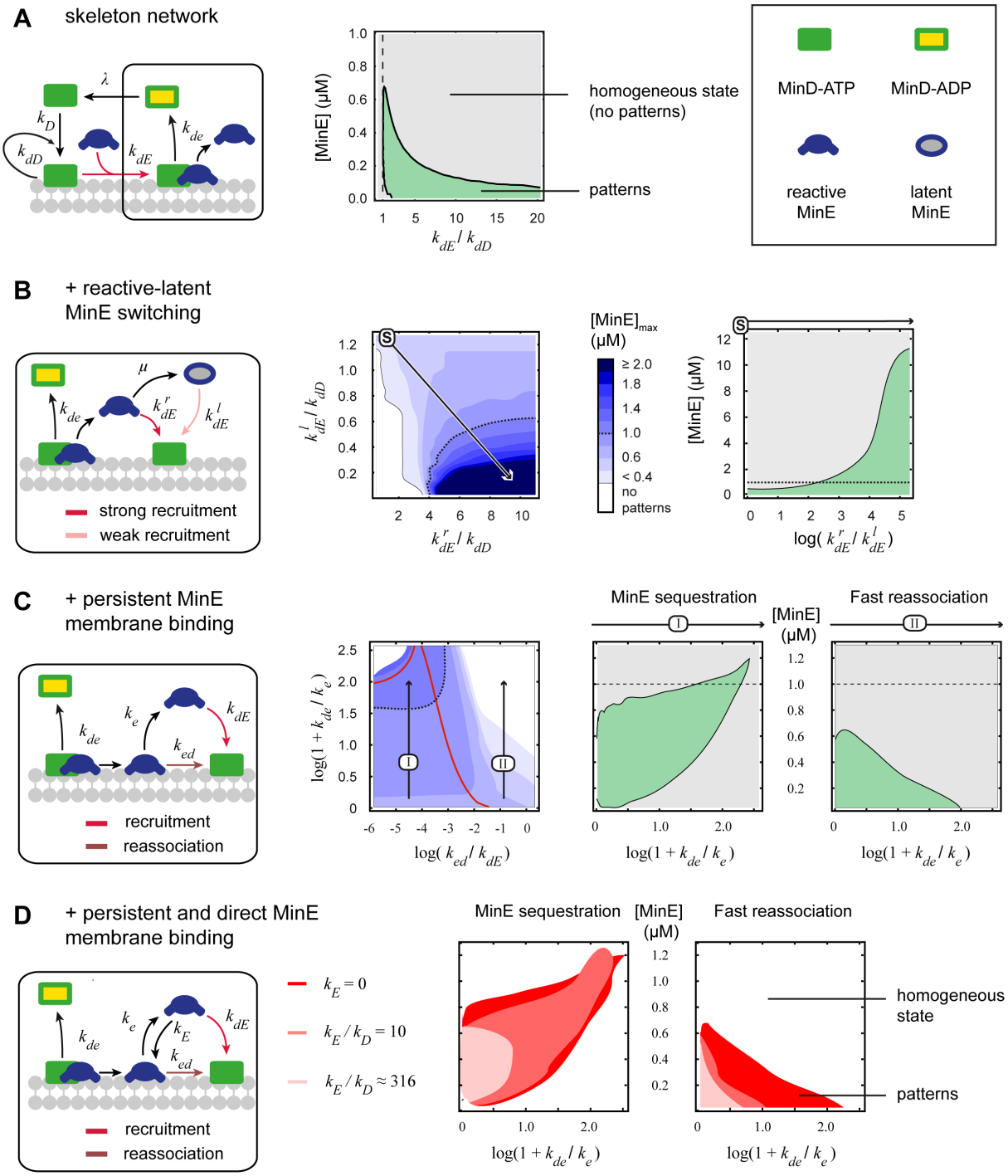

Figure 4.12: Theoretical evaluation, by linear stability analysis, of extensions to the skeleton network incorporating either a reactive-latent switch or membrane interaction of MinE. [MinD] = 1 μM, in all cases. **A)** The skeleton network only supports pattern formation when MinE/MinD < 1. **B)** A model extension including a switch from MinE's reactive to a latent state increases the maximal MinE concentration compatible with pattern formation ($[MinE]_{max}$) for high k^r_{dE} and low k^l_{dE}. In the skeleton network (S), $k^r_{dE} = k^l_{dE}$. The timescale for switching is set to 10 ms (μ = 100 s^{-1}), in the range of conformational changes in proteins (Shamir et al., 2016). **C)** Persistent and **D)** direct MinE membrane interaction theoretically allows for either increased or decreased $[MinE]_{max}$, depending if MinE's detachment or reassication with membrane-bound MinD dominates. The red line in C corresponds to equal detachment and reassociation. The theoretical analysis shown in this figure was performed by Jonas Denk (LMU Munich).

4.3.1.2 Experimental analysis of the role of MinE's conformational switch in Min protein pattern formation

In order to test the predictions of the different model extensions experimentally, we investigated the concentration range of pattern formation for MinE mutants impaired in conformational switching as well as membrane interaction. To disrupt switching to the latent state and lock MinE into the reactive conformation, we took advantage of the I24N mutation. MinE I24N has previously been shown to fold into the 4β-conformation, even in the absence of MinD (Park et al., 2011). Thus, it does not undergo the switch to the 6β-conformation, while being capable of membrane binding via its exposed MTS. In turn, to impair membrane binding, we employed the L3E mutation, which disrupts the amphipathicity of MinE's MTS (Park et al., 2011; Shih et al., 2011).

To analyze the effects of these mutations on the concentration range of Min protein patterns, we reconstituted WT MinE as well as MinE L3E, MinE I24N and MinE L3E/I24N at different concentrations together with 1 μM MinD on flat membranes and tested for pattern formation by confocal microscopy (Figure 4.13). All variants supported pattern formation in defined ranges of MinE concentration with a lower and upper threshold. Below the minimal MinE concentration, MinD homogeneously covered the membrane, whereas above the maximal MinE concentration, MinD was uniformly depleted from the membrane, as in other experiments with WT MinE and different mutants (section 4.1.1). Notably, our experiments show that Min patterns generally appear irregular around the lower MinE/MinD threshold allowing for pattern formation. This is consistent with a recent theoretical analysis that predicted chemical turbulence, i.e. irregular patterns, at the onset of instability within the homogeneous state (Halatek and Frey, 2018).

WT MinE supported pattern formation in a broad range of MinE concentrations and at MinE/MinD ratios above and below one, consistent with previous studies (Loose et al., 2011a; Loose et al., 2008; Vecchiarelli et al., 2016; Vecchiarelli et al., 2014). Moreover, impairing MinE membrane interaction by means of the L3E mutation had no apparent effect on the concentration range of pattern formation (Figure 4.13).

Strikingly, inserting the I24N mutation into either of the two variants, and thereby locking MinE into the reactive state, strongly decreased the maximal MinE/MinD ratio compatible with pattern formation (Figure 4.13). In particular, Min protein patterns only formed below a MinE/MinD ratio of one. This clearly indicates that the switch between reactive and latent MinE is critical for robust pattern formation at varying MinE/MinD ratios.

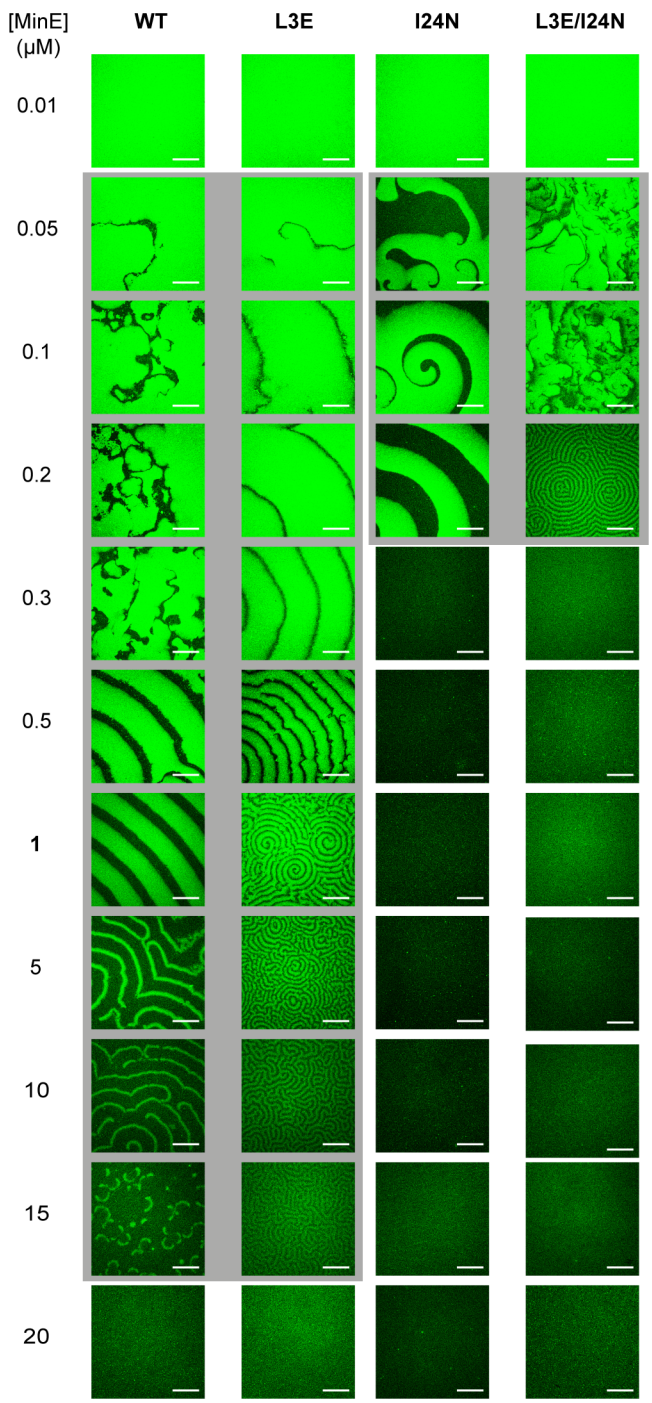

Figure 4.13: The MinE concentration range compatible with pattern formation (highlighted in grey background) is strongly reduced, when MinE's conformational switch is impaired. The I24N mutation locks MinE into the reactive state, while the L3E mutation disrupts MinE membrane interaction. Images show confocal micrographs of *in vitro* reconstitution experiments, in which 1 µM MinD incl. 20 % eGFP-MinD was reconstituted with MinE of varying concentration on flat membranes. MinE L3E/I24N at 0.3 µM showed patterns in only 50 % of cases and this condition was therefore not classified as supporting pattern formation reliably. The ranges shown here were observed in at least three independent experiments. Scale Bar: 50 µm.

4.3.2 Additional results

4.3.2.1 Biochemical characterization of the tested MinE variants

4.3.2.1.1 Membrane interaction of the tested MinE variants

The choice of MinE mutants for our comparison to the model extensions was based on a previous study showing that the I24N mutation locks MinE into the 4β-state with exposed MTS, while the L3E mutation disrupts membrane interaction (Park et al., 2011). In this study, the I24N mutant bound to the cell membrane when expressed in the absence of MinD and MinC *in vivo*, and this interaction was abolished by the L3E mutation (Park et al., 2011). We sought to confirm the effects of these mutations *in vitro* by performing a liposome co-sedimentation assay with WT MinE as well as MinE L3E, I24N and L3E/I24N (Figure 4.14).

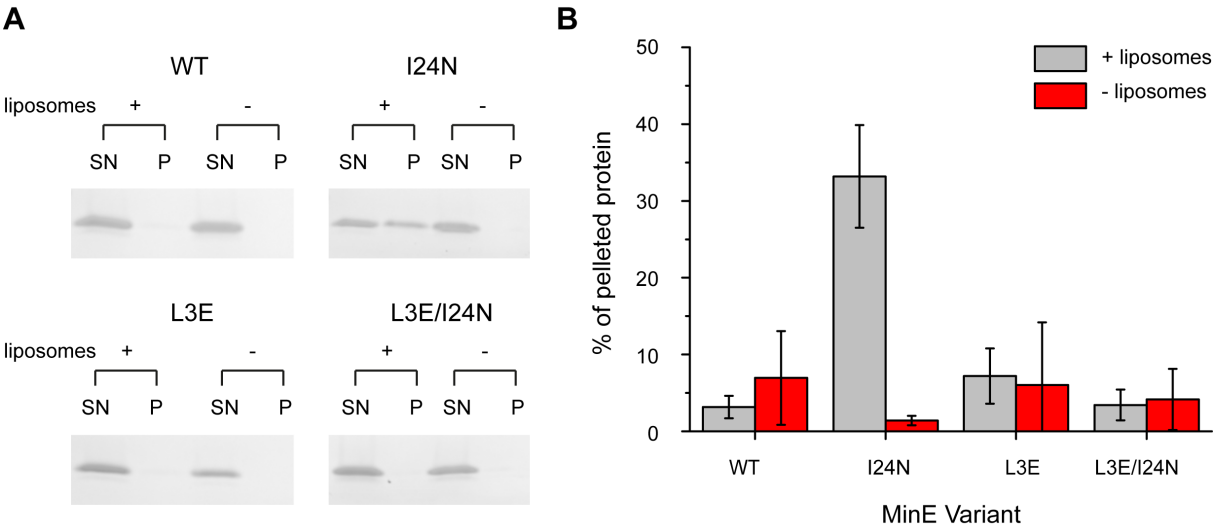

Figure 4.14: Liposome co-sedimentation assay with MinE mutants impaired in conformational switching and/or membrane binding. A) Representative SDS-PAGE fractions from the co-sedimentation experiments with 5 µM WT or mutant MinE and 0.5 mg/mL *E. coli* polar lipid SUVs. **B)** Percentage of pelleted protein for the different MinE variants (N=3). The data shown for MinE I24N and L3E/I24N is identical to Figure 7.5. All variants were characterized in the same set of experiments

In our co-sedimentation experiment, MinE I24N was the only variant capable of significant membrane binding, consistent with *in vivo* localization profiles in the absence of MinD (Park

et al., 2011; Raskin and de Boer, 1997). All other MinE variants did not co-sediment with the liposomes significantly compared to the negative control without vesicles.
Notably, the question whether WT MinE can attach to the membrane in the absence of MinD has been the subject of some debate with experimental evidence both in favor (Ayed et al., 2017; Hsieh et al., 2010; Renner and Weibel, 2012) and against (Hu et al., 2002; Loose et al., 2011a; Raskin and de Boer, 1997) direct MinE membrane attachment independent of recruitment by MinD. Although we did not observe direct membrane attachment of WT MinE in our co-sedimentation assay, it is possible that binding can be detected with more sensitive techniques. In any case, the result that membrane binding of WT MinE could not be shown by co-sedimentation suggests that its membrane affinity is weak in MinD's absence and underscores the latter's role in inducing and stabilizing MinE's 4β-state with exposed MTS, as was also recently emphasized (Ayed et al., 2017).
In the future, quantitative experiments on the membrane affinities of different MinE variants could shed further light on their binding properties. Nevertheless, in our co-sedimentation experiment, the tested MinE mutants showed effects that were broadly consistent with the effects described previously for the mutations (Park et al., 2011).

4.3.2.1.2 MinD ATPase stimulation by the tested MinE variants

To investigate the effect of locking MinE into its reactive state on the Min system's apparent ATPase rate, we compared MinE I24N and L3E/I24N to WT MinE and MinE L3E in terms of their ability to stimulate MinD's ATPase activity. For this, we performed an ATPase assay with MinD and liposomes in the presence and absence of the different MinE variants (Figure 4.15).
We found that MinE I24N, which is locked in the reactive state but can interact with the membrane (Park et al., 2011), showed similar ATPase stimulation as WT MinE under the tested conditions (Figure 4.15). As discussed previously (section 4.2.1.2), impairing MinE membrane interaction through the L3E mutation increased the Min system's ATPase rate. Interestingly, while the I24N mutation did not enhance stimulation in WT background, it resulted in a higher stimulated ATPase rate when inserted into MinE L3E (Figure 4.15).

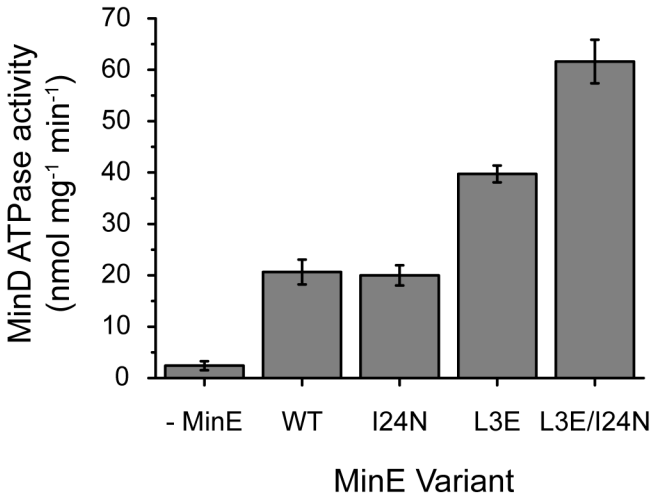

Figure 4.15: MinD ATPase stimulation assay with MinE mutants impaired in conformational switching and/or membrane binding. NADH-linked ATPase assays were performed with 4 µM MinD and 0.2 mg/mL *E. coli* polar lipid SUVs with and without 4 µM WT or mutant MinE. Error Bars represent standard deviation (N=3). The data shown for the samples without (-) MinE and with WT MinE and MinE L3E is identical to Figure 4.7. All variants were characterized in the same set of experiments.

These different effects of the I24N mutation in WT and L3E background have interesting implications regarding the rate-determining step of the ATPase cycle, which essentially depends on the slowest step therein. As suggested previously, detachment of MinE from the membrane likely limits the ATPase rate observed for WT MinE (section 4.2.1.2) (Ayed et al., 2017). However, for mutants that do not interact with the membrane or when mutations generate a slower process, another step can become rate-limiting. The observed increase by the I24N mutation in the background of the L3E mutant but not WT MinE suggests that processes related to MinE's conformational switch may become limiting to the system's apparent ATPase rate only in the absence of MinE membrane interaction. In the future, it would be interesting to further compare the variants in their capability to stimulate MinD's ATPase activity, e.g. by analyzing the dependence of stimulation on MinE concentration. In this way, the maximal ATPase stimulation, as well as the required concentrations to reach it, could be determined for the different MinE variants, which would provide more detailed insights into their behavior and the rate-limiting steps of the ATPase cycle.

4.3.2.2 Wave profiles for MinE mutants impaired in conformational switching

Finally, we investigated how MinE's conformational switch affects Min protein wave profiles. For this, we co-reconstituted labeled MinD and labeled WT or mutant MinE on flat membranes (Figure 4.16). As traveling waves did not emerge at identical MinE/MinD concentration ratios for the tested MinE variants (section 4.3.1.2), protein concentrations were adjusted individually for the variants with and without the conformational switch.

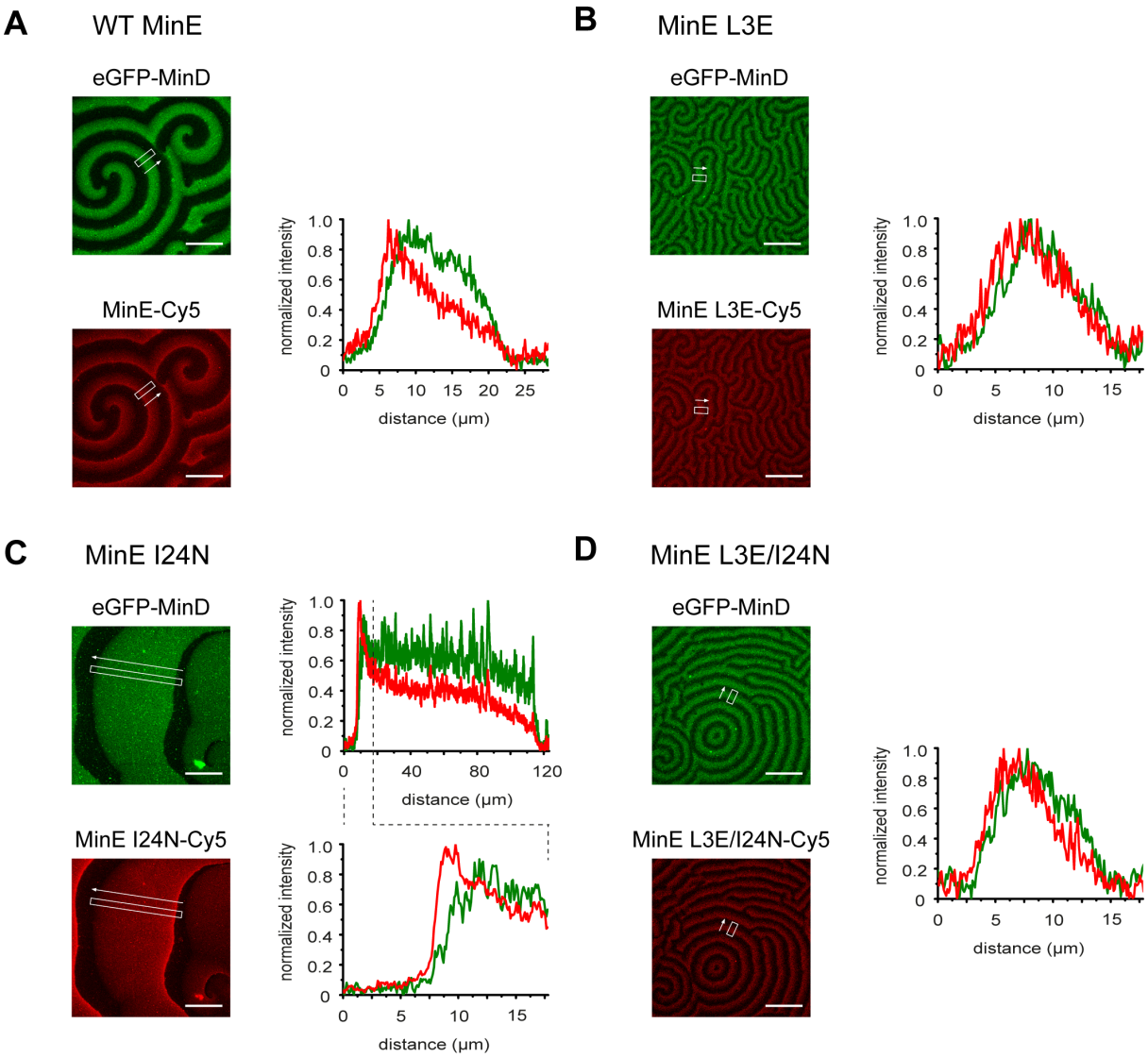

Figure 4.16: Normalized, spatial wave profiles for MinE mutants impaired in conformational switching and/or membrane binding. Fluorescence profiles were measured at concentrations compatible with wave formation for the respective mutants. Protein concentrations: 1 µM MinD incl. 20 % eGFP-MinD and **A)** 3 µM WT MinE, **B)** 3 µM MinE L3E, **C)** 0.2 µM MinE I24N, **D)** 0.2 µM MinE L3E/I24N, each including 10 % of the respective Cy5-labeled MinE variant. Scale Bar: 50 µm.

As discussed previously (sections 4.1.2.1 and 4.2.2.2) (Loose et al., 2008), the profiles of WT MinD and MinE assume characteristic shapes with MinE forming a clear peak at the wave's rear. As expected for mutations compromising MinE membrane interaction (section 4.2.2.2) (Vecchiarelli et al., 2016), this effect appeared attenuated in the shorter waves arising from the L3E mutation (Figure 4.16).

On the other hand, our analysis of MinE I24N showed that the MinD and MinE profiles had distinct shapes and that the mutant formed a strong peak at the wave's rear (Figure 4.16). While more detailed nuances between the profiles of the different variants remain to be investigated, this analysis shows that the characteristic features of Min protein wave profiles are retained when MinE is locked into the reactive form.

4.3.3 Discussion

Here, we investigated the role of MinE's conformational switch in pattern formation. With mathematical modeling, we showed that incorporating a switch from reactive to latent MinE into the skeleton model strongly increased the concentration range of Min patterns, enabling pattern formation both below and above a MinE/MinD ratio of one (Figure 4.12). Consistently, experimentally locking MinE into the reactive state through the I24N mutation strongly decreased the concentration range of Min patterns and only allowed for pattern formation when MinE was less abundant than MinD (Figure 4.13). Notably, the I24N mutant only formed patterns below the MinE/MinD ratio observed for WT Min proteins *in vivo* (Shih et al., 2002), consistent with its inability to restore WT cell morphology when co-expressed with MinD and MinC in an *E. coli* strain lacking the Min system (Zheng et al., 2014). Taken together, our complementary experimental and theoretical approach demonstrates that MinE's conformational switch is critical for the robustness of Min protein patterns against variations in protein concentration. Moreover, as MinE's switch from the latent to the reactive state depends on membrane-bound MinD and is therefore coupled to MinD's switch from its ADP- to its ATP-bound state, this result suggests that robustness arises from the interlinking of two protein switches, compared to the presence of a single switch (Figure 4.17).

Theoretical considerations suggest a mechanistic basis for how this interlinking may promote robustness against high MinE/MinD ratios. Here, it is important to note that dynamic Min protein patterns are essentially based on cycles of MinD-dominated recruitment followed by MinE-dominated detachment (Figure 4.17) (Frey et al., 2018). In these cycles, cooperative MinD recruitment initially dominates during the growth of a new MinD-covered zone on the membrane. However, with progressing MinD accumulation, MinE recruitment and the resulting removal of MinD ultimately outpace further MinD binding. During the MinE-dominated phase, reactive MinE rapidly rebinds another membrane-bound MinD molecule upon detachment to progressively remove MinD from the membrane. In this view, MinE dominance is only possible if the rate of recruitment to MinD is higher for released MinE than MinD, as MinE would otherwise not be able to outpace MinD binding and promote fast MinD detachment. In turn, for a new MinD-dominated zone to arise on the membrane, MinD's recruitment has to become transiently more probable than MinE's, for which MinD has to be present at a higher concentration than (reactive) MinE. This condition for MinD dominance restricts the range of MinE/MinD ratios compatible with pattern formation in the skeleton

model. Yet, if MinE switches to a latent state with lower recruitment rate upon removal of MinD from the membrane, MinD dominance is possible, even for higher total concentrations of MinE. In this way, the condition on the higher concentration of MinD relative to MinE is alleviated via MinE's switch to the latent state. Taken together, the dynamic, functional separation of reactive and latent MinE facilitates an alternating dominance of MinD and MinE in a broad range of MinE/MinD ratios, in particular also when MinE is more abundant than MinD.

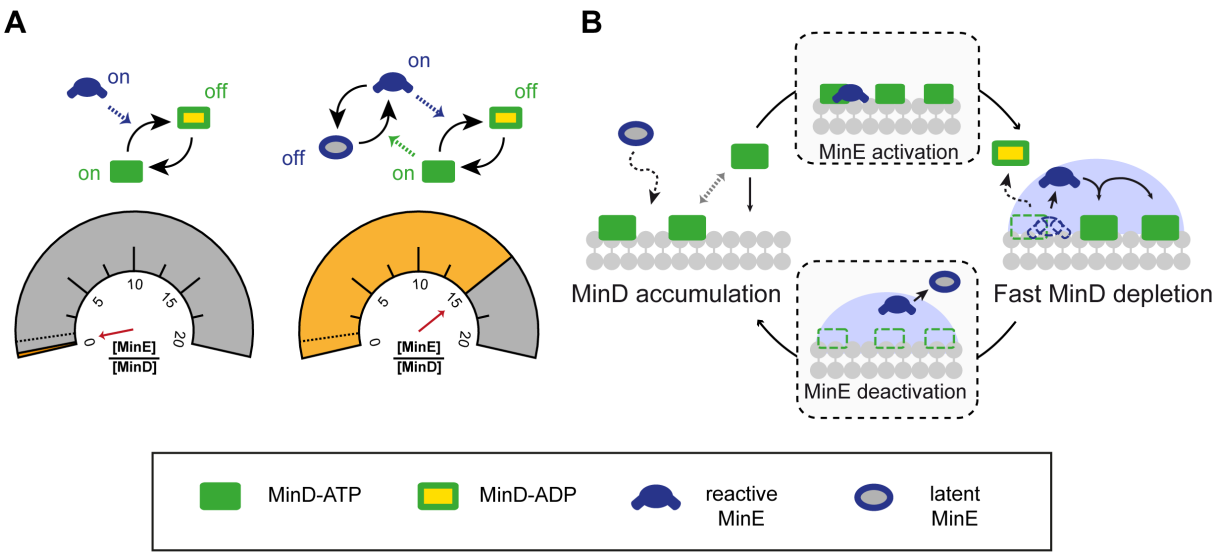

Figure 4.17: Interlinking protein switches in MinD and MinE confers robustness against variations in protein concentration on Min protein patterns. A) Comparison of MinD-MinE networks with only one or two interlinked switches. MinD's switch refers to ATP-dependent membrane binding and protein recruitment (activation) and MinE-dependent ATP hydrolysis and detachment (deactivation). MinE's switch refers to the MinD-dependent conformational change from the latent to the reactive state (activation) and spontaneous reversion after MinD detachment (deactivation). **B)** Mechanistically, the latent MinE conformation allows for MinD accumulation on the membrane even for high total MinE concentrations, whereas the reactive state locally enables fast MinD depletion due to rapid rebinding of detached MinE to membrane-bound MinD. In the reactive state, MinE may effectively act through a thin layer due to fast recruitment to membrane-bound MinD. Upon removal of MinD, reactive MinE switches to the latent form and becomes diffusely distributed in the bulk.

Theoretical considerations suggest that this dynamic separation is effectively accompanied by the spatial separation of latent MinE in the extended bulk and reactive MinE in a thin layer above the membrane. The thickness of this layer is essentially given by the bulk region reactive MinE can traverse before switching to the latent state. Interestingly, calculating this thickness suggests that, with 0.77 µm, this layer is orders of magnitude thinner than the system's bulk height of 5 mm ($l = \sqrt{D_c/\mu}$, with a switching rate µ of 100 s^{-1} and a bulk

diffusion coefficient D_c of 60 $\mu m^2 s^{-1}$). The emergence of this thin layer of reactive MinE is particularly interesting from a theoretical perspective, as MinE's switching is much faster than other processes in the system. Such fast processes are often treated as "instantaneous" and therefore neglected in mathematical approaches. However, the analysis discussed here shows that neglecting such fast processes would miss an important, emergent feature of the system. Accordingly, it highlights the importance of explicitly accounting for the bulk phase in general.

Impairing membrane interaction of either WT MinE or MinE I24N through the L3E mutation showed no apparent change in the concentration range allowing for pattern formation under the tested conditions (Figure 4.13). This demonstrates that MinE membrane interaction does not account for the robustness of pattern formation at MinE/MinD ratios below and above one. As no difference in the range of patterns was observed with or without the L3E mutation, the current experiment could not distinguish between the two different predicted scenarios of MinE "sequestration" on the membrane or "fast reassociation" with membrane-bound MinD (Figure 4.12). However, it is possible that effects of MinE membrane interaction may become apparent when comparing the MinE variants employed here with ones of higher membrane affinity in future experiments.

The MinE L3E/I24N double mutant only supported pattern formation in a narrow range of MinE concentration below a MinE/MinD ratio of one (Figure 4.13). Notably, this is consistent with theoretical predictions using the skeleton model (Figure 4.12) (Halatek and Frey, 2012). Moreover, the observed patterns for MinE L3E/I24N suggest that, while critical for the robustness and spatiotemporal properties of Min patterns respectively, neither MinE's conformational switch nor membrane binding is strictly required for pattern formation *per se*.

In this context, another interesting molecular aspect of MinE is that it forms a dimer via its C-terminal domain, historically referred to as a topological specificity domain (TSD) (Pichoff et al., 1995). This domain was also shown to be important for MinE's conformational switch (Park et al., 2011) and proposed to enable intermolecular MinE interactions (Zheng et al., 2014), although the latter remain to be confirmed *in vivo*. While all results reported herein relate to MinE with intact TSD, different experiments suggest that a monomeric peptide comprising just the MinD-interactive part of MinE's anti-MinCD domain ($MinE^{13-31}$) can stimulate MinD's ATPase activity but not support pattern formation (Vecchiarelli et al., 2016). In the skeleton network, dimerization or intermolecular MinE interactions are not explicitly accounted for, such that it is also suitable for comparison with $MinE^{13-31}$. However, the model is not necessarily in conflict with the different experimental observations in the

presence and absence of the TSD, as the biochemical properties of MinE variants with or without this domain are likely different. This would also impact the choice of parameters and, indeed, pattern formation is lost in certain parameter regimes. Nevertheless, the further refinement of models, e.g. by accounting for dimerization, and comparison to experimentally well-characterized MinE variants is an important future prospect.

How does robustness against variations in protein concentration benefit the Min system? First, it is important to note that changes in the MinE/MinD ratio determine not only the emergence of patterns, but also serve to modulate their detailed characteristics, such as the wavelength and velocity of Min waves or the periodicity of pole-to-pole oscillations (Hale et al., 2001; Loose et al., 2008) (sections 4.1 and 4.2). Thus, robustness against variations in protein concentration enables a large parameter regime allowing for pattern formation, which can be advantageous for both the maintenance and modulation of Min protein patterns. For example, if a bigger absolute change in MinD or MinE concentration were required to alter the wavelength via a change in the MinE/MinD ratio, a pattern of particular length scale would be more robust to small fluctuations in concentration. On the other hand, in the course of evolution, mutations or the duplication of genes can advantageously adapt the Min system's properties. As it is essential that such changes do not compromise pattern formation *per se*, a large parameter regime compatible with pattern formation may thus facilitate the evolutionary adaptation of the Min system.

Notably, the ATPase MinD and its activator MinE are part of the larger family of ParA/MinD NTPases and respective activating proteins (Lutkenhaus, 2012). Protein systems in this family regulate important intracellular processes, including chromosome segregation, cytokinesis, chemtaxis and the positioning of flagella (Kretschmer and Schwille, 2016; Schofield et al., 2010; Schuhmacher et al., 2015; Sourjik and Wingreen, 2012). It is thus intriguing to speculate that interlinked protein switches also play a role in mediating robustness in these systems. It is also interesting to put MinE into perspective with other proteins containing switchable tertiary structures. In this regard, so-called "metamorphic proteins" have recently been described in a variety of contexts (Murzin, 2008). Protein metamorphism essentially refers to a protein's ability to exist in two different conformations with distinct functional properties. One prominent example of a metamorphic protein is KaiB, which is part of a well-studied circadian clock in cyanobacteria, namely the KaiABC system (Chang et al., 2015; Snijder et al., 2017; Tseng et al., 2017). Here, a major structural rearrangement in KaiB to a "fold-switched" state controls its protein interactions, which leads to a phase transition in the Kai oscillator that regulates downstream signaling (Chang et al., 2015). Thus, the critical roles

of conformational changes in the MinCDE and KaiABC systems suggest a broader relevance of such functional switches in intracellular biochemical networks.

4.4 Modulation of Min protein patterns by MinD's membrane affinity

This section focuses on how Min protein patterns are modulated by changes in MinD membrane affinity. The underlying research was performed in collaboration with Andrea Tassinari, who conducted important preliminary experiments.

Using *in vitro* reconstitution approaches, the influence of MinE's biochemical features on pattern formation has systematically been explored (sections 4.1 - 4.3) (Loose et al., 2011a; Vecchiarelli et al., 2016). However, the impact of MinD's molecular motifs on the characteristics of Min protein patterns has so far received little attention. Therefore, we investigated how Min protein patterns are modulated by MinD's membrane affinity. While it is generally believed that MinD's interaction with the lipid membrane is crucial for pattern formation, it has not been characterized experimentally how different interaction strengths of MinD with the membrane affect Min protein patterns.

MinD interacts with the lipid membrane via a C-terminal membrane targeting sequence (MTS) folding into an amphipathic helix (Hu and Lutkenhaus, 2003; Szeto et al., 2002) (section 2.3.3.2). *In vivo* experiments with a GFP fusion of the *E. coli* MinD MTS as well as co-sedimentation experiments of MinD with liposomes have suggested that the affinity of one *E. coli* MinD MTS is too low for membrane interaction, while the simultaneous presence of two MTSs enables binding (Hu and Lutkenhaus, 2003; Lackner et al., 2003; Szeto et al., 2003). Accordingly, ATP-dependent dimerization has been proposed to promote membrane interaction (Hu and Lutkenhaus, 2003; Lackner et al., 2003).

The affinity of MinD to the membrane depends on the MTS sequence and defined mutations have been described that either impair or enhance MinD's interaction with the membrane (Szeto et al., 2002; Zhou and Lutkenhaus, 2003). Here, using *in vitro* reconstitution, we take advantage of such MinD mutants to dissect the effects of altered MinD membrane interaction on Min protein patterns.

4.4.1 MinD membrane interaction is required for pattern formation

First, we tested how pattern formation is affected, when MinD is defective in membrane interaction. For this, we characterized MinD L267E, a mutant shown to be impaired in membrane binding *in vivo* (Szeto et al., 2002). To confirm the reported deficiency in membrane binding, eGFP-labeled WT MinD or MinD L267E were added to a flat SLB in the presence of ATP. To assess membrane binding, the intensity along the z-axis was then measured. Whereas WT MinD clearly accumulated on the bilayer, the mutant did not bind the membrane, even at a five-fold elevated concentration (Figure 4.18). Unsurprisingly, in the presence of MinE, MinD L267E did not form patterns at either concentration (Figure 4.18). This confirms that MinD membrane interaction is essential for Min protein pattern formation (Hu et al., 2002; Szeto et al., 2002) and highlights that, similar to our observations with MinE's MTS (section 4.2), single mutations can abrogate membrane binding.

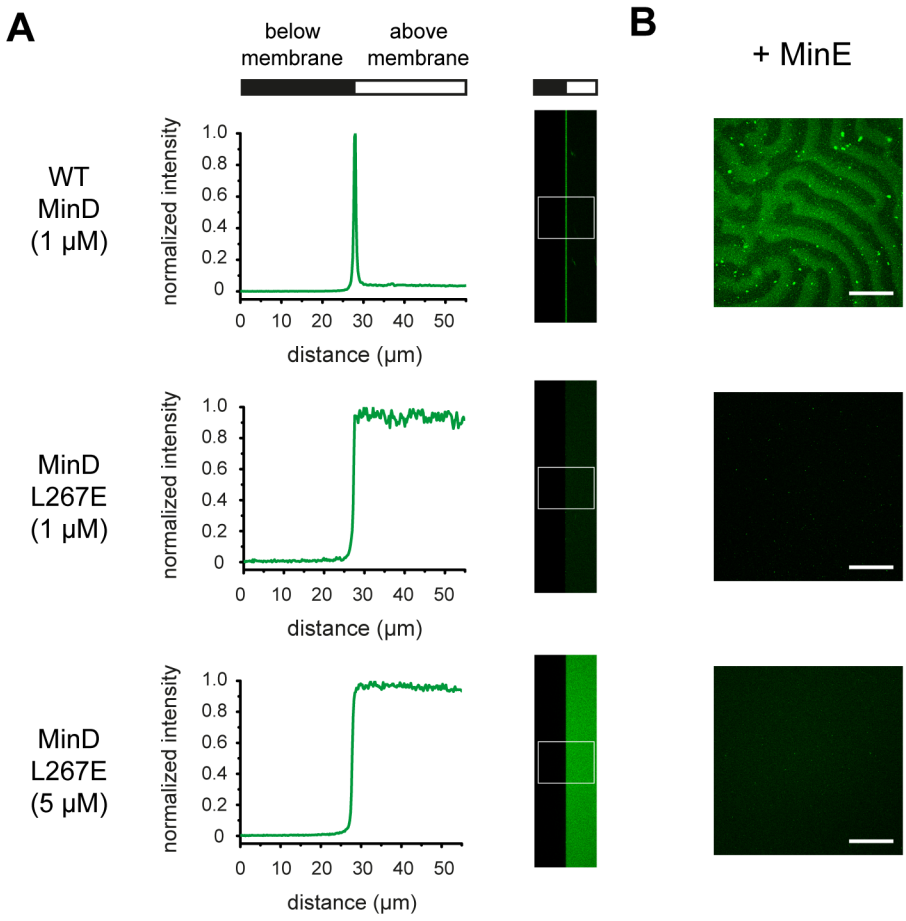

Figure 4.18: A mutation impairing MinD membrane interaction disrupts pattern formation. A) Intensity profiles along the z-axis, individually normalized to a 0-1 range, after incubation of WT MinD or MinD L267E incl. 20% WT or mutant eGFP-MinD respectively and 2.5 mM ATP with SLBs composed of *E. coli* polar lipids for 4 h. **B)** xy-images of self-organization assays in the additional presence of 1 µM MinE. Scale Bar: 50 µm.

4.4.2 Increasing MinD's membrane affinity modulates the type and properties of Min protein patterns

4.4.2.1 Membrane interaction of MinD Ins3, a mutant with increased length of the MTS

Next, we sought to characterize potential effects of increased MinD membrane affinity. For this, the amino acid sequence AKI was inserted between residues L264 and K265 of MinD's MTS, to increase its length by approximately one turn (Figure 4.19). Previously, this insertion mutant has been termed "MinD Ins3" (Szeto et al., 2002) and displayed membrane localization *in vivo*, indicating that the helicity and amphipathicity of the MTS are maintained in the mutant (Szeto et al., 2002). With its increased length, the engineered MTS is similar to the MTS of *B. subtilis* MinD, which does not require ATP-dependent dimerization for membrane binding, in contrast to *E. coli* MinD (Szeto et al., 2002). To test if our mutant also binds the membrane as an ADP-bound monomer, we performed liposome co-sedimentation assays with WT MinD and the Ins3 mutant in the presence of either ATP or ADP (Figure 4.19). As expected, the WT only co-sedimented significantly with the vesicles in the presence of ATP, but not ADP. In contrast, the Ins3 mutant showed membrane binding in the presence of both ATP and ADP (Figure 4.19). Surprisingly, the amount of ATP-bound MinD Ins3 in the pellet was not markedly higher compared to ATP-bound WT MinD or ADP-bound MinD Ins3. This may be due to saturation of membrane binding at the tested protein and vesicle concentrations in line with previously published co-sedimentation experiments (Lackner et al., 2003) and QCM-D studies (Renner and Weibel, 2012).

Future experimental studies on MinD membrane interaction with more sophisticated techniques, in particular investigations into the concentration dependence and kinetics of binding, should clarify differences between the WT and Ins3 mutant in more intricate detail. Moreover, it would be interesting to systematically compare membrane binding of MinD Ins3 in the ATP- and ADP-bound forms at lower concentrations. Nevertheless, the co-sedimentation experiment shown here is already a first indication that increasing the length of the *E. coli* MinD MTS facilitates MinD membrane interaction.

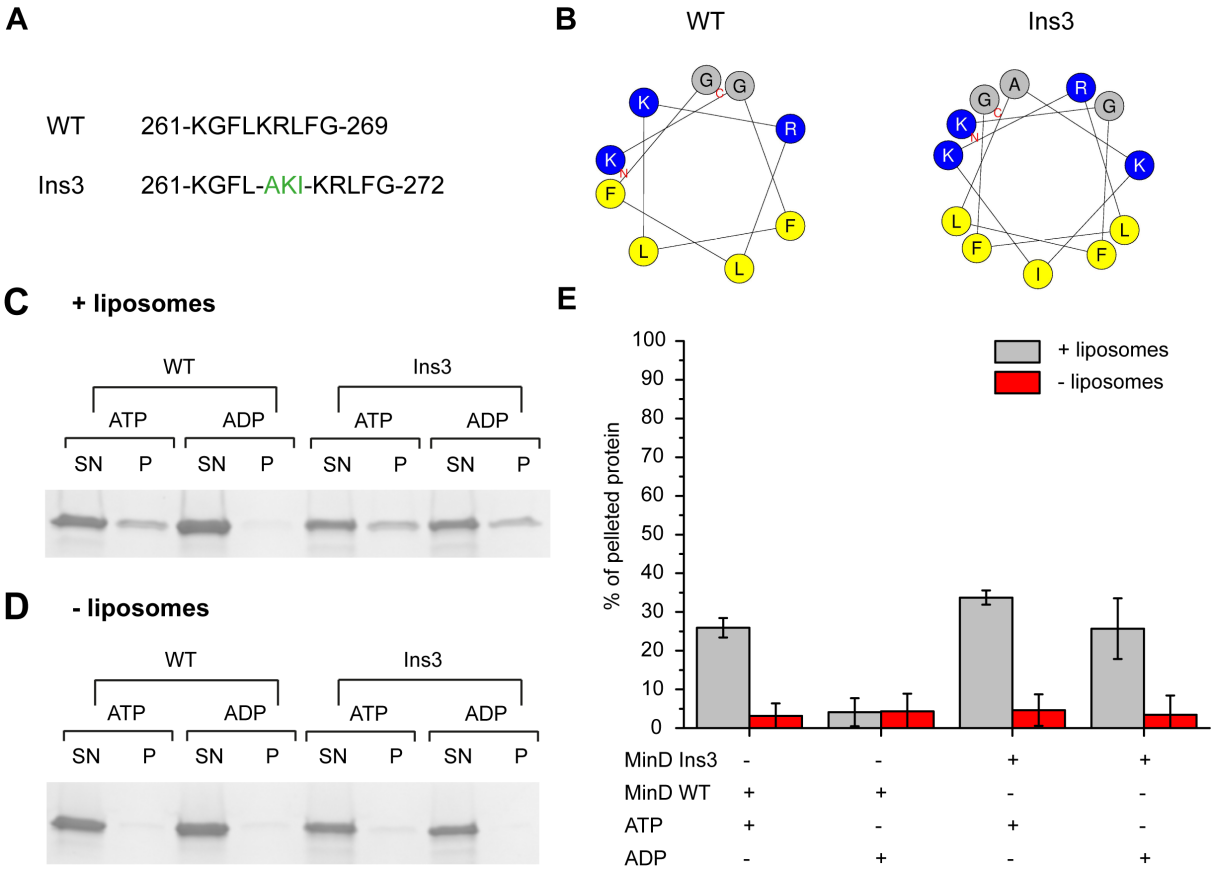

Figure 4.19: Membrane binding by a MinD mutant with increased length of the MTS. A) In the Ins3 mutant, amino acids AKI are inserted between L264 and K265 of *E. coli* MinD. **B)** Helix-wheel representation of the sequences shown in A (generated with HeliQuest Version 2). **C**, **D)** Representative SDS-PAGE fractions of liposome co-sedimentation experiments performed with 5 µM MinD in the presence of either 1 mM ATP or ADP, **C)** with, or **D)** without 0.5 mg/mL liposomes (SUVs composed of *E. coli* polar lipids). SN: supernatant. P: pellet. **E)** Percentage of pelleted protein corresponding to the gels in C and D. Error bars show standard deviations from three independent experiments.

4.4.2.2 Concentration range of pattern formation for MinD Ins3

We then investigated how increased MinD membrane affinity modulates Min protein pattern formation by reconstituting MinD Ins3 together with MinE on flat membranes. As Min protein concentrations are important regulators of pattern formation, we tested MinD concentrations ranging from 0.1 to 4 µM with MinE fixed at 1 µM (Figure 4.20). It is interesting to note that in this experiment, the WT formed patterns in a smaller range of the MinD/MinE ratio, compared to our experiments in which the MinD concentration was fixed and the MinE concentration varied (section 4.3.1.2). This observed difference is consistent with theoretical studies suggesting that both the total and relative concentrations of MinD and

MinE are important control parameters of pattern formation (Frey et al., 2018; Halatek and Frey, 2018).

Notably, we observed that both the upper and lower limits of the MinD/MinE concentration ratio supporting pattern formation were slightly reduced for the Ins3 mutant compared to the WT (Figure 4.20). Considering the antagonistic roles of MinD and MinE in pattern formation (Frey et al., 2018), this is not surprising. Below a critical MinD/MinE ratio, MinE detaches MinD so efficiently from the membrane that it cannot initiate pattern formation. On the other hand, above the upper limit of the MinD/MinE ratio, MinD membrane binding is too strong to be effectively antagonized by MinE, resulting in a homogeneous “carpet” of MinD on the membrane.

Thus, a higher membrane affinity facilitates sufficient MinD accumulation on the membrane at reduced concentrations than for the WT, leading to a reduction in the lower MinD/MinE threshold for pattern formation. Moreover, higher MinD membrane affinity would be expected to more effectively impede MinE’s removal of MinD from the membrane, such that pattern formation would cease at a reduced MinD/MinE ratio compared to the WT. In other words, for MinD variants with higher membrane affinity, a greater excess of MinE is necessary to detach MinD from the membrane, both for symmetry breaking at the upper limit and for comprehensive MinD depletion at the lower limit in the MinD/MinE ratio. Taken together, these considerations on the range of pattern formation indicate that increasing MinD membrane affinity shifts the antagonistic balance of MinD and MinE in favor of the former.

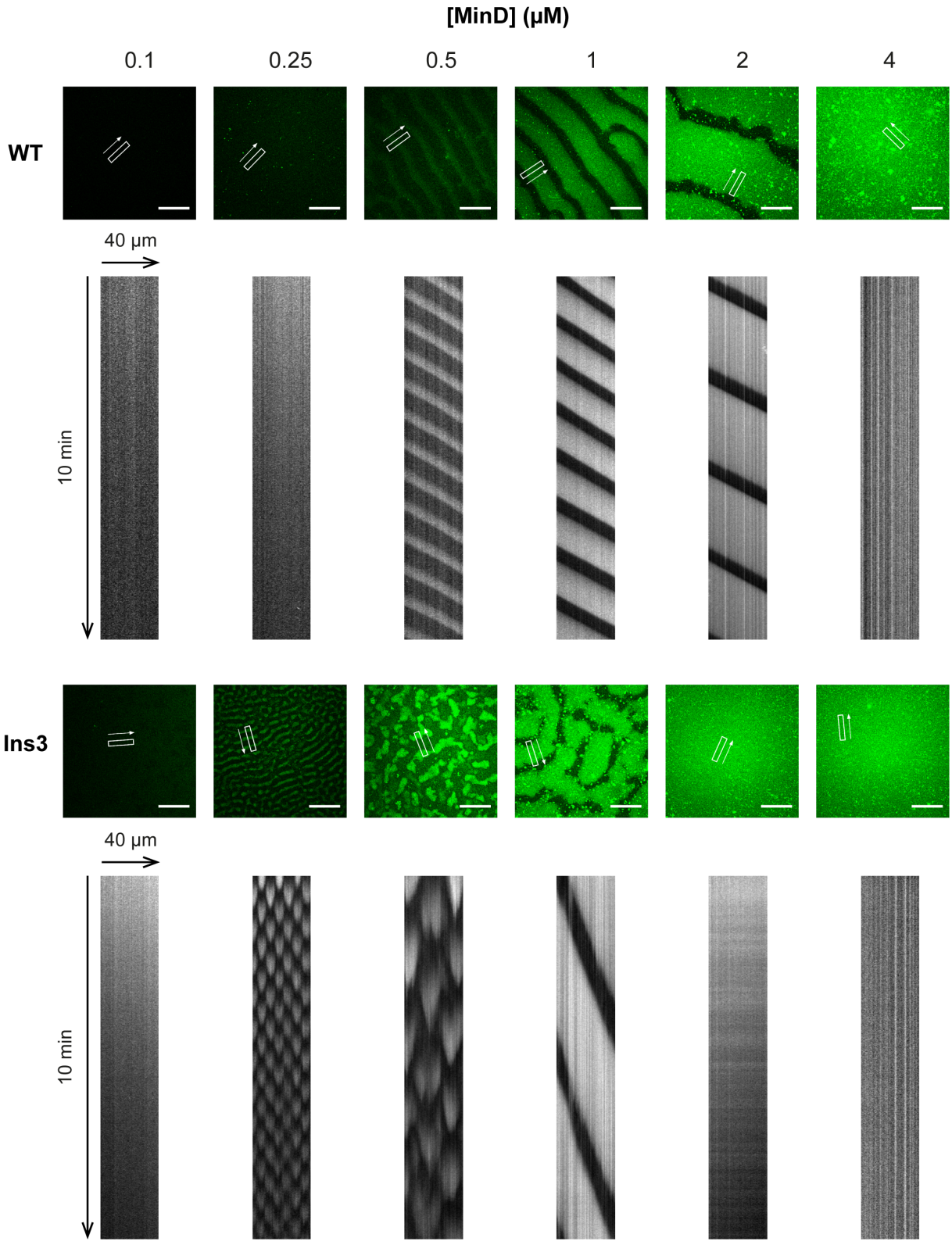

Figure 4.20: Concentration range of Min protein patterns forming with MinD Ins3. MinD incl. 20 % eGFP-MinD was reconstituted at varying concentration with 1 µM MinE incl. 10 % MinE-LD650 on flat SLBs. Confocal fluorescence micrographs and kymographs from the MinD channels are shown. (A slight decrease in intensity in some kymographs is due to bleaching or focus drift during the observation.) Scale Bar: 50 µm.

4.4.2.3 Traveling waves forming with MinD Ins3 show a reduced wave velocity

At a MinD concentration of 1 µM, we observed traveling waves for MinD Ins3, which qualitatively appeared similar to WT waves based on characteristic stripes observable in kymographs (Figure 4.20). However, compared to the WT, the mutant waves typically took longer to form, appeared more erratic and were only observed in a part of the sample's membrane.

Most notably, while the wavelength was not significantly changed between the WT and mutant patterns (Figure 4.21 A), traveling waves formed by MinD Ins3 were markedly slower than WT waves (Figure 4.21 B). This strong reduction in wave velocity demonstrates that changes in MinD membrane affinity can alter the quantitative characteristics of traveling Min protein waves.

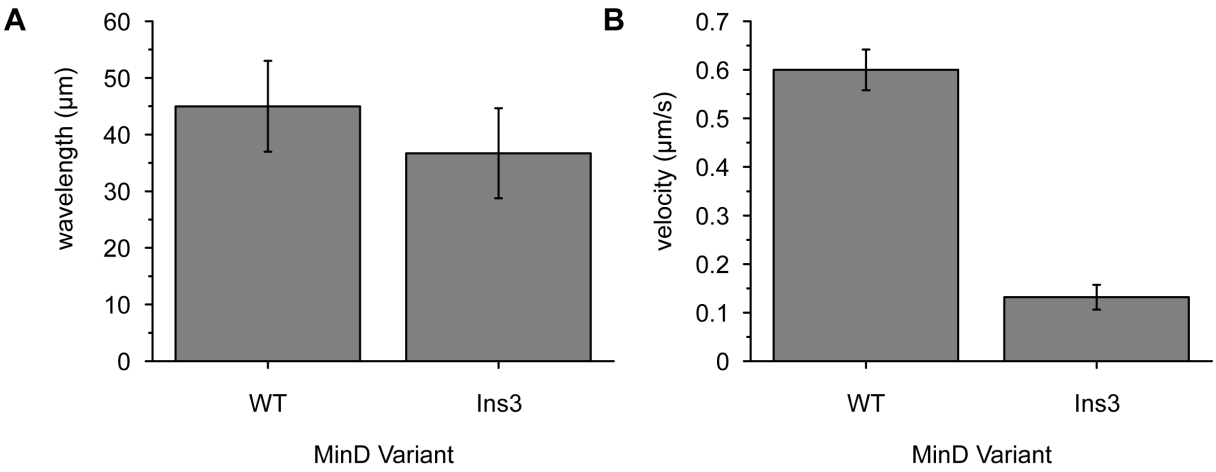

Figure 4.21: Quantitative modulation of traveling Min protein waves by MinD membrane affinity. A) Wavelength, and **B)** velocity of traveling waves formed by WT MinD or MinD Ins3 at 1 µM MinD incl. 20 % eGFP-MinD and 1 µM MinE incl. 10 % MinE-Cy5. N ≥ 6 waves from three independent experiments.

4.4.2.4 Emergence of standing wave oscillations for MinD Ins3

Next, we compared the types of patterns formed by WT MinD and the Ins3 mutant at low MinD concentrations. WT MinD formed traveling wave patterns at all concentrations within its concentration range of pattern formation. In contrast, MinD Ins3 displayed qualitatively different spatiotemporal dynamics at low MinD concentrations (0.25 – 0.5 µM) (Figure 4.20). Here, time-lapse imaging and kymograph analysis revealed that, instead of uniformly traversing a given area as traveling waves, Min proteins assembled and disassembled in two

defined and alternating membrane zones, giving rise to oscillation-type dynamics (Figure 4.20, Figure 4.22). Such spatiotemporal behavior can be described as a "standing wave" pattern and different manifestations of such dynamics have been experimentally observed in various reaction-diffusion systems (Glock et al., 2018; Kim et al., 2001; Vanag and Epstein, 2001; Vecchiarelli et al., 2016).

We further investigated MinD Ins3's standing wave dynamics by analyzing the spatiotemporal dynamics of both MinD and MinE (Figure 4.22 A-H). Similar to traveling waves, MinD and MinE co-localized on the membrane in a standing wave cycle (Figure 4.22 A-H). Moreover, within the temporal sequence of a standing-wave oscillation, MinE followed MinD (Figure 4.22 E). Thus, as is the case for traveling waves, MinE is recruited by MinD and lags behind MinD during detachment.

Perhaps the most striking difference between traveling and standing Min protein waves became apparent when averaging the fluorescence intensity over time (Figure 4.22 I-L). In this regard, traveling waves give rise to a nearly homogeneous distribution on the membrane aside from small defects that could be attributed to protein/lipid aggregates or related effects (Figure 4.22 J, L). This is expected because traveling waves uniformly traverse a given area, as evident by kymograph analysis (Figure 4.22 D, H). In contrast, in a standing-wave cycle, Min proteins oscillate between two defined spatial zones (Figure 4.22 C, G). During this process, the areas between these zones appear excluded from the Min proteins taking part in the oscillation. On time average, this gives rise to an inhomogeneous distribution of Min proteins on the membrane (Figure 4.22 I, K). In other words, standing wave oscillations cause symmetry breaking of the time-averaged protein distribution on the membrane.

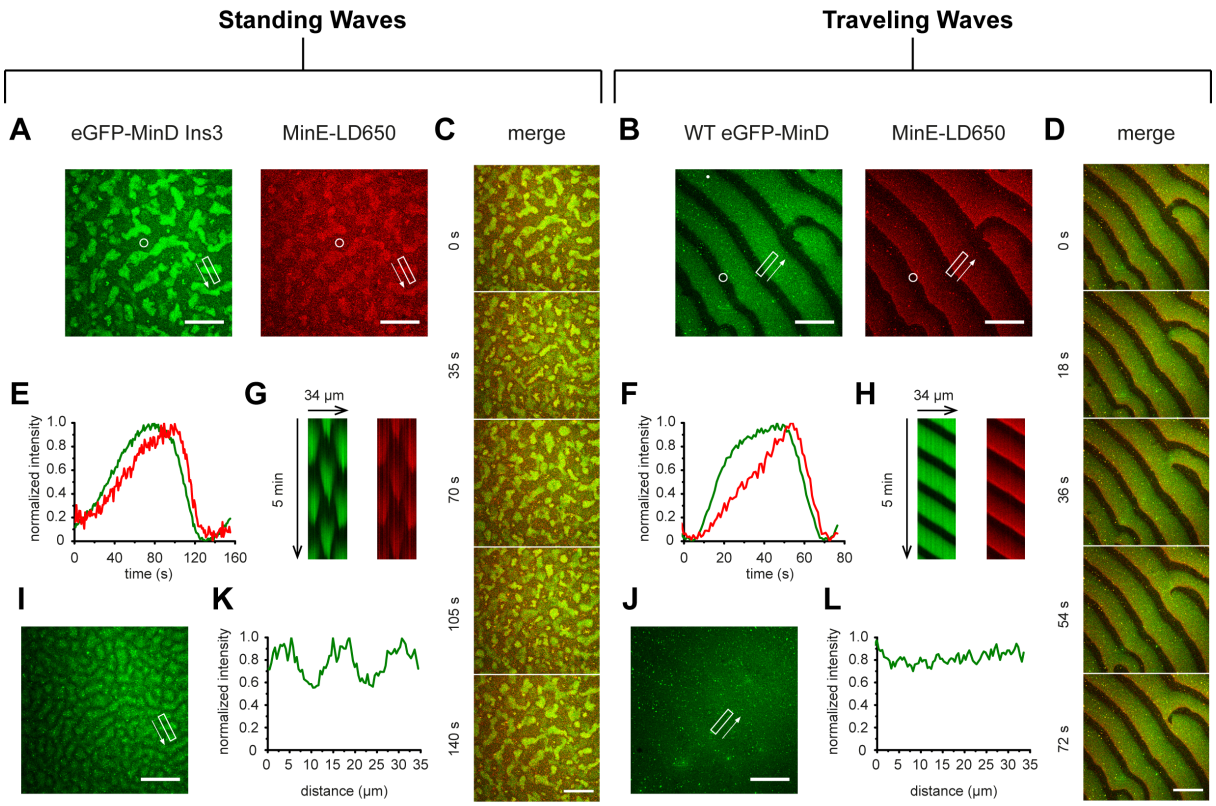

Figure 4.22: Comparison of standing and traveling Min protein waves. A, B) Confocal micrographs for **A)** standing and **B)** traveling Min waves. **C**, **D)** Temporal sequence of approximately one **C)** standing and **D)** traveling wave cycle. **E**, **F)** Wave profiles measured in the circular areas above and individually normalized to a 0-1 range. **G, H)** Kymographs measured along the rectangular areas above. **I**, **J)** eGFP-MinD intensity averaged over 5 min. **K**, **L)** Plotted time-averaged eGFP-MinD intensities for the same areas of which kymographs were obtained (G, H), individually normalized to the respective maximum value. The data for standing and traveling waves corresponds to the samples with 0.5 µM MinD Ins3 and 1 µM WT MinD respectively, each containing 20 % WT or mutant eGFP-MinD and 1 µM MinE incl. 10 % MinE-LD650, which are also shown in Figure 4.20. Scale Bar: 50 µm.

4.4.3 Discussion

Here, we demonstrated that 1) MinD membrane interaction is required for self-organization, and that 2) Min protein patterns are modulated in multiple ways by increasing MinD's membrane affinity. Besides shifting the concentration range in which patterns form, a defined insertion in MinD's MTS resulted in Min protein patterns that were either quantitatively or qualitatively distinct from WT waves depending on the MinD/MinE ratio. These diverse effects establish MinD membrane affinity as an important modulatory parameter controlling the emergent behaviors of the Min system.

The most surprising result was the occurrence of standing wave oscillations for MinD Ins3. These dynamics are qualitatively similar to patterns that have previously been observed when Min proteins were optically forced into a "resonance pattern" (Glock et al., 2018) or were depleted from the bulk using a flow-cell (Vecchiarelli et al., 2016). In the latter study, standing wave oscillations were described as "bursts" or "zebra" patterns based on their appearance as roundish patches or more regular waves respectively (Vecchiarelli et al., 2016). Although we also observed different degrees of regularity at varying MinD/MinE ratios, we base our classification as standing waves on a characteristic oscillation-type kymograph pattern (Figure 4.20 and Figure 4.22). In this regard, the mutant's standing waves also resemble the *in vivo* oscillations of WT Min proteins (Figure 2.7 in section 2.3.2) (Raskin and de Boer, 1999b). Remarkably, just as a concentration gradient with minimum at mid-cell forms on time average *in vivo*, we observed time-averaged symmetry breaking for MinD Ins3's standing wave oscillations on flat membranes. In future experiments, it will be interesting to test if this time-averaged pattern can localize downstream targets on flat membranes when the system is combined with effector molecules.

As standing waves can be brought about by different means, the question arises if there is a common mechanistic basis to generate this specific pattern as opposed to other outcomes of self-organization. Although more experimental and theoretical studies will be required to definitively address this point, comparisons with *in vivo* oscillations and standing-wave-like patterns in the presence of flow may suggest a common feature. In both cases, MinD is largely depleted from the bulk during membrane association. Similarly, for low concentrations of MinD Ins3, it may be possible that MinD Ins3's high membrane affinity allows for the mutant's depletion from the bulk during membrane association, thus enabling locally synchronized binding and unbinding cycles. Although such hypothetical depletion

remains to be confirmed experimentally, this would explain why standing waves did not form at higher mutant concentrations or for WT MinD, as the pool of excess proteins in the bulk would eventually grow with higher protein concentrations in the bulk volume and lower membrane affinity.

Assuming that bulk depletion is indeed associated with the standing waves observed for MinD Ins3, it would be interesting to theoretically analyze its role in standing wave formation by means of mathematical modeling. Furthermore, it would be interesting to test theoretically if current mathematical models of the Min system reproduce the shift in the concentration range of pattern formation, observed for MinD Ins3 (Figure 4.20) and if so, under which conditions on the rate constants in the system. This could reveal new insights into the interdependence of different processes in the Min system, such as nucleotide exchange, MinD membrane attachment and MinD and MinE protein interactions.

With regard to future experiments, it would be important to further characterize MinD membrane binding for the WT and Ins3 mutant under the concentrations giving rise to the different patterns. For example, the fraction of ADP- and ATP-bound proteins attached to the membrane could be determined for the different concentrations. Furthermore, it would be intriguing to determine potential thresholds in the attachment and detachment rates allowing for pattern formation as well as those separating the standing and traveling wave regimes. Lastly, it would be interesting to systematically investigate, in a concentration-dependent fashion, how such factors influence the Min system's ATPase rate and the system's behavior in cell-like geometry. A better understanding of binding and unbinding processes, as well their interdependence with other factors like concentration, could ultimately reveal a mechanistic basis for the emergence of standing waves as well as the reduction in wave velocity observed for traveling waves forming at higher concentrations of MinD Ins3.

In summary, MinD membrane affinity is both an essential requirement for Min protein patterns to form, and also an important modulatory parameter to tune their qualitative and quantitative characteristics. The mechanistic basis for both types of modulation constitutes an important direction for future experimental and theoretical studies.

5 Concluding remarks and outlook

The objective of this thesis was to gain novel insights into how the emergent properties of large-scale protein patterns are determined by the molecular features of the underlying self-organizing proteins. To address this question, we applied a reverse engineering approach to the *E. coli* Min system, an archetypal example of protein pattern formation on lipid membranes. In particular, we analyzed pattern formation by mutant proteins of the peripherally membrane-binding ATPase MinD and its activating protein MinE by combining *in vitro* self-organization experiments, biochemical assays and, in one case, mathematical modeling.

First, our study confirmed that both MinD's attachment to the lipid membrane and the stimulation of its ATPase activity by MinE are essential for pattern formation (sections 4.1 and 4.4). Second, our analysis yielded detailed insights into how the degree of MinD ATPase stimulation by MinE, the membrane affinities of MinD and MinE as well as Min protein concentrations regulate the emergent properties of Min protein patterns (all sections). Of particular note, we demonstrated that MinE membrane interaction is not required for pattern formation *per se* but restrains MinE's capacity to stimulate MinD's ATPase activity, increases the lower limit of the patterns' length scale and adapts the system for robust gradient formation in cell-like geometry (section 4.2). Third, our study generally highlights that the emergent properties of Min protein patterns are remarkably sensitive to changes in the molecular properties and concentrations of Min proteins. Such sensitivity makes the Min system vulnerable, as a desired pattern or gradient can easily be lost, but also versatile, allowing for facile adaptation of its dynamic behavior.

Importantly, while an easy adjustment of a pattern's detailed features may be desirable, the propensity of pattern formation *per se* (regardless of the patterns' detailed characteristics) should be robust in a broad range of parameters. With a combination of mathematical modeling and *in vitro* reconstitution, we revealed that robustness against variations in protein concentration is conferred by conformational switching between reactive and latent MinE conformations (section 4.3). Besides resolving a point of conflict between previous experiments and models, this demonstrates that MinE's conformational change is another non-essential, but regulatory important molecular feature for pattern formation.

In summary, the attachment of MinD to the membrane and its subsequent release by MinE constitutes the core cycle underlying Min protein dynamics, as is also reflected in mathematical models of Min protein self-organization (Frey et al., 2018). On top of this cycle, molecular features like MinE's conformational switch or its interaction with the membrane serve to confer robustness and, together with the essential processes of MinD membrane interaction and ATPase stimulation as well as protein concentrations, determine the detailed properties of Min protein patterns.

It is generally known that reaction-diffusion networks are sensitive to changes in the system's components. However, the resulting effects can typically not be predicted intuitively due to the interplay of different parameters as well as the non-linearity of the underlying interactions. For example, our research as well as previous studies have established that the Min system's dynamic behavior in cell-like geometry is modulated by at least three types of independent, experimentally tractable variables, including 1) the biochemical properties of Min proteins, 2) Min protein concentrations, as well as 3) the geometric boundary conditions, and that changes in different parameters partially result in similar effects (sections 4.1 and 4.2) (Amiranashvili et al., 2016; Bonny et al., 2013; Caspi and Dekker, 2016; Hale et al., 2001; Wu et al., 2016; Zieske and Schwille, 2014). All of these variables affect interaction kinetics, which in turn regulate the system's effective ATPase rate and the length scale of Min patterns. While this example illustrates the challenge of disentangling the influence of various parameters, it also affirms the notion that the Min system's emergent behavior is ultimately determined by a combination of different factors (Frey et al., 2018). Although a comprehensive mechanistic framework integrating all known regulatory features remains to be developed through future experimental and theoretical studies, our systematic investigation of the effects of protein features and concentrations can serve as a valuable resource of how various factors influence pattern formation. As such, it can support a fruitful cycle between theory and experiment by providing a test bed for mathematical models of Min protein formation, as already started in this work (section 4.3)

Thus, in the near term, experimental studies could further characterize the conditions allowing for pattern formation as well as those giving rise to specific types of patterns. For example, by characterizing MinD membrane interaction quantitatively for the WT and Ins3 mutant, it may be possible to reveal thresholds in kinetic rates that separate the traveling and standing wave regimes. Similarly, elucidating the mechanisms underlying the formation of distinct types of Min patterns would greatly benefit from a better understanding of the molecular-level processes giving rise to the observed cooperativity during MinD membrane binding (Lackner

et al., 2003; Renner and Weibel, 2012). Furthermore, it will be interesting to experimentally and theoretically deepen the focus on other properties of Min proteins that are currently not incorporated in mathematical models, such as Min protein dimerization (Pichoff et al., 1995) or potential higher-order oligomerization (Miyagi et al., 2018; Zheng et al., 2014).

In the long term, the results gained here could guide the *de novo* design and synthesis of an artificial self-organizing system. Such a system, based on proteins or other biomolecules, could be used to test the generality of the conclusions drawn here from the Min system. As the components would not be constrained by the outcome of natural evolution, it could also serve as an alternative platform to systematically investigate parameters' roles in reaction-diffusion systems. Thus, reverse and forward engineering approaches promise to synergistically uncover novel principles of protein pattern formation.

6 Bibliography

Adler, H.I., Fisher, W.D., Cohen, A., and Hardigree, A.A. (1967). Miniature *Escherichia coli* cells deficient in DNA. Proceedings of the National Academy of Sciences of the United States of America *57*, 321-326.

Agladze, K., Krinsky, V., and Pertsov, A. (1984). Chaos in the non-stirred Belousov–Zhabotinsky reaction is induced by interaction of waves and stationary dissipative structures. Nature *308*, 834.

Amiranashvili, A., Schnellbacher, N.D., and Schwarz, U.S. (2016). Stochastic switching between multistable oscillation patterns of the Min-system. New J Phys *18*.

Arumugam, S., Petrasek, Z., and Schwille, P. (2014). MinCDE exploits the dynamic nature of FtsZ filaments for its spatial regulation. Proceedings of the National Academy of Sciences of the United States of America *111*, E1192-1200.

Ayed, S.H., Cloutier, A.D., McLeod, L.J., Foo, A.C.Y., Damry, A.M., and Goto, N.K. (2017). Dissecting the role of conformational change and membrane binding by the bacterial cell division regulator MinE in the stimulation of MinD ATPase activity. The Journal of Biological Chemistry *292*, 20732-20743.

Bader, S., Kuhner, S., and Gavin, A.C. (2008). Interaction networks for systems biology. FEBS Letters *582*, 1220-1224.

Bange, G., and Sinning, I. (2013). SIMIBI twins in protein targeting and localization. Nature Structural & Molecular Biology *20*, 776-780.

Belousov, B. (1958). Sbornik Referator po Radiatsioni Medizin (conference proceedings) p. 145.

Bement, W.M., Leda, M., Moe, A.M., Kita, A.M., Larson, M.E., Golding, A.E., Pfeuti, C., Su, K.C., Miller, A.L., Goryachev, A.B.*, et al.* (2015). Activator-inhibitor coupling between Rho signalling and actin assembly makes the cell cortex an excitable medium. Nature Cell Biology *17*, 1471-1483.

Berman, H.M. (2008). The Protein Data Bank: A historical perspective. Acta Crystallographica Section A, Foundations of Crystallography *64*, 88-95.

Bernhardt, T.G., and de Boer, P.A. (2005). SlmA, a nucleoid-associated, FtsZ binding protein required for blocking septal ring assembly over chromosomes in *E. coli*. Molecular Cell *18*, 555-564.

Bi, E., and Lutkenhaus, J. (1993). Cell division inhibitors SulA and MinCD prevent formation of the FtsZ ring. Journal of Bacteriology *175*, 1118-1125.

Bi, E.F., and Lutkenhaus, J. (1991). FtsZ ring structure associated with division in *Escherichia coli*. Nature *354*, 161-164.

Bisson-Filho, A.W., Hsu, Y.P., Squyres, G.R., Kuru, E., Wu, F., Jukes, C., Sun, Y., Dekker, C., Holden, S., VanNieuwenhze, M.S.*, et al.* (2017). Treadmilling by FtsZ filaments drives peptidoglycan synthesis and bacterial cell division. Science *355*, 739-743.

Bonny, M., Fischer-Friedrich, E., Loose, M., Schwille, P., and Kruse, K. (2013). Membrane Binding of MinE Allows for a Comprehensive Description of Min-Protein Pattern Formation. PLoS Computational Biology *9*, e1003347.

Bornhorst, J.A., and Falke, J.J. (2000). Purification of proteins using polyhistidine affinity tags. Methods in Enzymology *326*, 245-254.

Bradford, M.M. (1976). A rapid and sensitive method for the quantitation of microgram quantities of protein utilizing the principle of protein-dye binding. Analytical Biochemistry *72*, 248-254.

Bramkamp, M., Emmins, R., Weston, L., Donovan, C., Daniel, R.A., and Errington, J. (2008). A novel component of the division-site selection system of *Bacillus subtilis* and a new mode of action for the division inhibitor MinCD. Molecular Microbiology *70*, 1556-1569.

Bramkamp, M., and van Baarle, S. (2009). Division site selection in rod-shaped bacteria. Current Opinion in Microbiology *12*, 683-688.

Camazine, S., Deneubourg, J.-L., Franks, N.R., Sneyd, J., Theraulaz, G., and Bonabeau, E. (2001). Self-organization in biological systems (Princeton, N.J.: Princeton University Press).

Caspi, Y., and Dekker, C. (2016). Mapping out Min protein patterns in fully confined fluidic chambers. eLife *5*, e19271

Chang, Y.G., Cohen, S.E., Phong, C., Myers, W.K., Kim, Y.I., Tseng, R., Lin, J., Zhang, L., Boyd, J.S., Lee, Y., *et al.* (2015). Circadian rhythms. A protein fold switch joins the circadian oscillator to clock output in cyanobacteria. Science *349*, 324-328.

Chen, A.H., Lubkowicz, D., Yeong, V., Chang, R.L., and Silver, P.A. (2015). Transplantability of a circadian clock to a noncircadian organism. Science Advances *1*, no. 5, e1500358 DOI: 10.1126/sciadv.1500358

Coltharp, C., Buss, J., Plumer, T.M., and Xiao, J. (2016). Defining the rate-limiting processes of bacterial cytokinesis. Proceedings of the National Academy of Sciences of the United States of America *113*, E1044-1053.

Corbin, B.D., Yu, X.C., and Margolin, W. (2002). Exploring intracellular space: Function of the Min system in round-shaped *Escherichia coli*. The EMBO Journal *21*, 1998-2008.

Cordell, S.C., Anderson, R.E., and Lowe, J. (2001). Crystal structure of the bacterial cell division inhibitor MinC. The EMBO Journal *20*, 2454-2461.

Coyle, S.M., and Lim, W.A. (2016). Mapping the functional versatility and fragility of Ras GTPase signaling circuits through *in vitro* network reconstitution. eLife *5*, e12435

D'Avino, P.P., Giansanti, M.G., and Petronczki, M. (2015). Cytokinesis in animal cells. Cold Spring Harbor Perspectives in Biology *7*, a015834.

Dajkovic, A., Lan, G., Sun, S.X., Wirtz, D., and Lutkenhaus, J. (2008). MinC spatially controls bacterial cytokinesis by antagonizing the scaffolding function of FtsZ. Current Biology : CB *18*, 235-244.

de Boer, P.A., Crossley, R.E., Hand, A.R., and Rothfield, L.I. (1991). The MinD protein is a membrane ATPase required for the correct placement of the *Escherichia coli* division site. The EMBO Journal *10*, 4371-4380.

de Boer, P.A., Crossley, R.E., and Rothfield, L.I. (1988). Isolation and properties of *minB*, a complex genetic locus involved in correct placement of the division site in *Escherichia coli*. Journal of Bacteriology *170*, 2106-2112.

de Boer, P.A., Crossley, R.E., and Rothfield, L.I. (1989). A division inhibitor and a topological specificity factor coded for by the minicell locus determine proper placement of the division septum in *E. coli*. Cell *56*, 641-649.

Denk, J., Kretschmer, S., Halatek, J., Hartl, C., Schwille, P., and Frey, E. (2018). MinE conformational switching confers robustness on self-organized Min protein patterns. Proceedings of the National Academy of Sciences of the United States of America. 201719801; https://doi.org/10.1073/pnas.1719801115

Di Ventura, B., and Sourjik, V. (2011). Self-organized partitioning of dynamically localized proteins in bacterial cell division. Molecular Systems Biology *7*, 457.

Driever, W., and Nusslein-Volhard, C. (1988a). The bicoid protein determines position in the *Drosophila* embryo in a concentration-dependent manner. Cell *54*, 95-104.

Driever, W., and Nusslein-Volhard, C. (1988b). A gradient of bicoid protein in *Drosophila* embryos. Cell *54*, 83-93.

Elowitz, M.B., and Leibler, S. (2000). A synthetic oscillatory network of transcriptional regulators. Nature *403*, 335-338.

Fange, D., and Elf, J. (2006). Noise-induced Min phenotypes in *E. coli*. PLoS Computational Biology *2*, e80.

Fleurie, A., Lesterlin, C., Manuse, S., Zhao, C., Cluzel, C., Lavergne, J.P., Franz-Wachtel, M., Macek, B., Combet, C., Kuru, E.*, et al.* (2014). MapZ marks the division sites and positions FtsZ rings in *Streptococcus pneumoniae*. Nature *516*, 259-262.

Frey, E., Halatek, J., Kretschmer, S., and Schwille, P. (2018). Protein Pattern Formation. In Physics of Biological Membranes, eds. P. Bassereau P.C.A. Sens (Springer-Verlag GmbH, Heidelberg), *In press*; Preprint: arXiv:1801.01365.

Fu, X., Shih, Y.L., Zhang, Y., and Rothfield, L.I. (2001). The MinE ring required for proper placement of the division site is a mobile structure that changes its cellular location during the *Escherichia coli* division cycle. Proceedings of the National Academy of Sciences of the United States of America *98*, 980-985.

Gardner, T.S., Cantor, C.R., and Collins, J.J. (2000). Construction of a genetic toggle switch in *Escherichia coli*. Nature *403*, 339-342.

Ghasriani, H., Ducat, T., Hart, C.T., Hafizi, F., Chang, N., Al-Baldawi, A., Ayed, S.H., Lundstrom, P., Dillon, J.A., and Goto, N.K. (2010). Appropriation of the MinD protein-interaction motif by the dimeric interface of the bacterial cell division regulator MinE. Proceedings of the National Academy of Sciences of the United States of America *107*, 18416-18421.

Ghosal, D., Trambaiolo, D., Amos, L.A., and Lowe, J. (2014). MinCD cell division proteins form alternating copolymeric cytomotive filaments. Nature Communications *5*, 5341.

Gierer, A., and Meinhardt, H. (1972). Theory of Biological Pattern Formation. Kybernetik *12*, 30-39.

Glock, P., Broichhagen, J., Kretschmer, S., Blumhardt, P., Mucksch, J., Trauner, D., and Schwille, P. (2018). Optical Control of a Biological Reaction-Diffusion System. Angewandte Chemie *57*, 2362-2366.

Goehring, N.W., Trong, P.K., Bois, J.S., Chowdhury, D., Nicola, E.M., Hyman, A.A., and Grill, S.W. (2011). Polarization of PAR proteins by advective triggering of a pattern-forming system. Science *334*, 1137-1141.

Haeusser, D.P., and Margolin, W. (2016). Splitsville: Structural and functional insights into the dynamic bacterial Z ring. Nature Reviews Microbiology *14*, 305-319.

Halatek, J., and Frey, E. (2012). Highly canalized MinD transfer and MinE sequestration explain the origin of robust MinCDE-protein dynamics. Cell Reports *1*, 741-752.

Halatek, J., and Frey, E. (2014). Effective 2D model does not account for geometry sensing by self-organized proteins patterns. Proceedings of the National Academy of Sciences of the United States of America *111*, E1817.

Halatek, J., and Frey, E. (2018). Rethinking pattern formation in reaction–diffusion systems. Nat Phys, 10.1038/s41567-017-0040-5.

Hale, C.A., and de Boer, P.A. (1997). Direct binding of FtsZ to ZipA, an essential component of the septal ring structure that mediates cell division in *E. coli*. Cell *88*, 175-185.

Hale, C.A., Meinhardt, H., and de Boer, P.A. (2001). Dynamic localization cycle of the cell division regulator MinE in *Escherichia coli*. The EMBO Journal *20*, 1563-1572.

Howard, M., Rutenberg, A.D., and de Vet, S. (2001). Dynamic compartmentalization of bacteria: Accurate division in *E. coli*. Phys Rev Lett *87*, 278102.

Hsieh, C.W., Lin, T.Y., Lai, H.M., Lin, C.C., Hsieh, T.S., and Shih, Y.L. (2010). Direct MinE-membrane interaction contributes to the proper localization of MinDE in *E. coli*. Molecular Microbiology *75*, 499-512.

Hu, L., Vecchiarelli, A.G., Mizuuchi, K., Neuman, K.C., and Liu, J. (2017). Brownian ratchet mechanisms of ParA-mediated partitioning. Plasmid *92*, 12-16.

Hu, Z., Gogol, E.P., and Lutkenhaus, J. (2002). Dynamic assembly of MinD on phospholipid vesicles regulated by ATP and MinE. Proceedings of the National Academy of Sciences of the United States of America *99*, 6761-6766.

Hu, Z., and Lutkenhaus, J. (1999). Topological regulation of cell division in *Escherichia coli* involves rapid pole to pole oscillation of the division inhibitor MinC under the control of MinD and MinE. Molecular Microbiology *34*, 82-90.

Hu, Z., and Lutkenhaus, J. (2000). Analysis of MinC reveals two independent domains involved in interaction with MinD and FtsZ. Journal of Bacteriology *182*, 3965-3971.

Hu, Z., and Lutkenhaus, J. (2001). Topological regulation of cell division in *E. coli*: Spatiotemporal oscillation of MinD requires stimulation of its ATPase by MinE and phospholipid. Molecular Cell *7*, 1337-1343.

Hu, Z., and Lutkenhaus, J. (2003). A conserved sequence at the C-terminus of MinD is required for binding to the membrane and targeting MinC to the septum. Molecular Microbiology *47*, 345-355.

Hu, Z., Mukherjee, A., Pichoff, S., and Lutkenhaus, J. (1999). The MinC component of the division site selection system in *Escherichia coli* interacts with FtsZ to prevent polymerization. Proceedings of the National Academy of Sciences of the United States of America *96*, 14819-14824.

Hu, Z., Saez, C., and Lutkenhaus, J. (2003). Recruitment of MinC, an inhibitor of Z-ring formation, to the membrane in *Escherichia coli*: Role of MinD and MinE. Journal of Bacteriology *185*, 196-203.

Huang, K.C., Meir, Y., and Wingreen, N.S. (2003). Dynamic structures in *Escherichia coli*: Spontaneous formation of MinE rings and MinD polar zones. Proceedings of the National Academy of Sciences of the United States of America *100*, 12724-12728.

Hutchison, C.A., 3rd, Chuang, R.Y., Noskov, V.N., Assad-Garcia, N., Deerinck, T.J., Ellisman, M.H., Gill, J., Kannan, K., Karas, B.J., Ma, L.*, et al.* (2016). Design and synthesis of a minimal bacterial genome. Science *351*, aad6253.

Isalan, M., Lemerle, C., and Serrano, L. (2005). Engineering gene networks to emulate *Drosophila* embryonic pattern formation. PLoS Biology *3*, e64.

Ivanov, V., and Mizuuchi, K. (2010). Multiple modes of interconverting dynamic pattern formation by bacterial cell division proteins. Proceedings of the National Academy of Sciences of the United States of America *107*, 8071-8078.

Jakubith, S., Rotermund, H.H., Engel, W., Vonoertzen, A., and Ertl, G. (1990). Spatiotemporal Concentration Patterns in a Surface-Reaction - Propagating and Standing Waves, Rotating Spirals, and Turbulence. Phys Rev Lett *65*, 3013-3016.

Karr, J.R., Sanghvi, J.C., Macklin, D.N., Gutschow, M.V., Jacobs, J.M., Bolival, B., Jr., Assad-Garcia, N., Glass, J.I., and Covert, M.W. (2012). A whole-cell computational model predicts phenotype from genotype. Cell *150*, 389-401.

Karsenti, E. (2008). Self-organization in cell biology: A brief history. Nature Reviews Molecular Cell Biology *9*, 255-262.

Karzbrun, E., Tayar, A.M., Noireaux, V., and Bar-Ziv, R.H. (2014). Synthetic biology. Programmable on-chip DNA compartments as artificial cells. Science *345*, 829-832.

Kasten, F.H. (1996). Paul Ehrlich: Pathfinder in Cell Biology. 1. Chronicle of His Life and Accomplishments in Immunology, Cancer Research, and Chemotherapy. Biotechnic & Histochemistry : official publication of the Biological Stain Commission *71*, 2-37. p. 5

Kim, M., Bertram, M., Pollmann, M., von Oertzen, A., Mikhailov, A.S., Rotermund, H.H., and Ertl, G. (2001). Controlling chemical turbulence by global delayed feedback: Pattern formation in catalytic CO oxidation on Pt(110). Science *292*, 1357-1360.

Kondo, S., and Miura, T. (2010). Reaction-diffusion model as a framework for understanding biological pattern formation. Science *329*, 1616-1620.

Kozubowski, L., Saito, K., Johnson, J.M., Howell, A.S., Zyla, T.R., and Lew, D.J. (2008). Symmetry-breaking polarization driven by a Cdc42p GEF-PAK complex. Current Biology : CB *18*, 1719-1726.

Kretschmer, S., Harrington, L., and Schwille, P. (2018). Reverse and forward engineering of protein pattern formation. Philosophical transactions of the Royal Society of London Series B, Biological Sciences *373*: 20170104. http://dx.doi.org/10.1098/rstb.2017.0104.

Kretschmer, S., and Schwille, P. (2016). Pattern formation on membranes and its role in bacterial cell division. Current Opinion in Cell Biology *38*, 52-59.

Kretschmer, S., Zieske, K., and Schwille, P. (2017). Large-scale modulation of reconstituted Min protein patterns and gradients by defined mutations in MinE's membrane targeting sequence. PloS One *12*, e0179582.

Kruse, K. (2002). A dynamic model for determining the middle of *Escherichia coli*. Biophys J *82*, 618-627.

Kuhner, S., van Noort, V., Betts, M.J., Leo-Macias, A., Batisse, C., Rode, M., Yamada, T., Maier, T., Bader, S., Beltran-Alvarez, P.*, et al.* (2009). Proteome organization in a genome-reduced bacterium. Science *326*, 1235-1240.

Lackner, L.L., Raskin, D.M., and de Boer, P.A. (2003). ATP-dependent interactions between *Escherichia coli* Min proteins and the phospholipid membrane *in vitro*. Journal of Bacteriology *185*, 735-749.

Laemmli, U.K. (1970). Cleavage of structural proteins during the assembly of the head of bacteriophage T4. Nature *227*, 680-685.

Lee, P.Y., Costumbrado, J., Hsu, C.Y., and Kim, Y.H. (2012). Agarose gel electrophoresis for the separation of DNA fragments. Journal of Visualized Experiments : JoVE *62*, 3923

Leipe, D.D., Wolf, Y.I., Koonin, E.V., and Aravind, L. (2002). Classification and evolution of P-loop GTPases and related ATPases. Journal of Molecular Biology *317*, 41-72.

Lenarcic, R., Halbedel, S., Visser, L., Shaw, M., Wu, L.J., Errington, J., Marenduzzo, D., and Hamoen, L.W. (2009). Localisation of DivIVA by targeting to negatively curved membranes. The EMBO Journal *28*, 2272-2282.

Loose, M., Fischer-Friedrich, E., Herold, C., Kruse, K., and Schwille, P. (2011a). Min protein patterns emerge from rapid rebinding and membrane interaction of MinE. Nature Structural & Molecular Biology *18*, 577-583.

Loose, M., Fischer-Friedrich, E., Ries, J., Kruse, K., and Schwille, P. (2008). Spatial regulators for bacterial cell division self-organize into surface waves *in vitro*. Science *320*, 789-792.

Loose, M., Kruse, K., and Schwille, P. (2011b). Protein self-organization: Lessons from the Min system. Annual Review of Biophysics *40*, 315-336.

Loose, M., and Mitchison, T.J. (2014). The bacterial cell division proteins FtsA and FtsZ self-organize into dynamic cytoskeletal patterns. Nature Cell Biology *16*, 38-46.

Lutkenhaus, J. (2012). The ParA/MinD family puts things in their place. Trends in Microbiology *20*, 411-418.

Lutkenhaus, J., and Sundaramoorthy, M. (2003). MinD and role of the deviant Walker A motif, dimerization and membrane binding in oscillation. Molecular Microbiology *48*, 295-303.

Ma, L., King, G.F., and Rothfield, L. (2004). Positioning of the MinE binding site on the MinD surface suggests a plausible mechanism for activation of the *Escherichia coli* MinD ATPase during division site selection. Molecular Microbiology *54*, 99-108.

Ma, L.Y., King, G., and Rothfield, L. (2003). Mapping the MinE site involved in interaction with the MinD division site selection protein of *Escherichia coli*. Journal of Bacteriology *185*, 4948-4955.

Marquardt, M. (1951) Paul Ehrlich (Springer-Verlag GmbH, Berlin-Goettingen-Heidelberg), p. 10

Martos, A., Jimenez, M., Rivas, G., and Schwille, P. (2012). Towards a bottom-up reconstitution of bacterial cell division. Trends in Cell Biology *22*, 634-643.

Martos, A., Petrasek, Z., and Schwille, P. (2013). Propagation of MinCDE waves on free-standing membranes. Environmental Microbiology *15*, 3319-3326.

McGill, R., Tukey, J.W., and Larsen, W.A. (1978). Variations of box plots. The American Statistician *32*, 12-16.

Meinhardt, H., and de Boer, P.A. (2001). Pattern formation in *Escherichia coli*: A model for the pole-to-pole oscillations of Min proteins and the localization of the division site. Proceedings of the National Academy of Sciences of the United States of America *98*, 14202-14207.

Mileykovskaya, E., and Dowhan, W. (2005). Role of membrane lipids in bacterial division-site selection. Current Opinion in Microbiology *8*, 135-142.

Mileykovskaya, E., Fishov, I., Fu, X., Corbin, B.D., Margolin, W., and Dowhan, W. (2003). Effects of phospholipid composition on MinD-membrane interactions *in vitro* and *in vivo*. The Journal of Biological Chemistry *278*, 22193-22198.

Misteli, T. (2001). The concept of self-organization in cellular architecture. The Journal of Cell Biology *155*, 181-185.

Miyagi, A., Ramm, B., Schwille, P., and Scheuring, S. (2018). High-Speed Atomic Force Microscopy Reveals the Inner Workings of the MinDE Protein Oscillator. Nano Letters *18*, 288-296.

Murzin, A.G. (2008). Biochemistry. Metamorphic proteins. Science *320*, 1725-1726.

Nakajima, M., Imai, K., Ito, H., Nishiwaki, T., Murayama, Y., Iwasaki, H., Oyama, T., and Kondo, T. (2005). Reconstitution of circadian oscillation of cyanobacterial KaiC phosphorylation *in vitro*. Science *308*, 414-415.

Niederholtmeyer, H., Sun, Z.Z., Hori, Y., Yeung, E., Verpoorte, A., Murray, R.M., and Maerkl, S.J. (2015). Rapid cell-free forward engineering of novel genetic ring oscillators. eLife *4*, e09771.

Oates, A.C., Morelli, L.G., and Ares, S. (2012). Patterning embryos with oscillations: structure, function and dynamics of the vertebrate segmentation clock. Development *139*, 625-639.

Osawa, M., Anderson, D.E., and Erickson, H.P. (2008). Reconstitution of contractile FtsZ rings in liposomes. Science *320*, 792-794.

Park, K.T., Du, S., and Lutkenhaus, J. (2015). MinC/MinD copolymers are not required for Min function. Molecular Microbiology *98*, 895-909.

Park, K.T., Villar, M.T., Artigues, A., and Lutkenhaus, J. (2017). MinE conformational dynamics regulate membrane binding, MinD interaction, and Min oscillation. Proceedings of the National Academy of Sciences of the United States of America *114*, 7497-7504.

Park, K.T., Wu, W., Battaile, K.P., Lovell, S., Holyoak, T., and Lutkenhaus, J. (2011). The Min oscillator uses MinD-dependent conformational changes in MinE to spatially regulate cytokinesis. Cell *146*, 396-407.

Park, K.T., Wu, W., Lovell, S., and Lutkenhaus, J. (2012). Mechanism of the asymmetric activation of the MinD ATPase by MinE. Molecular Microbiology *85*, 271-281.

Pichoff, S., and Lutkenhaus, J. (2005). Tethering the Z ring to the membrane through a conserved membrane targeting sequence in FtsA. Molecular Microbiology *55*, 1722-1734.

Pichoff, S., Vollrath, B., Touriol, C., and Bouche, J.P. (1995). Deletion analysis of gene *minE* which encodes the topological specificity factor of cell division in *Escherichia coli*. Molecular Microbiology *18*, 321-329.

Ramamurthi, K.S., and Losick, R. (2009). Negative membrane curvature as a cue for subcellular localization of a bacterial protein. Proceedings of the National Academy of Sciences of the United States of America *106*, 13541-13545.

Ramos, D., Ducat, T., Cheng, J., Eng, N.F., Dillon, J.A., and Goto, N.K. (2006). Conformation of the cell division regulator MinE: Evidence for interactions between the topological specificity and anti-MinCD domains. Biochemistry *45*, 4593-4601.

Raskin, D.M., and de Boer, P.A. (1997). The MinE ring: an FtsZ-independent cell structure required for selection of the correct division site in *E. coli*. Cell *91*, 685-694.

Raskin, D.M., and de Boer, P.A. (1999a). MinDE-dependent pole-to-pole oscillation of division inhibitor MinC in *Escherichia coli*. Journal of Bacteriology *181*, 6419-6424.

Raskin, D.M., and de Boer, P.A. (1999b). Rapid pole-to-pole oscillation of a protein required for directing division to the middle of *Escherichia coli*. Proceedings of the National Academy of Sciences of the United States of America *96*, 4971-4976.

Renner, L.D., and Weibel, D.B. (2012). MinD and MinE interact with anionic phospholipids and regulate division plane formation in *Escherichia coli*. The Journal of Biological Chemistry *287*, 38835-38844.

Sagués, F., and Epstein, I.R. (2003). Nonlinear chemical dynamics. Dalton T, 1201-1217.

Saiki, R.K., Gelfand, D.H., Stoffel, S., Scharf, S.J., Higuchi, R., Horn, G.T., Mullis, K.B., and Erlich, H.A. (1988). Primer-directed enzymatic amplification of DNA with a thermostable DNA polymerase. Science *239*, 487-491.

Schindelin, J., Arganda-Carreras, I., Frise, E., Kaynig, V., Longair, M., Pietzsch, T., Preibisch, S., Rueden, C., Saalfeld, S., Schmid, B.*, et al.* (2012). Fiji: An open-source platform for biological-image analysis. Nature Methods *9*, 676-682.

Schofield, W.B., Lim, H.C., and Jacobs-Wagner, C. (2010). Cell cycle coordination and regulation of bacterial chromosome segregation dynamics by polarly localized proteins. The EMBO Journal *29*, 3068-3081.

Scholes, N.S., and Isalan, M. (2017). A three-step framework for programming pattern formation. Current Opinion in Chemical Biology *40*, 1-7.

Schrödinger, E. (1944). What Is Life? The physical aspect of the living cell and mind (Cambridge University Press, Cambridge).

Schuhmacher, J.S., Thormann, K.M., and Bange, G. (2015). How bacteria maintain location and number of flagella? FEMS Microbiology Reviews *39*, 812-822.

Schumacher, D., Bergeler, S., Harms, A., Vonck, J., Huneke-Vogt, S., Frey, E., and Sogaard-Andersen, L. (2017). The PomXYZ Proteins Self-Organize on the Bacterial Nucleoid to Stimulate Cell Division. Developmental Cell *41*, 299-314 e213.

Schweizer, J., Loose, M., Bonny, M., Kruse, K., Monch, I., and Schwille, P. (2012). Geometry sensing by self-organized protein patterns. Proceedings of the National Academy of Sciences of the United States of America *109*, 15283-15288.

Schwille, P., and Diez, S. (2009). Synthetic biology of minimal systems. Crit Rev Biochem Mol *44*, 223-242.

Shamir, M., Bar-On, Y., Phillips, R., and Milo, R. (2016). SnapShot: Timescales in Cell Biology. Cell *164*, 1302-1302 e1301.

Shen, B., and Lutkenhaus, J. (2010). Examination of the interaction between FtsZ and MinCN in *E. coli* suggests how MinC disrupts Z rings. Molecular Microbiology *75*, 1285-1298.

Shih, Y.L., Fu, X., King, G.F., Le, T., and Rothfield, L. (2002). Division site placement in *E. coli*: Mutations that prevent formation of the MinE ring lead to loss of the normal midcell arrest of growth of polar MinD membrane domains. The EMBO Journal *21*, 3347-3357.

Shih, Y.L., Huang, K.F., Lai, H.M., Liao, J.H., Lee, C.S., Chang, C.M., Mak, H.M., Hsieh, C.W., and Lin, C.C. (2011). The N-terminal amphipathic helix of the topological specificity factor MinE is associated with shaping membrane curvature. PloS One *6*, e21425.

Shih, Y.L., and Zheng, M. (2013). Spatial control of the cell division site by the Min system in *Escherichia coli*. Environmental Microbiology *15*, 3229-3239.

Shiomi, D., and Margolin, W. (2007). The C-terminal domain of MinC inhibits assembly of the Z ring in *Escherichia coli*. Journal of Bacteriology *189*, 236-243.

Siegert, F., and Steinbock, O. (1994). Die Natur schlägt Wellen – Spiralwellen organisieren die Entwicklung sozialer Amöben. ed. A. Deutsch: Muster des Lebendigen - Faszination ihrer Entstehung und Simulation (Springer Fachmedien Wiesbaden; originally published by Vieweg-Verlag, Braunschweig, Wiesbaden.)

Sliusarenko, O., Heinritz, J., Emonet, T., and Jacobs-Wagner, C. (2011). High-throughput, subpixel precision analysis of bacterial morphogenesis and intracellular spatio-temporal dynamics. Molecular Microbiology *80*, 612-627.

Snijder, J., Schuller, J.M., Wiegard, A., Lossl, P., Schmelling, N., Axmann, I.M., Plitzko, J.M., Forster, F., and Heck, A.J. (2017). Structures of the cyanobacterial circadian oscillator frozen in a fully assembled state. Science *355*, 1181-1184.

Sourjik, V., and Wingreen, N.S. (2012). Responding to chemical gradients: bacterial chemotaxis. Current Opinion in Cell Biology *24*, 262-268.

Suefuji, K., Valluzzi, R., and RayChaudhuri, D. (2002). Dynamic assembly of MinD into filament bundles modulated by ATP, phospholipids, and MinE. Proceedings of the National Academy of Sciences of the United States of America *99*, 16776-16781.

Szeto, T.H., Rowland, S.L., Habrukowich, C.L., and King, G.F. (2003). The MinD membrane targeting sequence is a transplantable lipid-binding helix. The Journal of Biological Chemistry *278*, 40050-40056.

Szeto, T.H., Rowland, S.L., Rothfield, L.I., and King, G.F. (2002). Membrane localization of MinD is mediated by a C-terminal motif that is conserved across eubacteria, archaea, and chloroplasts. Proceedings of the National Academy of Sciences of the United States of America *99*, 15693-15698.

Thanbichler, M., and Shapiro, L. (2006). MipZ, a spatial regulator coordinating chromosome segregation with cell division in Caulobacter. Cell *126*, 147-162.

Touhami, A., Jericho, M., and Rutenberg, A.D. (2006). Temperature dependence of MinD oscillation in *Escherichia coli*: running hot and fast. Journal of Bacteriology *188*, 7661-7667.

Treuner-Lange, A., Aguiluz, K., van der Does, C., Gomez-Santos, N., Harms, A., Schumacher, D., Lenz, P., Hoppert, M., Kahnt, J., Munoz-Dorado, J.*, et al.* (2013). PomZ, a ParA-like protein, regulates Z-ring formation and cell division in *Myxococcus xanthus*. Molecular Microbiology *87*, 235-253.

Tseng, R., Goularte, N.F., Chavan, A., Luu, J., Cohen, S.E., Chang, Y.G., Heisler, J., Li, S., Michael, A.K., Tripathi, S.*, et al.* (2017). Structural basis of the day-night transition in a bacterial circadian clock. Science *355*, 1174-1180.

Turing, A.M. (1952). The Chemical Basis of Morphogenesis. Philos T Roy Soc B *237*, 37-72.

Vanag, V.K., and Epstein, I.R. (2001). Pattern formation in a tunable medium: The Belousov-Zhabotinsky reaction in an aerosol OT microemulsion. Phys Rev Lett *87*, 228301.

Vecchiarelli, A.G., Li, M., Mizuuchi, M., Hwang, L.C., Seol, Y., Neuman, K.C., and Mizuuchi, K. (2016). Membrane-bound MinDE complex acts as a toggle switch that drives Min oscillation coupled to cytoplasmic depletion of MinD. Proceedings of the National Academy of Sciences of the United States of America. *113*, E1479–E1488

Vecchiarelli, A.G., Li, M., Mizuuchi, M., Ivanov, V., and Mizuuchi, K. (2017). MinE recruits, stabilizes, releases, and inhibits MinD interactions with membrane to drive oscillation. bioRxiv, 109637.

Vecchiarelli, A.G., Li, M., Mizuuchi, M., and Mizuuchi, K. (2014). Differential affinities of MinD and MinE to anionic phospholipid influence Min patterning dynamics *in vitro*. Molecular Microbiology *93*, 453-463.

Willemse, J., Borst, J.W., de Waal, E., Bisseling, T., and van Wezel, G.P. (2011). Positive control of cell division: FtsZ is recruited by SsgB during sporulation of Streptomyces. Genes & Development *25*, 89-99.

Wolpert, L. (1969). Positional information and the spatial pattern of cellular differentiation. Journal of Theoretical Biology *25*, 1-47.

Wu, F., van Schie, B.G., Keymer, J.E., and Dekker, C. (2015). Symmetry and scale orient Min protein patterns in shaped bacterial sculptures. Nature Nanotechnology *10*, 719-726.

Wu, F.B., Halatek, J., Reiter, M., Kingma, E., Frey, E., and Dekker, C. (2016). Multistability and dynamic transitions of intracellular Min protein patterns. Molecular Systems Biology *12*.

Wu, L.J., and Errington, J. (2004). Coordination of cell division and chromosome segregation by a nucleoid occlusion protein in Bacillus subtilis. Cell *117*, 915-925.

Wu, L.J., and Errington, J. (2012). Nucleoid occlusion and bacterial cell division. Nature Reviews Microbiology *10*, 8-12.

Wu, W., Park, K.T., Holyoak, T., and Lutkenhaus, J. (2011). Determination of the structure of the MinD-ATP complex reveals the orientation of MinD on the membrane and the relative location of the binding sites for MinE and MinC. Molecular Microbiology *79*, 1515-1528.

Xiao, J., and Goley, E.D. (2016). Redefining the roles of the FtsZ-ring in bacterial cytokinesis. Current Opinion in Microbiology *34*, 90-96.

Yang, X., Lyu, Z., Miguel, A., McQuillen, R., Huang, K.C., and Xiao, J. (2017). GTPase activity-coupled treadmilling of the bacterial tubulin FtsZ organizes septal cell wall synthesis. Science *355*, 744-747.

Zaikin, A.N., and Zhabotinsky, A.M. (1970). Concentration wave propagation in two-dimensional liquid-phase self-oscillating system. Nature *225*, 535-537.

Zhao, C.R., de Boer, P.A., and Rothfield, L.I. (1995). Proper placement of the *Escherichia coli* division site requires two functions that are associated with different domains of the MinE protein. Proceedings of the National Academy of Sciences of the United States of America *92*, 4313-4317.

Zheng, M., Chiang, Y.L., Lee, H.L., Kong, L.R., Hsu, S.T., Hwang, I.S., Rothfield, L.I., and Shih, Y.L. (2014). Self-assembly of MinE on the membrane underlies formation of the MinE ring to sustain function of the *Escherichia coli* Min system. The Journal of Biological Chemistry *289*, 21252-21266.

Zhou, H., and Lutkenhaus, J. (2003). Membrane binding by MinD involves insertion of hydrophobic residues within the C-terminal amphipathic helix into the bilayer. Journal of Bacteriology *185*, 4326-4335.

Zieske, K., Chwastek, G., and Schwille, P. (2016). Protein Patterns and Oscillations on Lipid Monolayers and in Microdroplets. Angew Chem Int Edit *55*, 13455-13459.

Zieske, K., Schweizer, J., and Schwille, P. (2014). Surface topology assisted alignment of Min protein waves. FEBS Letters *588*, 2545-2549.

Zieske, K., and Schwille, P. (2013). Reconstitution of pole-to-pole oscillations of Min proteins in microengineered polydimethylsiloxane compartments. Angewandte Chemie *52*, 459-462.

Zieske, K., and Schwille, P. (2014). Reconstitution of self-organizing protein gradients as spatial cues in cell-free systems. eLife *3*, e03949

Zieske, K., and Schwille, P. (2015). Reconstituting geometry-modulated protein patterns in membrane compartments. Methods in Cell Biology *128*, 149-163.

7 Appendix

7.1 Protein sequences

In the following, sequences of the His-tagged WT Min proteins are shown, which have been described previously (Loose et al., 2008; Zieske et al., 2014) and were used in this work. Mutations were introduced into these proteins with the numbering corresponding to the original Min protein sequence, consistent with previous literature. The original Min protein sequence is highlighted in black, the His-tag in red, eGFP in green and linker sequences in blue.

His-MinD

MGSSHHHHHHSSGLVPRGSHMASMTGGQQMGRGSEFARIIVVTSGKGGVGKTTSSAAIATGLAQKGK
KTVVIDFDIGLRNLDLIMGCERRVVYDFVNVIQGDATLNQALIKDKRTENLYILPASQTRDKDALTREG
VAKVLDDLKAMDFEFIVCDSPAGIETGALMALYFADEAIITTNPEVSSVRDSDRILGILASKSRRAENGE
EPIKEHLLLTRYNPGRVSRGDMLSMEDVLEILRIKLVGVIPEDQSVLRASNQGEPVILDINADAGKAYAD
TVERLLGEERPFRFIEEEKKGFLKRLFGG

His-eGFP-MinD:

MGSSHHHHHHSSGLVPRGSHMASMTGGQQMGRGSVSKGEELFTGVVPILVELDGDVNGHKFSVSGEG
EGDATYGKLTLKFICTTGKLPVPWPTLVTTLTYGVQCFSRYPDHMKQHDFFKSAMPEGYVQERTIFFK
DDGNYKTRAEVKFEGDTLVNRIELKGIDFKEDGNILGHKLEYNYNSHNVYIMADKQKNGIKVNFKIRH
NIEDGSVQLADHYQQNTPIGDGPVLLPDNHYLSTQSALSKDPNEKRDHMVLLEFVTAAGITLGMDELY
KEFARIIVVTSGKGGVGKTTSSAAIATGLAQKGKKTVVIDFDIGLRNLDLIMGCERRVVYDFVNVIQGD
ATLNQALIKDKRTENLYILPASQTRDKDALTREGVAKVLDDLKAMDFEFIVCDSPAGIETGALMALYFA
DEAIITTNPEVSSVRDSDRILGILASKSRRAENGEEPIKEHLLLTRYNPGRVSRGDMLSMEDVLEILRIKLV
GVIPEDQSVLRASNQGEPVILDINADAGKAYADTVERLLGEERPFRFIEEEKKGFLKRLFGG

His-MinE:

MGSSHHHHHHSSGLVPRGSHMASMTGGQQMGRGSEFALLDFFLSRKKNTANIAKERLQIIVAERRRSD
AEPHYLPQLRKDILEVICKYVQIDPEMVTVQLEQKDGDISILELNVTLPEAEELK

7.2 Purified proteins

The following figures show SDS-PAGE gels of the purified N-terminally His-tagged Min proteins used in the indicated sections. In all cases, Precision Plus Dual Xtra protein standard was used as ladder.

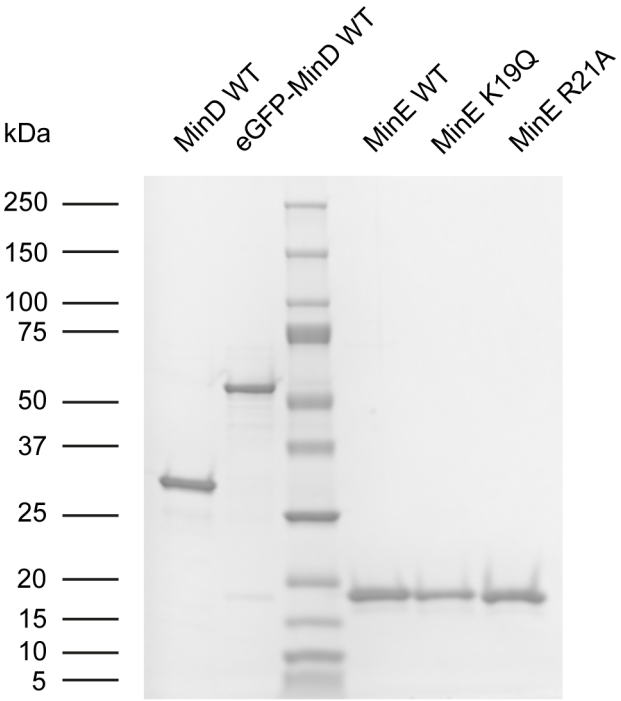

Figure 7.1: SDS-PAGE gel (Mini-Protean TGX 4-20%) stained with InstantBlue, showing samples of MinD, eGFP-MinD and MinE variants used in experiments reported in section 4.1.

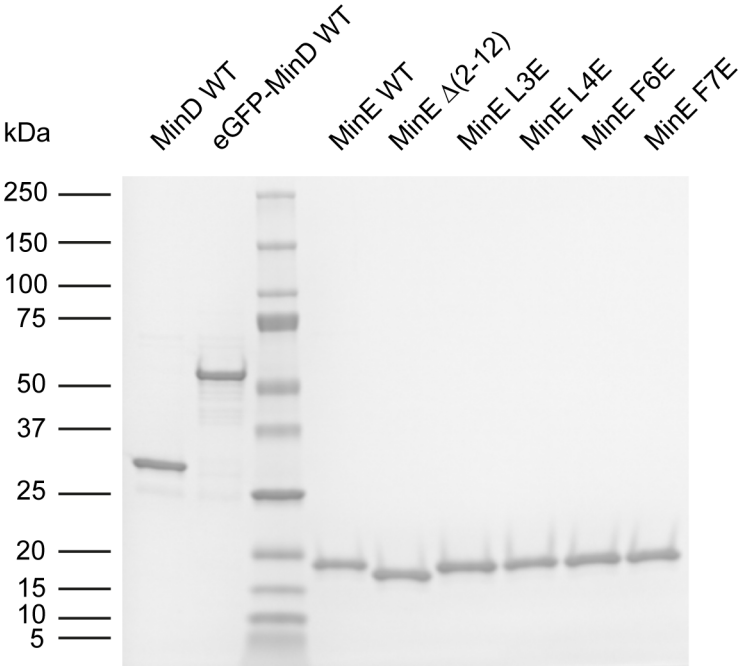

Figure 7.2: SDS-PAGE gel (Mini-Protean TGX 4-20 %), stained with InstantBlue, showing samples of MinD, eGFP-MinD and MinE variants used in experiments reported in sections 4.2 and 4.3.

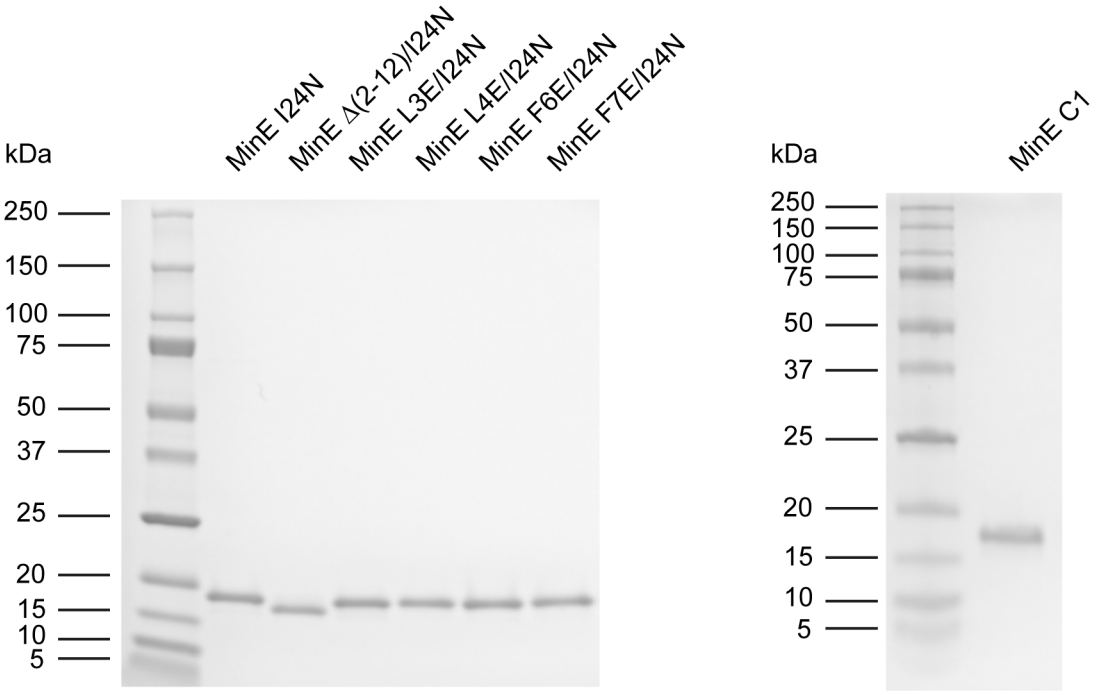

Figure 7.3: SDS-PAGE gels (left: Mini-Protean TGX 4-20 %, right: Mini-Protean TGX anyKd gel) stained with InstantBlue, showing samples of MinE I24N mutants and MinE C1 (R10G/K11E/K12E) used in experiments reported in sections 4.2 and 4.3. The SDS-PAGE with MinE C1 was performed by Tamara Heermann.

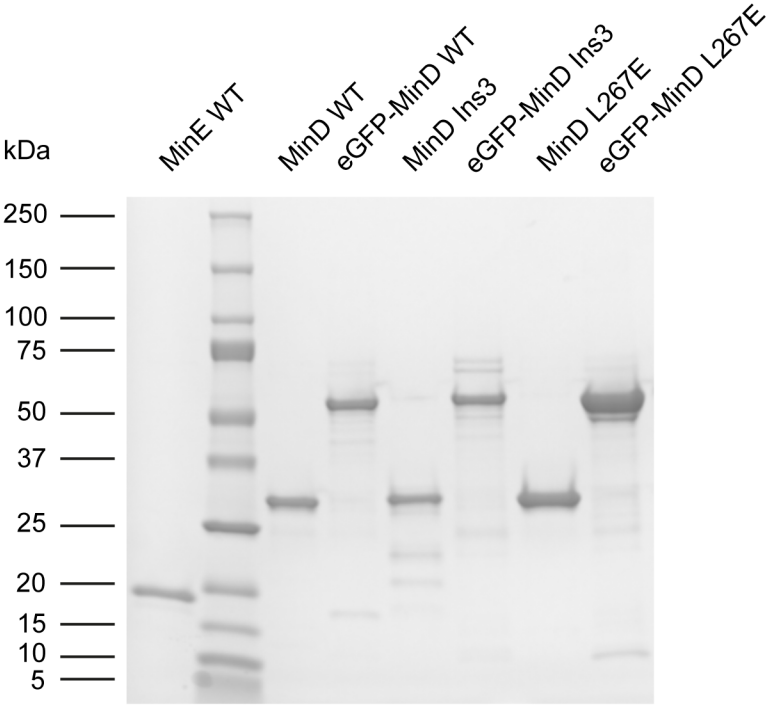

Figure 7.4: SDS-PAGE gel (Mini-Protean TGX 4-20 %), stained with InstantBlue, showing MinD, eGFP-MinD and MinE variants used in experiments reported in section 4.4.

7.3 Appendix for section 4.2.1

The following supplementary information for section 4.2.1 is adapted from, and in part identical to, the manuscript listed at the beginning of section 4.2 (Kretschmer et al., 2017)[11].

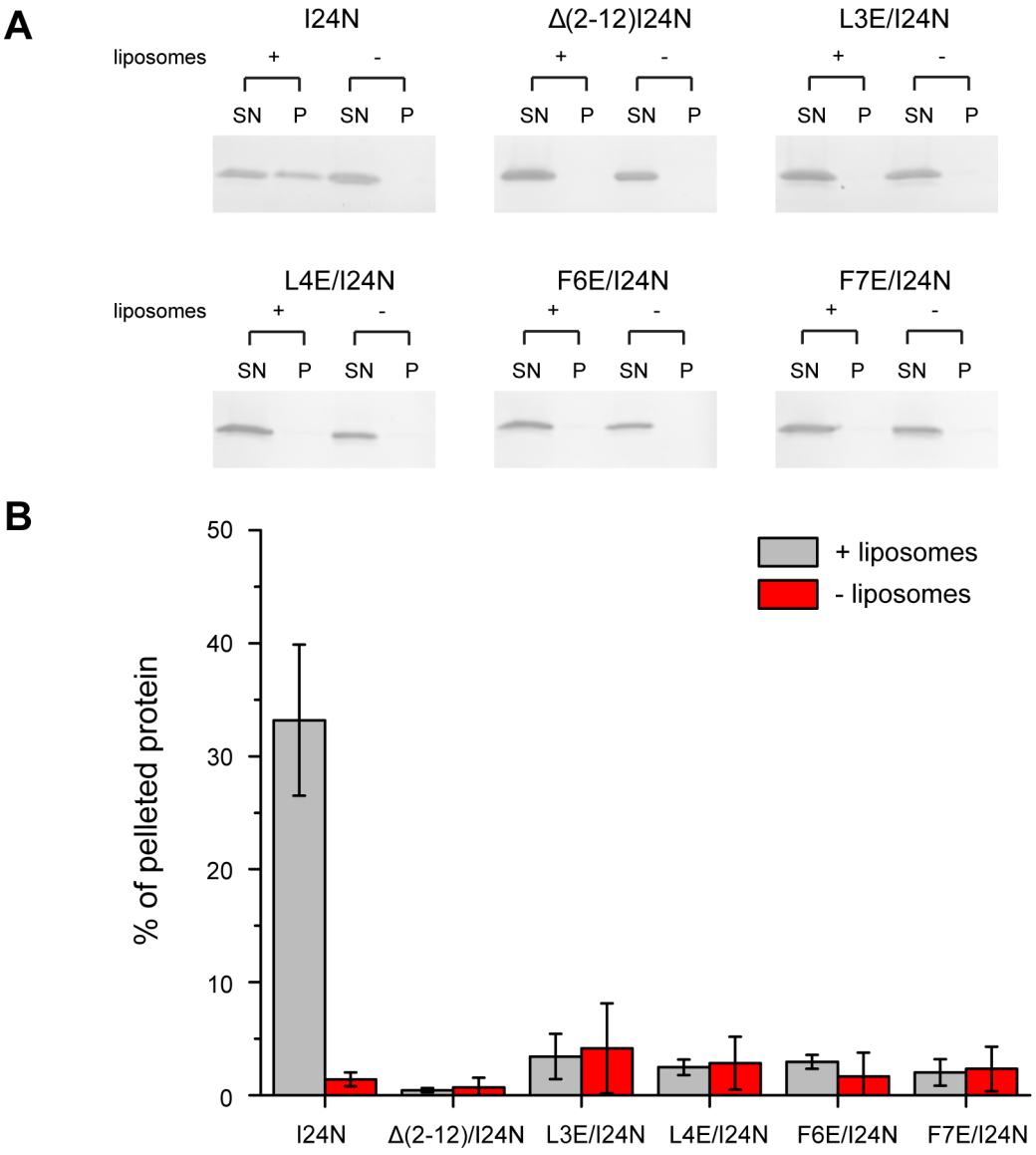

Figure 7.5: Truncation or mutation of MinE's membrane targeting sequence disrupts interaction of MinE with lipid membranes *in vitro*. Analogously to prior *in vivo* experiments, the effect of mutations in MinE's MTS was tested in the background of a mutation (here: I24N) that constitutively exposes Min's MTS and thereby facilitates detection of MinE membrane interaction (Park et al., 2011). **A)** Representative SDS-PAGE fractions from co-sedimentation experiments of MinE I24N mutants with small unilamellar vesicles. SN: supernatant. P: pellet. **B)** Percentage of pelleted protein for MinE I24N in the presence or absence of additional MTS mutations. Error bars represent standard deviation from three independent experiments.

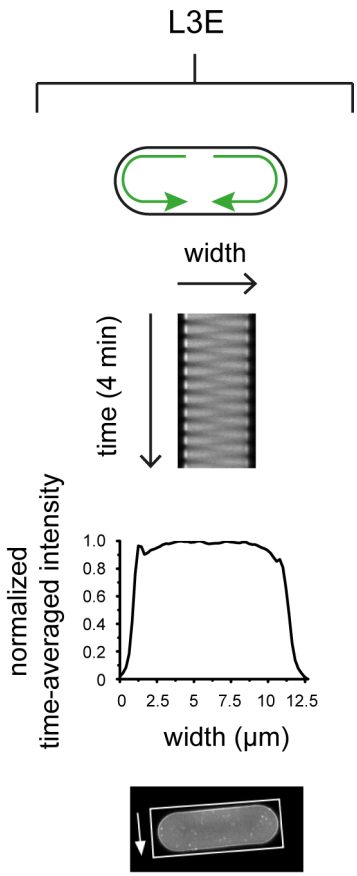

Figure 7.6: Bidirectional rotations emerging with MinE L3E appear like an oscillation along the minor axis. The kymograph along the compartment width and time-averaged fluorescence intensity, measured in the rectangular area highlighted below, are plotted for the same compartment exhibiting bidirectional rotations shown in Figure 4.8.

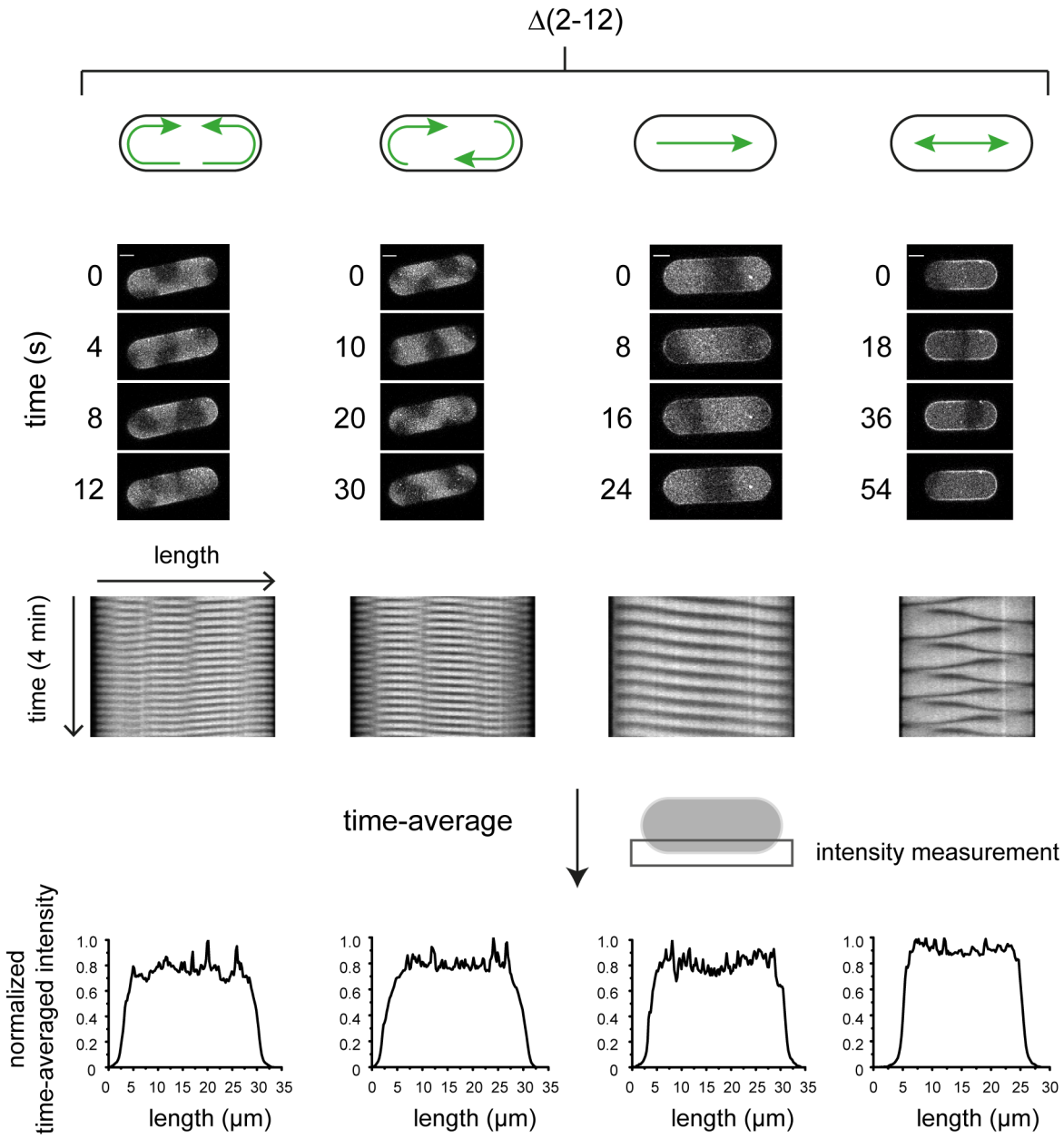

Figure 7.7: Unusual dynamics observed with MinE Δ(2-12). All images at 1 µM MinD with 20% eGFP-MinD and 1 µM MinE. Time-averaged protein distributions were measured as in Figure 4.8. Scale Bar: 5 µm.

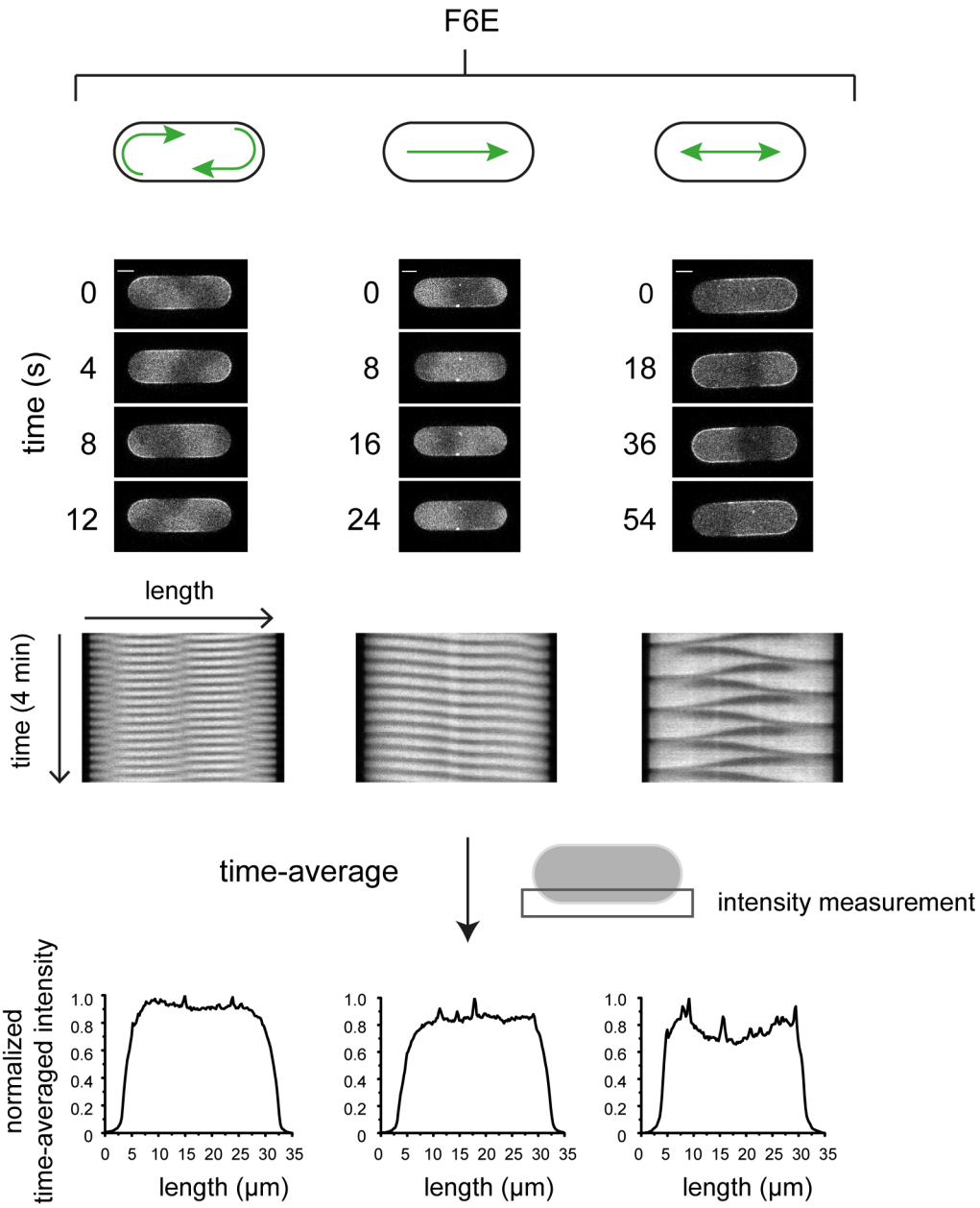

Figure 7.8: Unusual dynamics observed with MinE F6E. All images at 1 µM MinD with 20% eGFP-MinD and 1 µM MinE. Time-averaged protein distributions were measured as in Figure 4.8. Scale Bar: 5 µm.

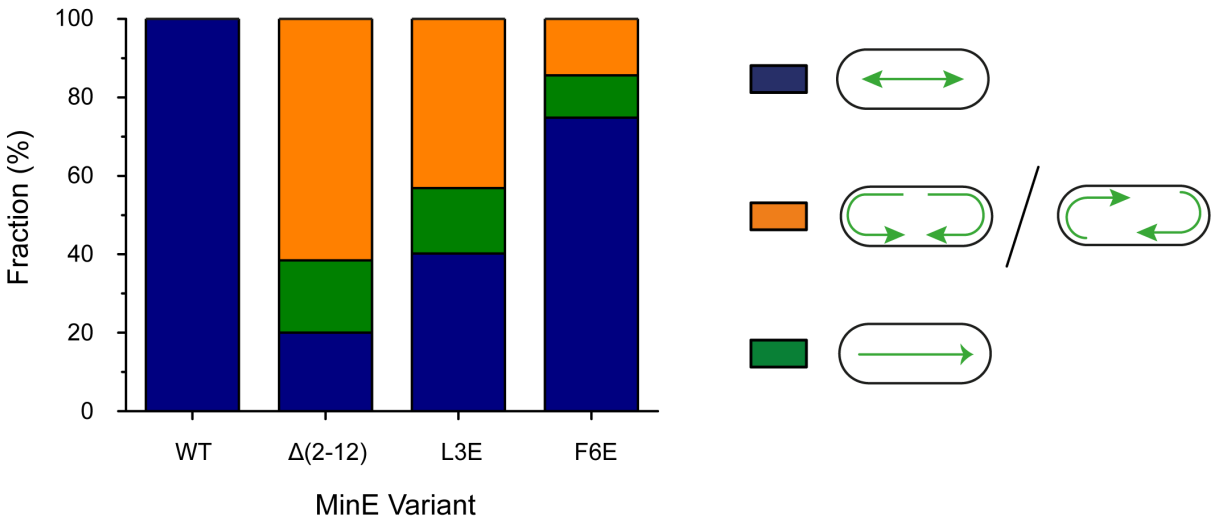

Figure 7.9: Relative fractions of observed modes for MinE Δ(2-12), L3E and F6E. Bi- and unidirectional rotations were classified together, as they were sometimes difficult to distinguish. Chaotic dynamics, which occasionally occurred but could not be clearly assigned, were not taken into account. Protein concentrations: 1 µM MinD incl. 20 % eGFP-MinD, 1 µM MinE. Absolute numbers of observed modes are shown in Table 7.1.

Table 7.1: Absolute numbers of different dynamic modes observed for WT MinE and MinE Δ(2-12), L3E and F6E in PDMS microcompartments. Modes were counted in three independent experiments imaging multiple compartments respectively (N ≥ 55 analyzed compartments). If mode switching occurred within the same compartment, both modes were counted.

MinE variant	**Pole-to-pole oscillations**	**Traveling waves**	**Rotations**
WT	81	0	0
Δ(2-12)	13	12	40
L3E	41	17	44
F6E	104	15	20

7.4 Appendix for section 4.3.1

The following contains supplementary information on the theoretical analysis performed by Jonas Denk (LMU Munich). This section is based on the manuscript listed at the beginning of section 4.3 (Denk et al., 2018)[12].

For linear stability analysis, a two-dimensional box geometry with the membrane at the bottom and bulk on top was used. The length of the box was 250 µm, whereas the bulk was 5 mm high. Nonlinear reactive boundary conditions at the membrane interface ensure that processes involving bulk and membrane-bound proteins equal the diffusive fluxes onto and off the membrane. For the sides of the analyzed two-dimensional box, periodic boundary conditions were employed. In turn, no-flux boundary conditions were employed at the top of the box.

In sections 7.4.1 and section 7.4.2, the basic equations underlying the models discussed in section 4.3 are stated. Values of parameters that were not varied in the linear stability analysis are given in Table 7.2 and Table 7.3 within section 7.4.3.

7.4.1 Model including a switch from reactive to latent MinE

The extended model including MinE's switch from the reactive to the latent state is described by the following system of partial differential equations, in coordinate-free form. The nomenclature is similar to section 2.3.5 with *E,r* and *E,l* denoting reactive and latent MinE respectively and μ denoting the switching rate. Note that the skeleton model is recovered for $k_{dE}^{r} = k_{dE}^{l}$, i.e. only one MinE conformation**.**

$$\partial_t u_{DD} = D_c \nabla_c^2 u_{DD} - \lambda u_{DD} \quad (7)$$

$$\partial_t u_{DT} = D_c \nabla_c^2 u_{DT} + \lambda u_{DD} \quad (8)$$

$$\partial_t u_{E,r} = D_c \nabla_c^2 u_{E,r} - \mu\, u_{E,r} \quad (9)$$

$$\partial_t u_{E,l} = D_c \nabla_c^2 u_{E,l} + \mu\, u_{E,r} \quad (10)$$

$$\partial_t u_d = D_m \nabla_m^2 u_d + f_d(u_d, \tilde{u}_{DT}, \tilde{u}_{E,r}, \tilde{u}_{E,l}) \quad (11)$$

$$\partial_t u_{de} = D_m \nabla_m^2 u_{de} + f_{de}(u_{de}, u_d, \tilde{u}_{E,r}, \tilde{u}_{E,l}) \quad (12)$$

with the following reactions occurring at the membrane-bulk interface and $\tilde{u}_i$ denoting bulk densities just above the membrane.

$$f_d(u_d, \tilde{u}_{DT}, \tilde{u}_{E,r}, \tilde{u}_{E,l}) := (k_D + k_{dD}u_d)\tilde{u}_{DT} - u_d(k_{dE}^l \tilde{u}_{E,l} + k_{dE}^r \tilde{u}_{E,r}) \quad (13)$$

$$f_{de}(u_{de}, u_d, \tilde{u}_{E,r}, \tilde{u}_{E,l}) := u_d(k_{dE}^l \tilde{u}_{E,l} + k_{dE}^r \tilde{u}_{E,r}) - k_{de}u_{de} \quad (14)$$

7.4.2 Models including MinE membrane interaction

The extended model including persistent MinE membrane interaction is described by the following system of partial differential equations, in coordinate-free form.

$$\partial_t u_{DD} = D_c \nabla_c^2 u_{DD} - \lambda u_{DD} \quad (15)$$

$$\partial_t u_{DT} = D_c \nabla_c^2 u_{DT} + \lambda u_{DD} \quad (16)$$

$$\partial_t u_E = D_c \nabla_c^2 u_E \quad (17)$$

$$\partial_t u_d = D_m \nabla_m^2 u_d + f_d(u_d, u_e\, \tilde{u}_{DT}, \tilde{u}_E) \quad (18)$$

$$\partial_t u_{de} = D_m \nabla_m^2 u_{de} + f_{de}(u_{de}, u_d, u_e, \tilde{u}_E) \quad (19)$$

$$\partial_t u_e = D_m \nabla_m^2 u_e + f_e(u_{de}, u_d, u_e) \quad (20)$$

with the following reactions occurring at the membrane-bulk interface and $\tilde{u}_i$ denoting bulk densities just above the membrane.

$$f_d(u_d, u_e\, \tilde{u}_{DT}, \tilde{u}_E) := (k_D + k_{dD}u_d)\tilde{u}_{DT} - u_d(k_{dE}\tilde{u}_E + k_{ed}u_e) \quad (21)$$

$$f_{de}(u_{de}, u_d, u_e, \tilde{u}_E) := u_d(k_{dE}\tilde{u}_E + k_{ed}u_e) - k_{de}u_{de} \quad (22)$$

$$f_e(u_{de}, u_d, u_e) := k_{de}u_{de} - u_d k_{ed} u_e - k_e u_e \quad (23)$$

For additionally analyzing direct MinE membrane binding independent of recruitment by MinD, attachment of MinE from the bulk to the membrane with a rate k_E is incorporated, such that:

$$f_E(u_e, u_d, \tilde{u}_E) := k_e u_e - k_{dE} u_d \tilde{u}_E - k_E \tilde{u}_E \quad (24)$$

$$f_e(u_{de}, u_d, u_e, \tilde{u}_E) := k_E \tilde{u}_E + k_{de}u_{de} - u_d k_{ed} u_e - k_e u_e \quad (25)$$

7.4.3 Values of parameters

Table 7.2: Values of parameters for analyzing the network with reactive-latent switch

Parameter	Value
Diffusion coefficient for MinD and MinE in the bulk (D_c)	60 $\mu m^2 s^{-1}$
Diffusion coefficient for MinD and MinE on the membrane (D_m)	0.013 $\mu m^2 s^{-1}$
Rate constant for MinD attachment (k_D)	0.065 $\mu m\ s^{-1}$
Rate constant for MinD recruitment (k_{dD})	0.02 $\mu m^3\ s^{-1}$
Rate of MinDE disintegration (k_{de})	0.34 s^{-1}
Nucleotide exchange rate (λ)	6 s^{-1}
Switching rate (μ)	100 s^{-1}
MinD mean total density	638 μm^{-3}

Table 7.3: Values of parameters for analyzing the networks with MinE membrane interaction

Parameter	Value
Diffusion coefficient for MinD and MinE in the bulk (D_c)	60 $\mu m^2 s^{-1}$
Diffusion coefficient for MinD and MinE on the membrane (D_m)	0.013 $\mu m^2 s^{-1}$
Rate constant for MinD attachment (k_D)	0.065 $\mu m\ s^{-1}$
Rate constant for MinD recruitment (k_{dD})	0.02 $\mu m^3\ s^{-1}$
Rate constant for MinE recruitment (k_{dE})	0.126 $\mu m^3\ s^{-1}$
Rate of MinDE disintegration (k_{de})	0.34 s^{-1}
Nucleotide exchange rate (λ)	6 s^{-1}
MinD mean total density	638 μm^{-3}

7.5 Abbreviations

AAAS	American Association for the Advancement of Science
AAP	ATPase activating protein
ADP	Adenosine 3’ diphosphate
ATP	Adenosine 3’ triphosphate
DFG	Deutsche Forschungsgemeinschaft
DMF	Dimethylformamide
DMSO	Dimethylsulfoxide
DNA	Deoxyribonucleic acid
EDTA	Ethylenediaminetetraacetic acid
(e)GFP	(enhanced) green fluorescent protein
GTP	Guanosine 3’ triphosphate
GUVs	Giant unilamellar vesicles
Kan	Kanamycin
kDa	kiloDalton
Hepes	4-(2-hydroxyethyl)-1-piperazineethanesulfonic acid
incl.	including
IPTG	Isopropyl β-D-1-thiogalactopyranoside
LB	Lysogeny broth (medium)
LMU	Ludwig-Maximilians-Universität
LSM	Laser scanning microscope
MPI-B	Max-Planck-Institute of Biochemistry
MTS	Membrane targeting sequence
mRNA	Messenger ribonucleic acid
NAD	Nicotinamide adenine dinucleotide
NDP	Nucleoside 3’ diphosphate
(d)NTP	(deoxy)nucleoside 3’ triphosphate
NTA	Nitrilotriacetic acid
NO	Nucleoid occlusion
PALM	Photoactivated Localization Microscopy
PCR	Polymerase chain reaction
PDB	Protein Data Bank
PDMS	Polydimethylsiloxane

PEP	Phosphoenolpyruvate
PNAS	Proceedings of the National Academy of Science of the United States of America
QBM	Quantitative Biosciences Munich
QCM-D	Quartz crystal microbalance with dissipation monitoring
SDS-PAGE	Sodium dodecyl sulfate polyacrylamide gel electrophoresis
SFB	Sonderforschungsbereich
SLBs	Supported lipid bilayer
SOC	Super optimal broth with catabolite repression (medium)
SUVs	Small unilamellar vesicles
TB	Terrrific broth (medium)
TCEP	Tris(2-carboxyethyl)phosphin
TSD	Topological specificity domain
w/v	weight per volume

8 Acknowledgments

First and foremost, I would like to express my gratitude to Prof Dr. Petra Schwille for the opportunity to perform my PhD research in her laboratory. Petra's guidance and the inspiring lab environment she generated and maintained were very important for my research as well as my personal development as a scientist. I also greatly appreciated the chance to present my work at international conferences and am thankful for the opportunity to write review articles and otherwise expand my scientific horizon.

Moreover, I would like to thank Prof. Dr. F. Ulrich Hartl for taking over the official PhD mentorship ("Fachvertretung") at the Faculty for Chemistry and Pharmacy at LMU Munich and for evaluating my dissertation. Furthermore, I would like to thank both him and Prof. Dr. Erwin Frey for providing valuable feedback at my thesis advisory committee (TAC) meetings. I would also like to thank the members of my PhD examination committee.

I am grateful for having been a student of the Graduate School of Quantitative Biosciences Munich (QBM). Besides instructive lectures, workshops and retreats, this graduate school and the organizers provided a supportive community and enabled me to attend international events, including the q-bio summer school in San Diego. Many thanks to all involved in QBM, including Ulrike Gaul, Erwin Frey, Michael Mende, Julia Schlehe, Filiz Civril, Markus Hohle and Mara Kieke. I also acknowledge financial support from the Max-Planck-Society as well as the German Research Foundation (DFG) via QBM and the SFB 1032.

Within the Schwille group, I would like to thank Martin Loose, Ariadna Martos and Katja Zieske, who pointed out interesting research directions at the beginning, provided feedback and introduced me to experimental techniques used in this work. Later, I was fortunate to work in the company of Philipp Glock, Beatrice Ramm and more recently Tamara Heermann, whom I would all like to thank for their valuable comments, discussions and support. I am also highly grateful to Andrea Tassinari for her dedicated work during her master's thesis under my guidance. I would also like to thank Katja Zieske, Michael Heymann and Frank Siedler for microfabrication. Moreover, I would like to thank our technicians Sigrid Bauer, Kerstin Andersson, Michaela Schaper, Katharina Nakel, Beatrix Scheffer and Brigitte Hartl for their help with DNA-, protein- and lipid-related techniques. In particular, I would like to thank Michaela Schaper and Katharina Nakel for their help with cloning. I would also like to thank Sabine Suppmann and other members of the Core Facility at the Max-Planck-Institute

of Biochemistry for help with protein purification. Furthermore, I would like to thank Silke Leuze-Bütün for administrative help and Helge Vogl and Frank Siedler for technical support. Generally, I would like to thank all members of the Schwille lab for discussions, advice and the supportive atmosphere. Besides the ones named already, I particularly learned from Henri Franquelim, Jonas Mücksch, Kristina Ganzinger, Sven Vogel, Matías Hernandez and Leon Harrington.

I am also highly grateful for the close collaboration with Erwin Frey, Jacob Halatek and Jonas Denk, who analyzed the Min system theoretically. In particular, I would like to thank Jonas for his work and the good discussions we had.

Lastly, I am incredibly grateful for the support of my family and friends over the years. In particular, I would like to thank my parents Wolfgang and Angelika, my brothers Lorenz and Toby and my girlfriend Sabine, all for their unwavering support throughout.

9 Endnotes

The following endnotes contain additional information on selected citations, licenses and permissions.

[1] According to Martha Marquardt, Ehrlich stated in the context of his Abitur examinations: "Das Leben ist … ein chemischer Vorgang ... " (Marquardt, 1951).
English version ("Life is … a chemical incident …") cited from (Kasten, 1996).
[2] Photo by the National Park Service, Title: Ripples on Mesquite Flat Sand Dunes (http://www.nps.gov/media/photo/gallery.htm?id=F44A0841-155D-4519-3EA6EA1963D35111) [Public domain], via Wikimedia Commons, downloaded from https://commons.wikimedia.org/wiki/File:Ripples_on_Mesquite_Flat_Sand_Dunes.jpg on April 10, 2018.
[3] Photo by D. Dibenski, Title: Auklet flock, Shumagins 1986 (images.fws.gov) [Public domain], via Wikimedia Commons, downloaded from https://commons.wikimedia.org/wiki/File:Auklet_flock_Shumagins_1986.jpg on March 28, 2018.
[4] Link to Journal Homepage: https://www.nature.com/nature/, last accessed on April 23, 2018.
[5] Link to Book Homepage: https://link.springer.com/book/10.1007/978-3-663-05242-5, last accessed on April 23, 2018.
[6] Link to Journal Homepage: https://www.nature.com/nrmicro/, last accessed on April 23, 2018.
[7] For the CC BY 3.0 license, see also: https://creativecommons.org/licenses/by/3.0/, last accessed on April 23, 2018.
[8] For the CC BY 4.0 license, see also: https://creativecommons.org/licenses/by/4.0/, last accessed on April 23, 2018.
[9] Link to Journal Homepage: https://www.nature.com/nnano/, last accessed on April 23, 2018.
[10] "Authors are allowed to re-use parts of their own work in derivative works without seeking the Royal Society's permission. However, please ensure the paper is cited.";
"You are also free to … use it in a thesis or dissertation ... "
See: https://royalsociety.org/journals/permissions/, last accessed on April 23, 2018.
[11] "This is an open access article distributed under the terms of the Creative Commons Attribution License, which permits unrestricted use, distribution, and reproduction in any medium provided the original author and source are credited".
See: http://journals.plos.org/plosone/article?id=10.1371/journal.pone.0179582, last accessed on April 23, 2018.
For the CC BY 4.0 license, see also: https://creativecommons.org/licenses/by/4.0/, last accessed on April 23, 2018.
[12] "PNAS authors need not obtain permission for the following cases: 1. to use their original figures or tables in their future works; … 3. to include their articles as part of their dissertations; or 4. to use all or part of their articles in printed compilations of their own works. The full journal reference must be cited …"
See: http://www.pnas.org/page/about/rights-permissions, last accessed on April 23, 2018.